https://doi.org/10.1070/RCR5038

Porous porphyrin-based metal-organic frameworks: synthesis, structure, sorption properties and application prospects

Yulia G. Gorbunova,[a, b]* Yulia Yu. Enakieva,[b] Marina V. Volostnykh,[b] Anna A. Sinelshchikova,[b] Inna A. Abdulaeva,[b] Kirill P. Birin,[b] Aslan Yu. Tsivadze [a, b]

[a] *Kurnakov Institute of General and Inorganic Chemistry, Russian Academy of Sciences, Leninsky prosp. 31, 119991 Moscow, Russian Federation*
[b] *Frumkin Institute of Physical Chemistry and Electrochemistry, Russian Academy of Sciences, 31 Leninsky prosp. 31, stroenie 4, 119071 Moscow, Russian Federation*

The unique properties of porous metal-organic frameworks are responsible for the increasing research interest in the design and synthesis of this type of materials. A general strategy towards targeted design of metal-organic frameworks possessing desired properties is a choice of optimal linkers, which are usually represented by polytopic organic ligands. Porphyrins are promising building blocks for such frameworks due to their tunable physicochemical properties and wide possibilities of macrocycle modification. The achievements of the last decade in the development of synthetic approaches to porphyrin functionalization have promoted fast progress of tetrapyrrole chemistry as the basis of metal-organic frameworks. This review gives analysis of the current literature devoted to the synthesis of porphyrin-based metal-organic frameworks and the prospects for their application in modern materials science.
The bibliography includes 262 references.

Contents

1. Introduction 1
2. Synthetic strategies towards porphyrin-based metal-organic frameworks 3
2.1. Crystal engineering 3
2.1.1. Metal-organic frameworks based on A_4 type carboxy-substituted porphyrins 4
2.1.2. Metal-organic frameworks based on other A_4 type porphyrins 13
2.1.3. Metal-organic frameworks based on A_2 and A_2B_2 type carboxy-substituted porphyrins 17
2.2. Pillaring of two-dimensional layers by ditopic ligands 19
2.3. Post-synthetic modification strategy 21
3. Practical application prospects 25
3.1. Sorption and separation of gases 25
3.2. Catalysis of organic reactions 25
3.2.1. Oxidation reactions 30
3.2.2. CO_2 addition reactions 31
3.2.3. Carbene insertion 32
3.2.4. Photocatalytic reduction of CO_2 32
3.3. Photodynamic therapy of cancer and other biomedical applications 33
3.4. Utilization of CO_2 37
3.5. Photocatalytic production of hydrogen 37
3.6. Proton and electronic conduction 38
3.7. Films based on metal-organic frameworks 39
4. Conclusion 44
5. List of abbreviations 44
6. References 45

1. Introduction

Metal-organic frameworks (MOFs) are a relatively new class of porous materials possessing unique physicochemical properties and structural characteristics. Metal-organic frameworks are successfully used for sorption and separation of various gases and gas mixtures,[1–5] as active components of luminescent and photon devices,[6,7] in catalysis,[8–11] medicine[12–14] and in other fields of science and technology. In MOF structures, metal cations and/or metal clusters form framework nodes, which are connected into a common network by organic ligand molecules. The possibility of the targeted modification of the structural parameters of MOFs by varying the nature of inorganic and organic components may produce materials with different pore sizes and large surface areas.

Metal-organic frameworks in which organic ligands are represented by porphyrin macrocycles attract attention for several reasons. Owing to the aromatic nature of the macrocycle, porphyrins possess unique physicochemical properties and high thermal and chemical stability, which is important for the design of materials suitable for real technological applications.[15,16] In addition, a porphyrin molecule is a rigid macrocycle with linear dimensions of approximately 20–30 Å, which determines a relatively large size of MOF pores and channels, the diameters of which vary from 3.5 to 38 Å, depending on the tetrapyrrole structure. Metal-organic frameworks based on porphyrins are also characterized by additional interactions between

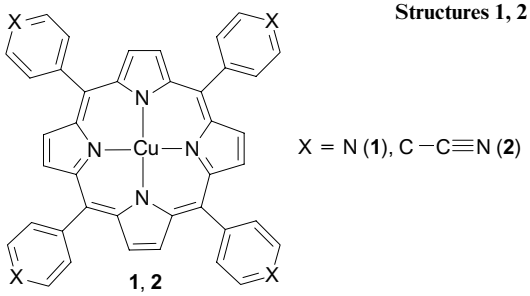
Received 23 August 2021
© 2022 Uspekhi Khimii, ZIOC RAS, Russian Academy of Sciences and IOP Publishing Limited

the π-system of the macrocycle and small guest molecules held in the pores and channels. It is also noteworthy that, owing to the appearance of efficient approaches to the synthesis of chemically diverse porphyrins, it is possible to design MOFs using tetrapyrrole macrocycles containing various receptor moieties and additional functional groups. This considerably expands the scope of potential applicability of these materials, which includes heterogeneous catalysis,[10] photocatalytic hydrogen generation processes,[17] electrochemical reactions,[18–20] photodynamic therapy of cancer [13, 21, 22] and other fields.

Porphyrins are multidentate ligands, in which the periphery can be modified by varying the type, nature and positions of receptor groups and the nature of the macrocyclic metal centre can also be varied. The peripheral receptor moieties can be represented by carboxyl, hydroxyl and phosphonate moieties and by pyridine, pyrazole and imidazole rings (Fig. 1). All porphyrins used for MOFs construction can be conventionally divided into two types according to the number, position and relative orientation of receptor groups. One type includes symmetrical A_4 type tetraaryl-substituted porphyrins, which contain receptor groups in each *meso*-aryl substituent. The second type includes less symmetrical A_2 and A_2B_2 type molecules containing identical aryl groups in each pair of two opposing *meso*-positions of porphyrin. The receptor groups can be located either in all four *meso*-positions or only in two of them.

The first porphyrin-containing MOFs were obtained by Abrahams research group [23] in 1994 as ruby-coloured crystals. The structures $\{[Cu^{II}(TPP)Cu^{I}]_n\}^{n+}$ [TPP is 5,10,15,20-tetra(4-pyridyl)porphyrin] and

Structures 1, 2



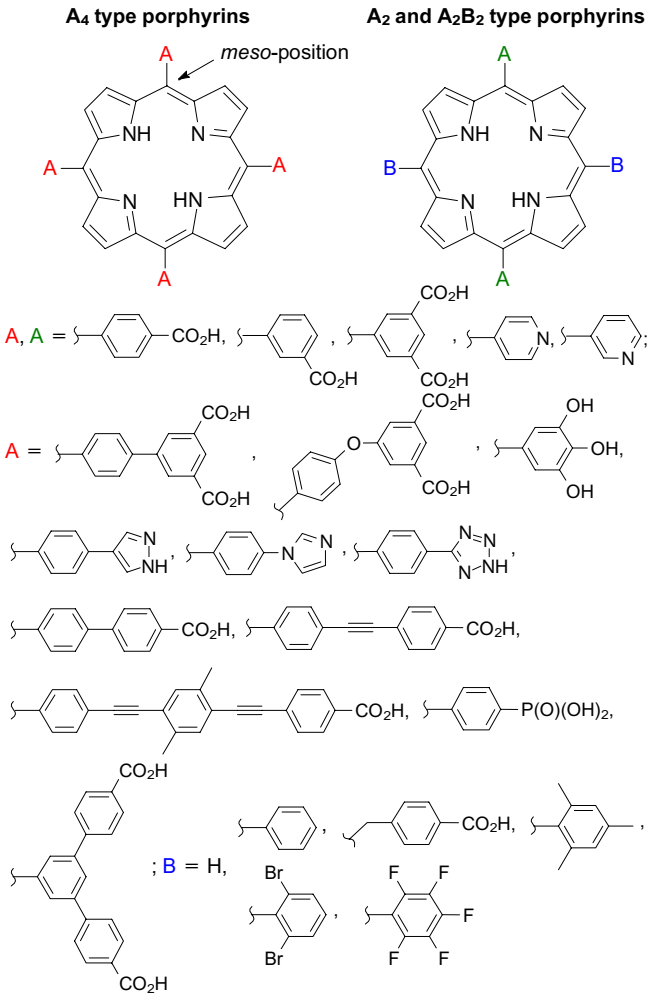


Figure 1. Types of porphyrin ligands for the synthesis of MOFs.

$\{[Cu^{II}(TCYP)Cu^{I}]_n\}^{n+}$ [TCYP is 5,10,15,20-tetrakis(4-cyanophenyl)porphyrin] were obtained by the reaction of a solution of tetrapyridyl- (**1**) or tetra(4-cyanophenyl)-substituted (**2**) copper porphyrin with $Cu(MeCN)_4BF_4$ by slow evaporation

Yu.G.Gorbunova. Corresponding Member of the RAS, Doctor of Chemical Sciences, Professor, Chief Researcher at IGIC RAS, Chief Researcher at IPCE RAS.
E-mail: yulia@igic.ras.ru, yulia.gorbunova@gmail.com
Current research interests: coordination and supramolecular chemistry of tetrapyrrole macrocycles and crown ethers, lanthanides, functional materials.
Yu.Yu.Enakieva. Candidate of Chemical Sciences, Leading Researcher at IPCE RAS.
E-mail: yulia.enakieva@gmail.com
Current research interests: coordination chemistry of tetrapyrrole macrocycles, porphyrins, porphyrin functionalization, porphyrinyl-phosphonates, metal-organic frameworks, proton conduction, functional materials.
M.V.Volostnykh. Candidate of Chemical Sciences, Researcher at IPCE RAS.
E-mail: marinavolostnykh@gmail.com
Current research interests: coordination chemistry of tetrapyrrole compounds, supramolecular assemblies, hybrid photoactive materials.
A.A.Sinelshchikova. Candidate of Chemical Sciences, Senior Researcher at IPCE RAS.
E-mail: asinelshchikova@gmail.com
Current research interests: X-ray diffraction, porphyrins, phthalocyanines, metal-organic frameworks, supramolecular chemistry of tetrapyrrole macrocycles.
I.A.Abdulaeva. Candidate of Chemical Sciences, Researcher at IPCE RAS.
E-mail: inna.a.abdulaeva@gmail.com
Current research interests: functionalization and coordination chemistry of tetrapyrrole macrocycles, porphyrins, catalysis.
K.P.Birin. Candidate of Chemical Sciences, Leading Researcher at IPCE RAS.
E-mail: kirill.birin@gmail.com
Current research interests: functionalization and coordination chemistry of tetrapyrrole macrocycles, porphyrins, hybrid functional materials, heterogeneous catalysis.
A.Yu.Tsivadze. Academician, Doctor of Chemical Sciences, Professor, head of laboratory and Scientific Supervisor of IPCE RAS, head of laboratory of IGIC RAS.
E-mail: tsiv@phyche.ac.ru
Current research interests: coordination and supramolecular chemistry of tetrapyrrole macrocycles and crown ethers, separation of isotopes, extraction.

Translation: Z.P.Svitanko

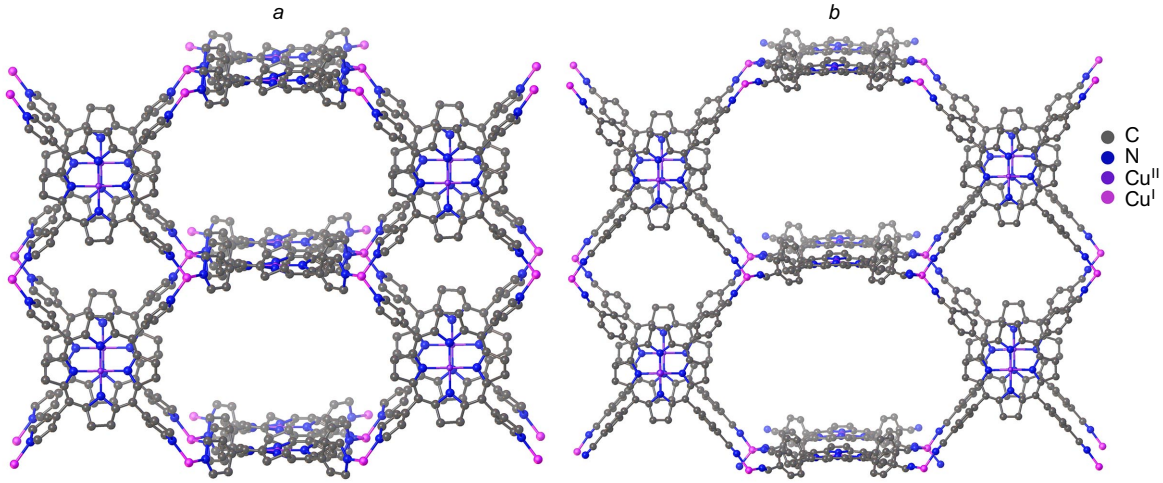


Figure 2. Crystal structures of the first porphyrin-based MOFs: $\{[Cu^{II}(TPP)Cu^{I}]_n\}^{n+}$ (*a*) and $\{[Cu^{II}(TCYP)Cu^{I}]_n\}^{n+}$ (*b*). The figure was created by the authors using the Cambridge Crystallographic Data Centre (Refcodes PIZJEN, PIZJAJ) and data of Ref. 23.

of solvents in a nitrogen flow. In both cases, single crystal XRD of the crystals showed the formation of a framework with large channels characterized by a window of ~20 Å size (Fig. 2).

However, these systems proved to be unstable and did not withstand removal of the solvent, being destroyed in air. Since then, various research groups have pursued the search for the optimal conditions for the synthesis of porphyrin-containing MOFs possessing higher stability. According to Web of Science, the number of publications in this field of research is more than a hundred per year, with their citation number being more than 6000 (Fig. 3).

It is noteworthy that the vast majority of synthetically available porphyrin MOFs that have most interesting and promising characteristics contain carboxy- and pyridyl-substituted porphyrins. There are only few reported examples of metal-organic frameworks containing porphyrins with other functional groups. Interestingly, synthetically available porphyrin analogues such as phthalocyanines, porphyrazines, subporphyrins, *etc*. are very rarely used to produce MOFs.[24–29]

The metal-organic frameworks based on pyridine-substituted porphyrins have been described rather comprehensively in reviews;[30–32] therefore, they are not considered here. It is noteworthy that porphyrin ligands with carboxyl receptor groups can form rather strong bonds with a broad range of metal ions; therefore, these ligand have been most studied as organic components for MOFs that would be stable after removal of the solvent. Therefore, this review is mainly focused on the scientific achievements in the synthesis, structure and physicochemical properties of particularly MOFs based on carboxy-substituted porphyrins. However, examples of using other functionalized porphyrins as organic building blocks for the preparation of these materials are also given.

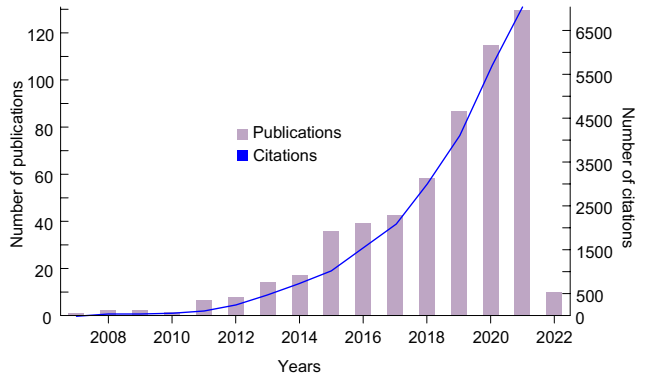


Figure 3. Variation of the number of publications devoted to porphyrin-based MOFs and publication citations starting from 2007 according to Web of Science.

2. Synthetic strategies towards porphyrin-based metal-organic frameworks

By analogy with other coordination polymers, all porphyrin-based MOFs can be divided into three types according to the crystal structure motif: 1D (chains), 2D (layers) and 3D ones (frameworks). Often, it is difficult to predict which motif will form; however, it is possible to distinguish the general synthetic strategies that are used to prepare frameworks of specified structure. The first strategy is the design of crystal structure by changing the topology of both organic and inorganic units and by varying the conditions of synthesis. This approach is called crystal engineering. The second approach is binding of 2D layers to one another by binding ligands (pillared MOFs). This may result in switching from 2D to 3D motifs, with the distance between the layers being controlled by varying the length of linkers. The third approach is post-synthetic modification of MOFs. Each strategy is considered in detail below, and examples of its application are given.

2.1. Crystal engineering

The type of porphyrin precursor used to design a MOF determines the crystal structure and, as a consequence, the physicochemical properties of the material. An important role belongs also to the structure of secondary building units (SBUs), which vary depending on the nature of metal sources and experimental conditions of MOF synthesis. Therefore, the published data describing approaches to the synthesis of porphyrin-based MOFs are analyzed according

to the type of porphyrin ligands and secondary building units and on the reaction conditions.

Among the described methods for the preparation of porphyrin MOFs, solvothermal synthesis is most popular. In this case, variation of the solvent nature, modulator, reaction temperature and time and component ratio can considerably affect the structure of the resulting porous MOF. This part of the review gives analysis of the effect of key factors (type of porphyrin ligand, nature of metal source used to form SBUs and conditions of synthesis) on the structure (pore size and shape) of porphyrin-based MOFs. The published data are arranged according to the above-indicated types of porphyrin ligands.

2.1.1. Metal-organic frameworks based on A_4 type carboxy-substituted porphyrins

Among A_4 type porphyrins, a special place is occupied by tetradentate 5,10,15,20-tetrakis(4-carboxyphenyl)porphyrin (TCPP, **3**) (Fig. 4), which was used to prepare the vast majority of porphyrin MOFs. The next most popular is 5,10,15,20-tetrakis(3,5-dicarboxyphenyl)porphyrin (TDCPP, **4**). In some cases, the distance between the tetrapyrrole macrocycle and the terminal receptor groups in the porphyrin ligand is increased by introducing additional linkers (see Fig. 4).

In all cases, porphyrins can participate in the formation of MOFs either as free bases or as metal complexes, which can be prepared in advance, *in situ* or by post-modification. A broad range of metals of various valence (two, three and four) can be used as the nodes of porphyrin MOFs.

Most often, reactions of porphyrin **3** with divalent metal ions (Zn^{2+}, Co^{2+}, Ni^{2+}) give rise to two-dimensional (2D) motifs. Choi *et al.*[33] described 2D structures, PPF-1 † and isostructural PPF-1Co, which were synthesized from zinc or cobalt porphyrins and Zn^{2+} cations; in this case, free porphyrin **3** is metallated *in situ*. The PPF-1 structure is a two-dimensional sheet containing square channels with dimensions of 11.8 × 11.8 Å (Fig. 5).

There are also reported examples of 3D frameworks based on TCPP ligand **3** and divalent metals that form secondary building units of a different structure. Sharma

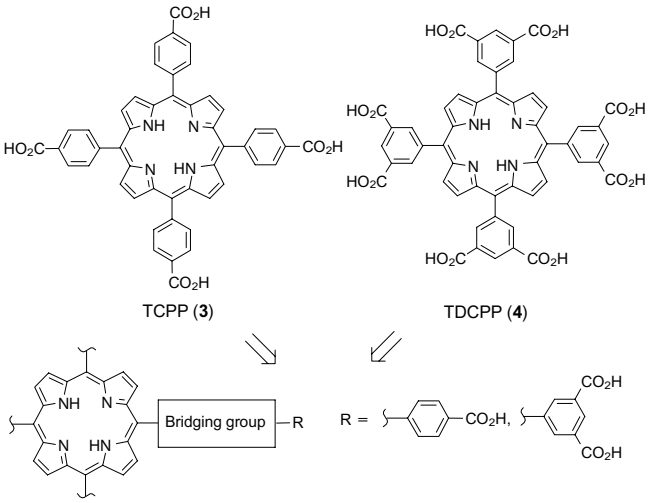


Figure 4. Carboxy-substituted A_4 type porphyrins for the design of MOFs.

† The designations (codes) of MOFs used here were taken from original publications.

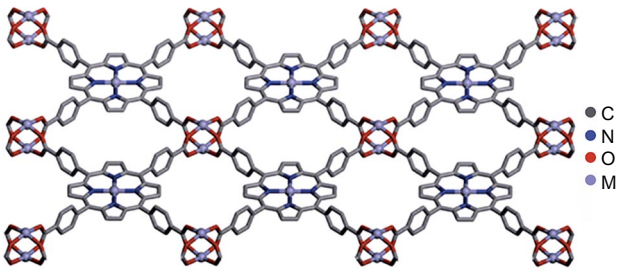


Figure 5. Part of the PPF-1 structure according to X-ray diffraction data. The water molecules are not shown. The figure was created by the authors using the Cambridge Crystallographic Data Centre (Refcode VUHJEO) and data of Ref. 33.

et al.[34] carried out the reaction of compound **3** with manganese(II) chloride (in 1 : 5 ratio) and thus obtained MOF1(Mn) containing 6.32 × 11.88 Å channels along the [001] crystallographic direction (Fig. 6 *a*,*b*). The 2D networks were formed *via* coordination of the porphyrin carboxyl groups to manganese cations. This was accompanied by simultaneous metallation of porphyrin molecules with the manganese cations that were additionally axially coordinated by two water molecules. The presence of water molecules promoted further assembly of two 2D layers of this MOF into a 3D framework due to hydrogen bonding to the oxygen atoms of free carboxylate groups of the neighbouring porphyrin molecule (see Fig. 6 *c*).

It is of interest that earlier the same research group[35] prepared a MOF that was also called MOF1. However, in this case, the authors used a lower amount of manganese(II) chloride (1 : 2 ratio) and synthesized a 3D MOF with two types of 1D channels with dimensions of 3.94 × 8.37 Å and 4.66 × 4.93 Å, in which extended Mn^{II} carboxylate 1D chains served as SBUs (Fig. 7). This structure had manganese cations only in the nodes and, owing to the presence of free porphyrin, MOF1 was capable of selective capture of CO_2. In addition, this material could be post-metallated with Fe^{3+} cations to give the framework Fe^{III}@MOF1, which behaved as an efficient, recycable catalyst for styrene oxidation.

The reaction of Ni^{2+} salt with porphyrin **3** afforded a porous 3D framework, MMPF-20,[36] containing

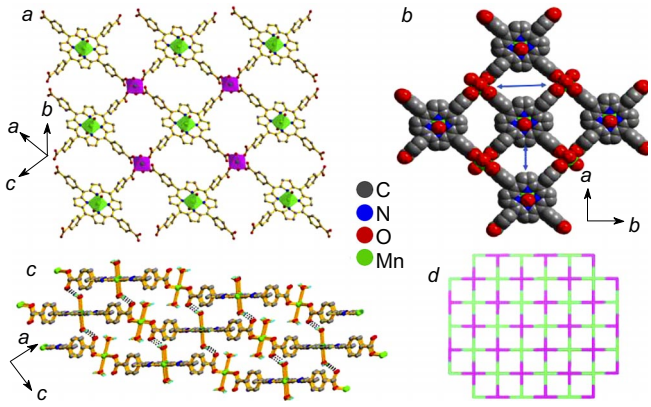


Figure 6. Structure of two-dimensional MOF1(Mn) (*a*, *b*), its topological image (*d*) and supramolecular 3D structure of this MOF formed by O···H–O hydrogen bonds between neighbouring 2D layers (*c*).[34] Published with permission from Elsevier.

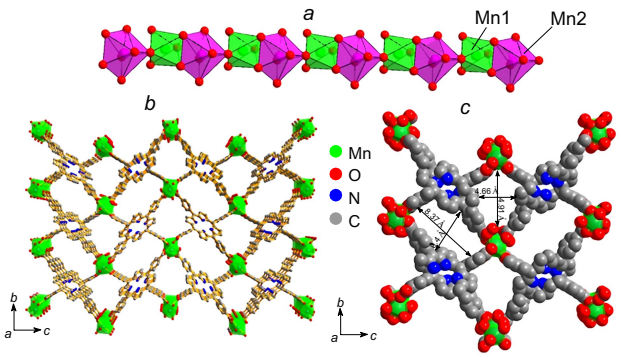


Figure 7. Mn^{II}-Carboxylate 1D channels in MOF1 (*a*); its structure with 1D channels (*b*) and space-filled image of 3D framework reflecting the presence of two types of 1D channels (*c*).[35] Published with permission from Wiley.

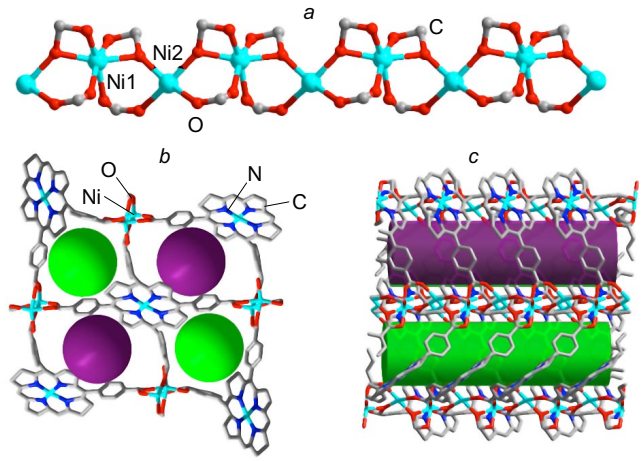


Figure 8. Ni^{II}-Carboxylate 1D channels in MMPF-20 (*a*) and its structure along the [100] (*b*) and [010] (*c*) crystallographic directions.[36] Published with permission from the American Chemical Society.

$\sim 4.6 \times 12.6$ Å 1D channels (Fig. 8). Owing to the presence of secondary building units such as extended 1D chains (see Fig. 8 *a*), MMPF-20 preserved its porosity after the removal of the guest solvent molecules, as was shown previously also for other analogous MOFs.[37]

A structure of this type was also obtained by a solvothermal reaction of cadmium nitrate with Pd-TCPP as a 3D framework with two types of channels sized $\sim 4.6 \times 12.6$ Å and 8.27×9.32 Å.[38]

Li *et al.*[39] reported an interesting example of the preparation of the anionic three-dimensional framework PMOF1, $[Cd_{3.2}(TCPP)_2][Me_2NH_2]_{1.6}$, based on cadmium(II) cations and porphyrin **3**. The $[Me_2NH_2]^+$ cations were present in the framework as counter-ions; they could be successfully replaced by Li^+ cations. Although the surface area of PMOF1 and its derivatives was moderate (407–672 $m^2\ g^{-1}$), these MOFs were able to adsorb CO_2 and CH_4 at elevated pressure (see Section 3.1). Using electrochemical methods, it was shown that the type of counter-ion does not considerably affect the semiconductor properties of the sample, while the crucial role is played by the charge of the framework.[39]

Zou *et al.*[40] used extended 1D chains based on Pb^{2+} cations as SBUs to modify the structure of obtained 3D MOFs by varying the nature of the metal within the porphyrin ligand. Five structurally different frameworks (Fig. 9) were obtained on the basis of free ligand **3** or its complexes with several metals (M-TCPP, where M = Co^{2+}, Ni^{2+}, Cu^{2+} and $V^{4+}O$) and Pb^{2+} salts.

The coordination of A_4 type carboxyphenylporphyrins to clusters based on trivalent metal cations (Al^{3+}, In^{3+} and Ga^{3+}) gives stable 3D framework. It is noteworthy that variation of synthetic conditions does not induce significant changes in their structure. The preparation of stable porous framework Al-PMOF by the reaction of $AlCl_3 \cdot 6H_2O$ with porphyrin **3** was reported.[41,42] The crystal structure of this MOF was determined by powder XRD. It was shown that Al-PMOF was a 3D framework consisting of 1D channels with elliptical pores of 6×11 Å size, which were connected by narrower channels to pores of 5 Å size. It is of interest that this MOF was stable in air up to 350 °C.

Rhauderwiek *et al.*[43] described the frameworks In-PMOF and Ga-PMOF, based on In^{3+} and Ga^{3+} cations and the TCPP ligand, isostructural to the aluminium-based MOF described above.[41] The variation of synthetic conditions did not result in significant structural changes; however, this allowed the authors to control the size and

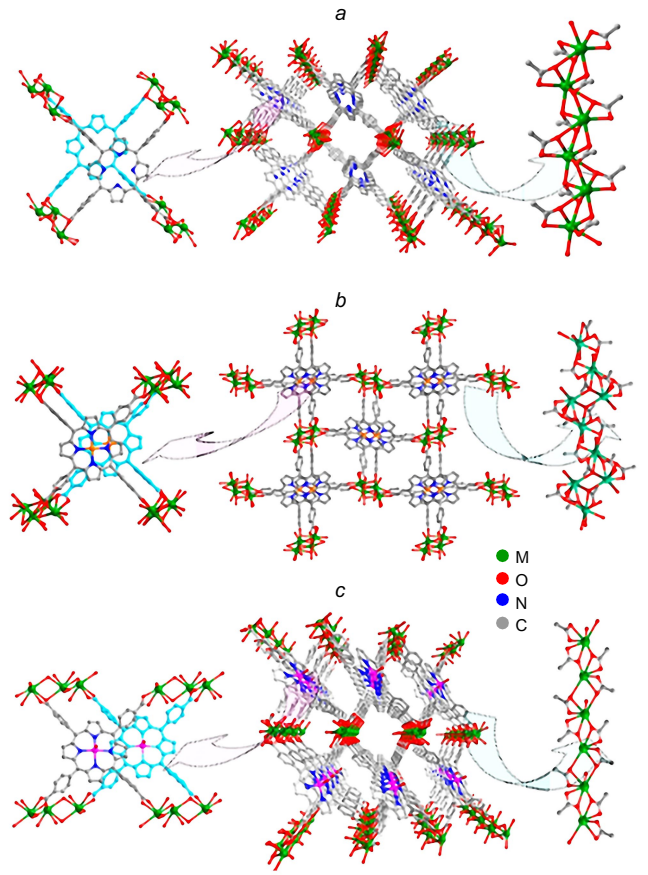


Figure 9. Crystal structures of MOFs formed upon interaction of Pb^{2+} with TCPP (*a*), M^{II}-TCPP (M = Co, Ni, Cu) (*b*) and VO-TCPP (*c*): on the left is a part of the structure containing a porphyrin ligand; on the right is the Pb^{2+}-carboxylate zigzag-like 1D chain; at the centre is a part of the open-channel porous 3D framework.[40] Published with permission from the Royal Society of Chemistry.

the surface area of crystallites (see Section 3.1). Another research group[44] also prepared a stable MOF based on In^{3+} (JLU-Liu7) similar to In-PMOF and characterized the product by single crystal XRD.

It was shown that the addition of alkali solutions to reaction mixtures considerably affects the structure of the resulting MOFs. For example, Fateeva *et al.*[45] described the synthesis of 3D frameworks MIL-141(A) based on Fe^{3+} cations and the Ni-TCPP complex in the presence of aqueous solutions of alkalis (AOH; A = Li^+, Na^+, K^+, Rb^+, Cs^+). In relation to a solution of caesium hydroxide, it was shown that the resulting MOF consisted of 3-fold interpenetrating anionic network with two types of channels (~4 and 6 Å in diameter), the charge of which was counter-balanced by alkali metal cations located inside the pores (Fig. 10).

Liu *et al.*[46] prepared a series of porphyrin MOFs, M-PMOF-3(Fe) based on TCPP complexes with various metals (M = $Fe^{3+}Cl$, Co^{2+}, Ni^{2+}, Cu^{2+}) and extended 1D chains containing Fe^{3+} ions. A specific feature of these MOFs is the use of a ternary mixture of modulators comprising benzoic and trifluoroacetic acids and water. The frameworks M-PMOF-3(Fe) possessed high chemical (in the pH range from 0 to 11) and thermal (up to 350 °C) stability.

An interesting example of formation of a series of multicomponent PCN-900(RE) frameworks (RE is a rare earth element) was reported by Zhang *et al.*[47] These structures were obtained in the presence of 2-fluorobenzoic acid by combining A_4 type porphyrin ligand **3**, a linear linker and the $(RE)_6(OH)_8(CO_2)_{12}$ cluster, where $(RE)^{3+}$ = Eu^{3+}, Y^{3+}, Yb^{3+}, Tb^{3+}, Dy^{3+} (Fig. 11). The post-synthetic metallation of PCN-900(Eu) based on free porphyrin ligand gave rise to the framework PCN-900(Eu)-MTCPP (M^{2+} = Zn^{2+}, Fe^{2+}, Co^{2+}, Ni^{2+}). The authors showed that a change in the molar ratio between the main building blocks — the linear 4,4′-dicarboxydiphenyl sulfone (DCDPS) linker and tetratopic TCPP ligand — directly affected the product composition. The composition of the phases was confirmed by powder XRD. When no DCDPS was added to the reaction mixture, the authors obtained poorly crystalline products. When this linker was used in a minor amount, the target PCN-900(Eu) phase was formed, but poorly crystallized products were present as impurities. The formation of pure PCN-900(Eu) phase was detected at a 25 : 1 molar ratio of DCDPS to TCPP.[47]

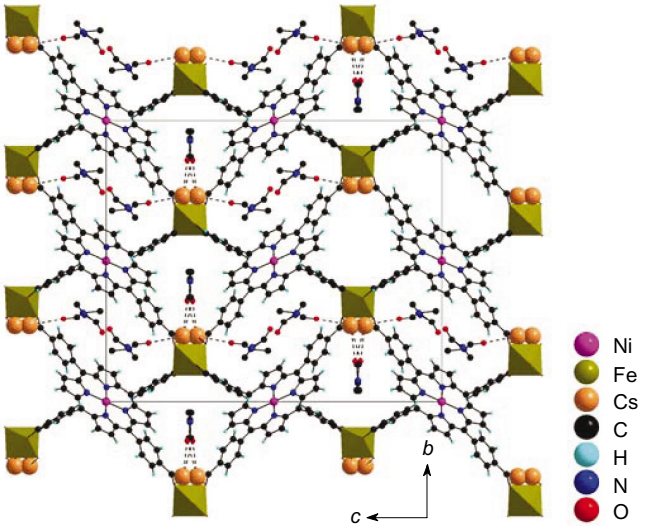


Figure 10. Crystal structure of MIL-141(Cs).[45] Published with permission from the American Chemical Society.

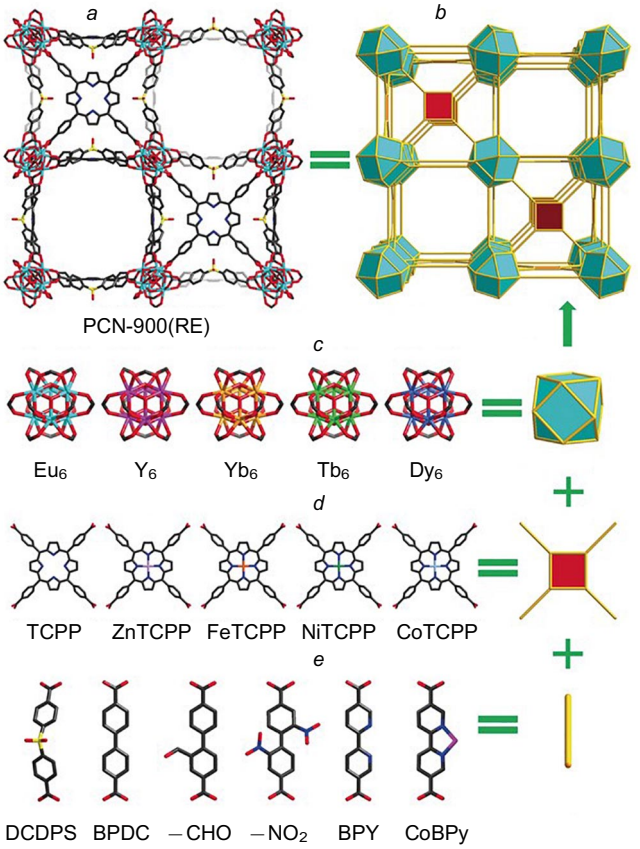


Figure 11. Crystal structure (*a*) and main topology (*b*) of the framework PCN-900(Eu) and structures (on the left) and schematic images (on the right) of cluster components: 12-connected clusters $(RE)_6$, where $(RE)^{3+}$ = Eu, Y, Yb, Tb and Dy (*c*); M-TCPP porphyrins, where M = H_2, Zn^{2+}, Fe^{2+}, Ni^{2+} and Co^{2+} (*d*); and linear linkers: 4,4′-dicarboxydiphenyl sulfone (DCDPS), biphenyl-4,4′-dicarboxylate (BPDC) derivatives with 2-aldehyde (–CHO) and 2,2′-dinitro groups ($-NO_2$), 2,2′-bipyridine-3,3′-dicarboxylate (BPY) and its cobalt complex (CoBPY) (*e*).[47] Published with permission from Wiley.

One more example of the synthesis of RE-based porphyrin MOF (YTMNs) was described by Wang *et al.*[48] The authors used yttrium (Y^{3+}) cations as metal centres in the framework nodes and porphyrin **3** as the organic ligand. It was shown that the YTMNs framework can be applied as a multifunctional fluorescent sensor for detecting F^- or OH^- ions with high sensitivity and selectivity.

Fu *et al.*[49] reported a highly selective and sensitive fluorescent sensor for Al^{3+}, Cr^{3+} and Fe^{3+} cations based on Tb-TCPP, which can also serve as an indicator for acidic and alkaline solutions for pH < 3 or > 9.

The increase in the oxidation state of the metal cation to four leads to the formation of more thermally and chemically stable MOFs due to the stronger $M^{4+}-O$ bonds. The most studied porphyrin-based MOFs containing tetravalent metal cations as the framework nodes are formed upon the reaction of porphyrin **3** with Zr^{4+} cations. It is noteworthy that by varying the reaction conditions (the ratio of the starting building blocks and the number or the type of the

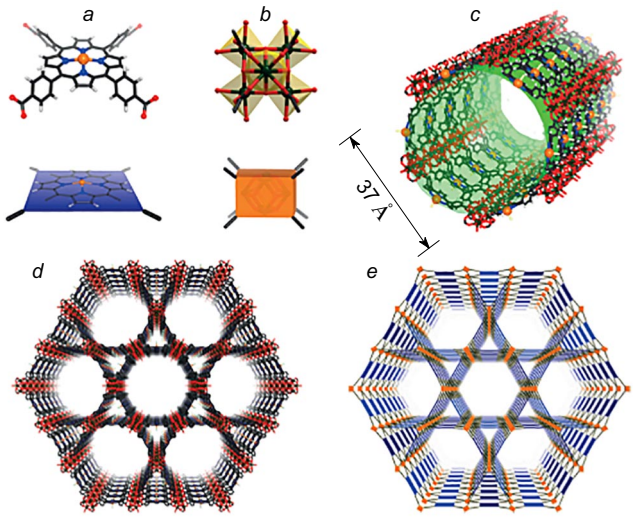


Figure 12. Crystal structure (above) and topological image (below) of Fe-TCPP (*a*) and 8-connected Zr_6 cluster (*b*), images of 1D channel structure (green cylinder) (*c*) and 3D PCN-222(Fe) framework with Kagome topology (*d*) and simplified view (*e*).[50] Published with permission from Wiley.

modulating reagents), it is possible to adjust the coordination sphere around the Zr_6 cluster‡ in the MOF; this is accompanied by a change in the structure topology to give new porphyrin MOFs with different properties. In a number of studies,[50–54] mesoporous framework PCN-222 [known also as MOF-545 (Ref. 55) and MMPF-6 (Ref. 56)] was prepared by the reaction of an eightfold excess of $ZrCl_4$ with TCPP in the presence of benzoic acid. PCN-222 represented a 3D framework composed of a network of one-dimensional hexagonal channels with a unique diameter of 37 Å and triangular pores of ~12 Å size (Fig. 12).

It was shown[57] that replacement of the metal source in SBU by hafnium oxychloride ($HfOCl_2 \cdot 8\,H_2O$) under the same reaction conditions did not induce structural changes: the MOF (Hf-2) thus formed with hafnium(IV) cations as the nodes was isostructural to PCN-222 polymers.

An increase in the amount of $ZrCl_4$ (a tenfold excess) and a decrease in the amount of modulating agent (benzoic acid) resulted in the synthesis[58] of a series of new porous MOFs, which were called PCN-224 and were based on the Zr_6 clusters and M-TCPP porphyrins (M = H_2, Ni^{2+}, Co^{2+} and Fe^{3+}). Unlike the 8-connected Zr_6 cluster in PCN-222, each Zr_6 unit in the framework PCN-224 is linked only to six TCPP ligands, which lowers the symmetry of the zirconium cluster. Owing to the decrease in the number of carboxylate linkers in this MOF, more free space appears, which finally promotes the formation of 3D channels up to 19 Å in diameter.

The reactions of porphyrin complexes of trivalent metals (Ir^{3+}, Rh^{3+}) and Ru^{2+} with $ZrCl_4$ or $HfCl_4$ under similar conditions gave a series of MOFs isostructural to PCN-224, which were called Ir-PMOF-1(Zr),[59] Ir-PMOF-1(Hf),[60] Ru-PMOF-1(Hf)[61] and Rh-PMOF-1(Zr).[62] The authors showed that the replacement of neither the cation within the porphyrin ligand nor the cation in the salt, with the other reaction conditions being invariable, induces significant structural changes of the framework.

A considerable decrease in the amount of $ZrCl_4$ (down to a 2.5-fold excess relative to the M-TCPP ligand, where M = H_2, Fe^{3+}) resulted in the formation of the framework PCN-223.[63] This MOF contained a Zr_6 cluster that was linked to twelve carboxyl groups of porphyrin molecules, which had not been observed previously in structures of this type. The structure PCN-223 was a system one-dimensional triangular channels with a diameter of 12 Å (Fig. 13).

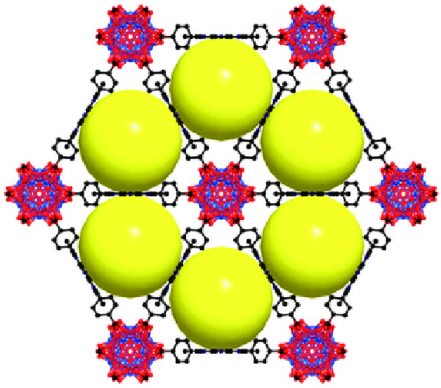


Figure 13. Crystal structure of PCN-223.[63] Published with permission from the American Chemical Society.

Thus, it was found that variation reaction conditions can be used to deliberately change the size and shape of pores in Zr^{IV}-MOFs based on porphyrin **3**. Moreover, structural transformation affects the chemical stability of the obtained MOFs, which defines their potential applications. For example, the framework PCN-222 is highly slable in acid media, whereas analogous PCN-224 is more stable in alkaline solutions, while the framework PCN-223 is stable over a broad pH range (0 to 10).

One more way to change the structure of MOFs is to introduce an additional organic ligand of a different nature. For example, Yuan *et al.*[64] obtained a multifunctional zirconium-containing MOF (PCN-134) based on porphyrin ligand **3** and 1,3,5-tris(4-carboxyphenyl)benzene (BTB).[64] The use of nickel(II) TCPP complex under similar conditions gave framework PCN-134(Ni) (Fig. 14). The Zr_6 clusters in this framework were linked to 1,3,5-tris(4-carboxyphenyl)benzene molecules to give 2D layers, which were, in turn, connected by porphyrin ligands, giving rise to a 3D layer pillar structure.

Yan *et al.*[65] showed that zirconium and hafnium are not the only tetravalent metals that can be used to build the MOF crystal lattice. Metal-organic frameworks based on titanium(IV) have attracted considerable attention owing to their numerous photocatalytic applications. The authors reported an original approach to fabrication of the framework PCN-22 based on porphyrin **3** and Ti^{4+} cations (Fig. 15). Instead of a titanium salt, the pre-synthesized $Ti_6O_6(OPr^i)_6(abz)_6$ cluster (abz is 4-aminobenzoate) was employed as the secondary building unit for the formation of this material. This not only slowed down crystallization, but also made it possible to avoid the formation of TiO_2 upon hydrolysis of the Ti^{4+} cation. The structure of PCN-22 is a 3D framework containing tetragonal channels

‡ The Zr_6 symbol designates hydroxo or oxo clusters of variable composition with six zirconium atoms.

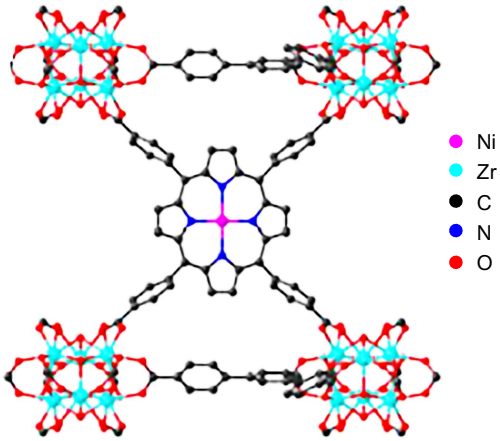


Figure 14. Structure of PCN-134(Ni) formed by the Zr_6 cluster, nickel(II) TCPP complex and 1,3,5-tris(4-carboxyphenyl)benzene molecules.[64] Published with permission from the American Chemical Society.

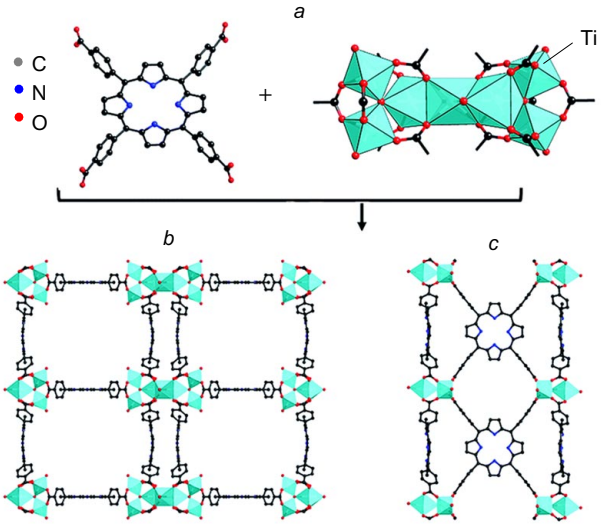


Figure 15. Scheme of formation of the PCN-22 crystal structure from TCPP (on the left) and from Ti_7O_6 clusters (on the right) (*a*) and views along the [100] (*b*) and [010] (*c*) directions.[65] Published with permission from the Royal Society of Chemistry.

with a diameter of 15 Å, which has relatively high thermal stability.

Keum *et al.*[66] described another example of Ti^{IV}-containing carboxylate MOF (DGIST-1), which consisted of pre-synthesized titanium(IV) oxo-cluster $Ti_6O_6(OPr^i)_6(t\text{-BA})_6$ (*t*-BA is *tert*-butyl acetate) and porphyrin ligand **3**. This MOF had high crystallinity, and after activation, a surface area of 1957.3 $m^2\ g^{-1}$, which is higher compared to known Ti^{IV}-MOFs (PCN-22) reported earlier.[65]

Hu *et al.*[67] described the first example of actinide porphyrin MOF based on uranium. The material U-IHEP-4 was synthesized by the reaction of Co-TCPP with uranyl nitrate $UO_2(NO_3)_2$. The framework U-IHEP-4 contained three types of cages of 16, 27 and 37 Å diameters, respectively (Fig. 16). Owing to the presence of a negative charge in the porous framework, this material can selectively adsorb positively charged dye molecules — methyl green and rhodamine B.

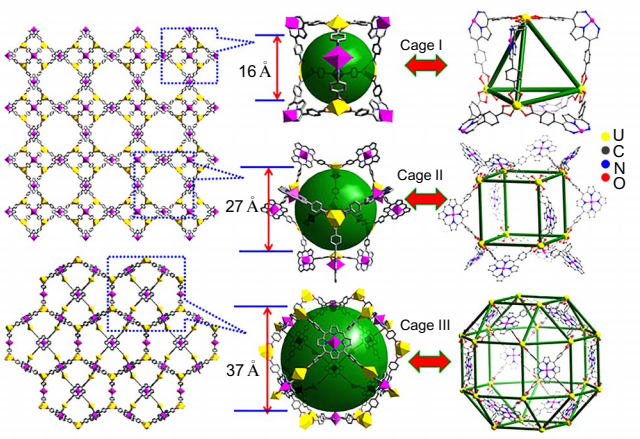


Figure 16. Three types of cages in the U-IHEP-4 framework.[67] Published with permission from Wiley.

Later, another actinide porphyrin-based MOF (named as NU-905) was obtained on the basis of Th^{IV} and free TCPP ligand.[68] This framework consisted of hexanuclear thorium secondary building units $[Th_6(\mu_3\text{-}O)_2(HCO_2)_4(H_2O)_6]$, which were additionally stabilized *via* binding to the carboxylate groups of porphyrin **3**. In order to determine the porosity, the solvent (water) in NU-905 was replaced by ethanol, and then the sample was activated by supercritical (sc) CO_2. The NU-905-scCO_2 structure activated in this way retained the crystallinity and showed thermal stability when heated up to 500 °C. The specific surface area calculated from the argon adsorption data was 800 $m^2\ g^{-1}$.

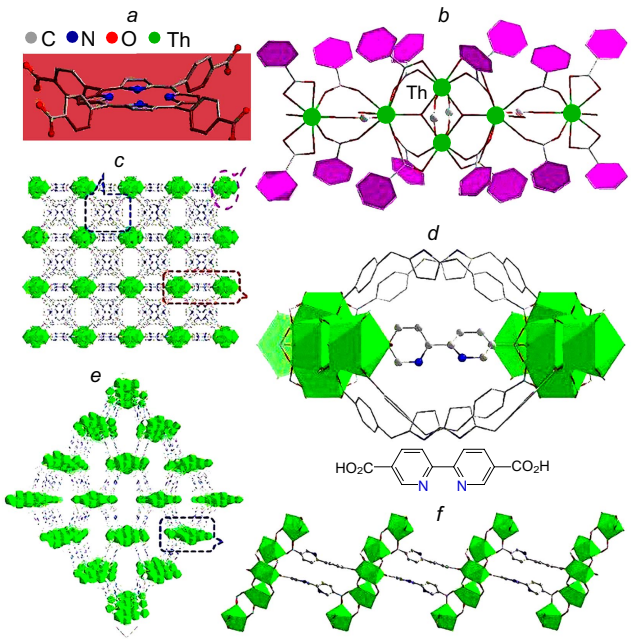
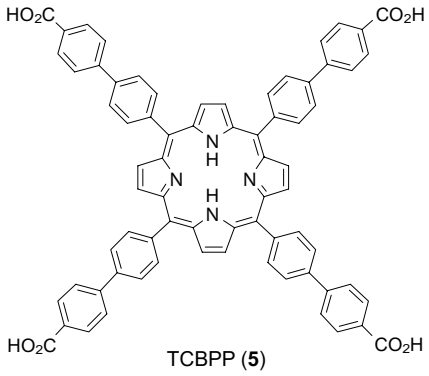


Figure 17. Schematic view of planar TCPP structure (*a*), hexanuclear thorium cluster (*b*), part of the framework Th-IHEP-5 (*c*), thorium(IV) clusters connected by porphyrin and H_2bpydc linker (*d*); Th-IHEP-5 3D structure (*e*) and 1D chain of Th_6 clusters connected by the H_2bpydc linker (*f*).[69] Published with permission from the Royal Society of Chemistry.

Huang *et al.*[69] described Th^{IV} porphyrin MOF (called Th-IHEP-5) on the basis of the TCPP ligand and 2,2′-bipyridine-5,5′-dicarboxylic acid (H_2bpydc) (Fig. 17). The Th-IHEP-5 framework has a more complex topology than NU-905 considered above. It was shown that the introduction of an additional photosensitizer molecule (H_2bpydc) endows this MOF with a pronounced photocatalytic activity in the oxidation of 2-chloroethyl ethyl sulfide and in the binding of carbon dioxide.

There are examples of porphyrin MOFs containing 4-carboxyphenyl groups separated from the tetrapyrrole macrocycle by an additional bridging moiety with considerably variable length. Lin *et al.*[70] used 5,10,15,20-tetrakis(4-carboxybiphenyl)porphyrin (TCBPP, **5**) ligand in which the phenyl groups bearing carboxy groups were separated from the porphyrin ring by an additional phenyl bridge.

Structure 5



TCBPP (**5**)

A series of isostructural Zr^{IV}-MOFs (designated as CPM-99) based on free ligand **5** and its zinc, cobalt and iron complexes (M-TCBPP, where M = H_2, Zn^{2+}, Co^{2+}, Fe^{2+}) was obtained (Figs 18, 19). These 3D frameworks contain large cubic cavities of 25 Å size and slightly distorted octahedral cavities ~11 Å in diameter.

In parallel, ultrastable FJI-H6 and FJI-H7 metal-organic frameworks based on TCBPP and Zr^{4+} or Hf^{4+} cation were synthesized.[71] These products were isostructural to CPM-99, although the authors did not mention this fact.

It should be emphasized that the use of organic ligands with long peripheral substituents often not only leads to increasing pore size and surface area of MOFs, but also

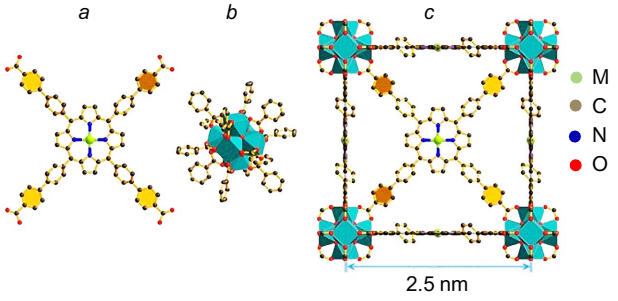


Figure 18. Molecular structures of M-TCBPP, where M = H_2, Zn, Co, Fe (*a*) and 12-connected Zr_6 cluster (*b*) and cubic cell of the CPM-99 framework (*c*).[70] Zr atoms are shown as turquoise-coloured cuboctahedra. Published with permission from the American Chemical Society.

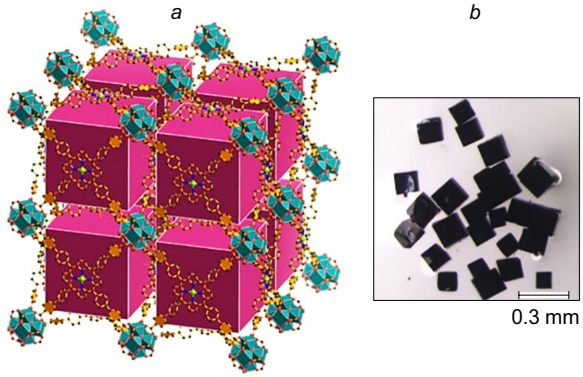
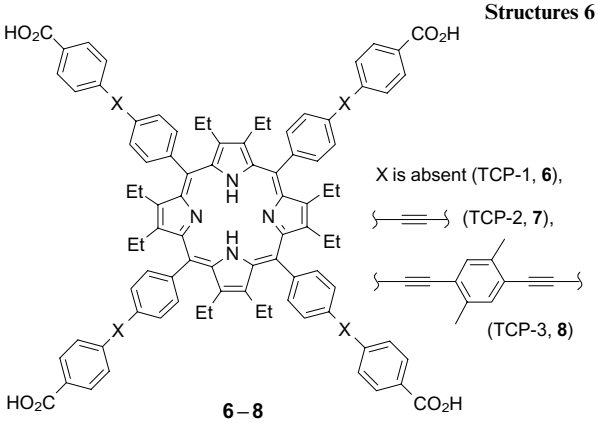


Figure 19. 3D network of Zr_6 clusters (shown as turquoise polyhedra) and cubic cavities (shown in deep red) in CPM-99 (*a*) and micrograph of this MOF (*b*).[70] Published with permission from the American Chemical Society.

induces the formation of interpenetrating networks or decreases the stability of the framework as a whole. However, in the case of FJI-H6, FJI-H7 and the series of isostructural metal-organic frameworks CPM-99, the authors demonstrated that no interpenetrating networks are formed and high stability of the materials is retained.

A reticular chemistry approach was used to obtain topologically similar (isoreticular) frameworks with increasing pore size.[72] The authors presented a detailed comparison of the physicochemical and sorption characteristics of porphyrin MOFs with different lengths of the bridging moieties at the periphery of the ligands: 5,10,15,20-tetrakis(4′-carboxybiphenyl-4-yl)octaethylporphyrin (TCP-1, **6**), 5,10,15,20-tetrakis[4-(4-carboxyphenylethynyl)phenyl]octaethylporphyrin (TCP-2, **7**), 5,10,15,20-tetrakis(4-{[4-(2,5-dimethyl-4-(4-carboxyphenylethynyl)phenyl]ethynyl}phenyl)octaethylporphyrin (TCP-3, **8**).

Structures 6–8



6–8

The reactions of porphyrins **6**–**8** with zirconium chloride give frameworks PCN-228, PCN-229 and PCN-230, respectively (Fig. 20). These structures are also isoreticular analogues of above-described CPM-99 and FJI-H6.

The synthesized MOFs are mesoporous, with the pore size varying from 25 to 38 Å. The framework PCN-230 has the maximum pore size among zirconium MOFs described to date. Meanwhile, PCN-229 has the highest porosity and surface area among the previously mentioned MOFs containing zirconium clusters as secondary building units (see

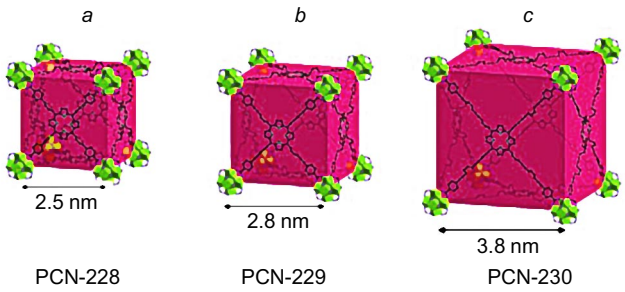


Figure 20. Crystal structure and dimensions of PCN-228 (*a*), PCN-229 (*b*) and PCN-230 (*c*). The figure was created by the authors using data of Ref. 72.

Table 1 in Section 3.1). These characteristics are comparable with the values obtained for FJI-H6, which was reported [71] at the same time. It is noteworthy that PCN-228, PCN-229 and PCN-230 possess outstanding chemical stability in aqueous solutions (at pH from 0 to 12).

A similar series of isoreticular mesoporous frameworks MOF-526, MOF-527 and MOF-528 with pore size from 19 to 37 Å were prepared [73] using copper complexes of 5,10,15,20-tetrakis(4-carboxybiphenyl)porphyrin, 5,10,15,20-tetrakis(4-carboxytriphenyl)porphyrin (TCTPP) and 5,10,15,20-tetrakis(4-carboxytetraphenyl)porphyrin (TCTTPP) as organic linkers, respectively. Elongation of the organic linker resulted in the pore size of MOF-526, MOF-527 and MOF-528 being 25.5, 31.4 and 37.6 Å, respectively, *i.e.*, the pore size gradually increased in arithmetic progression with a ~6 Å step, which corresponds to one phenyl moiety. It was shown that these frameworks possess a constant porosity with the Brunauer–Emmett–Teller surface area (BET) of 4260, 2000 and 3550 $m^2\ g^{-1}$, respectively.

The increase in the number of functional groups in the porphyrin ligand often gives MOFs with a new topology. Several sorts of A_4 type porphyrins containing eight carboxy groups that are used to prepare porous MOFs have been reported. Apart from TDCPP (**4**), this may be 5,10,15,20-tetrakis[3,5-bis(4-carboxyphenyl)phenyl]porphyrin (TBCPPP, **9**).

The reactions of TDCPP ligand with metal nitrates can furnish MOFs of various types. It should be noted that each carboxy group in these structures can act as both mono- and bidentate ligand, which determines the type of porphyrin binding to the metal or metal cluster as the framework nodes.

Compound **4** and cobalt(II) nitrate afford the framework MMPF-2,[74] in which one porphyrin molecule is linked to eight metal clusters *via* monodentate coordination of carboxyl groups, while the other porphyrin molecule is also bound to eight metal clusters, but in the bidentate manner. In the structure, it is possible to distinguish a small hydrophilic channel, with the terminal water molecules pointing into this channel. Each square hydrophilic channel is surrounded by four rows of 10.05×10.10 Å rectangular channels, which are formed by three cofacial porphyrin molecules. Smaller channels (6.2×7.8 Å) are located between the rectangular channels.

The framework MMPF-4 was obtained by the reaction of TDCPP with zinc(II) nitrate.[75] In this structure, all carboxy groups of porphyrin molecules act as bidentate ligands. This MOF is based on small cubicuboctahedral building blocks in which square faces are formed by the zinc(II) porphyrin complex formed *in situ*, while triangular faces are formed by $Zn_2(CO_2)_3$ clusters (Fig. 21, 22). This structure has cavities of two types: one type is formed by porphyrin molecules and metal clusters, while the other type is formed only by the clusters. These pores have diameters of 21.5 and 11.2 Å and differ in the size of reach-through windows (7.8×8.1 Å and 8.1×8.1 Å, respectively).

Cadmium(II) nitrate was used for the synthesis of MOF under the same conditions.[75] During the reaction, the authors observed the formation of the complex of porphyrin **4** with Cd^{2+} and the subsequent formation of

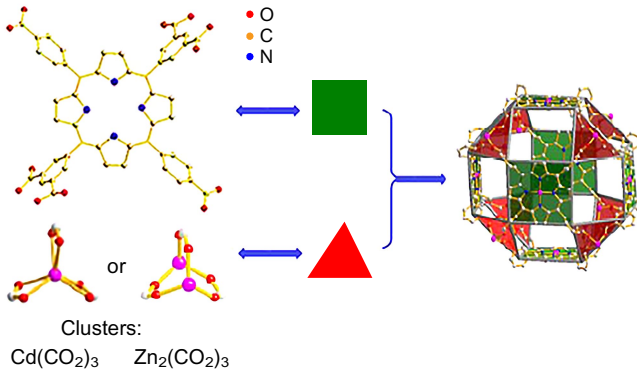
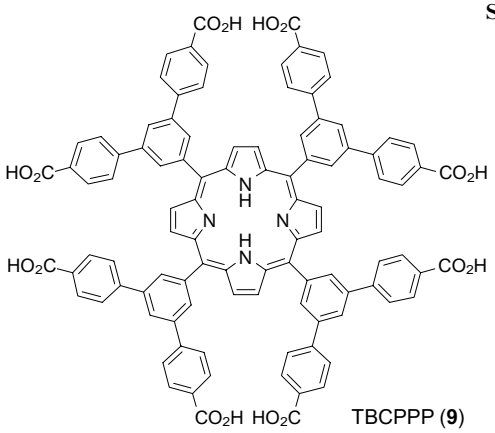


Figure 21. Fragment of the MMPF-4 (M = Zn) or MMPF-5 (M = Cd) structure.[75] Published with permission from the Royal Society of Chemistry.

Structure 9



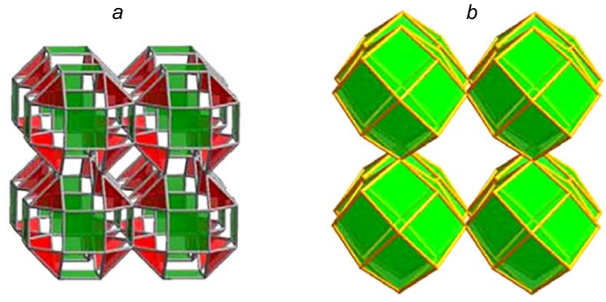


Figure 22. MMPF-4 or MMPF-5 (*a*) structure and its topological image (*b*).[75] Published with permission from the Royal Society of Chemistry.

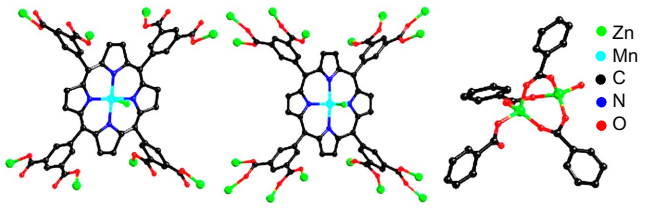


Figure 23. Three types of building units of the framework SZJ-4.[76] Published with permission from the American Chemical Society.

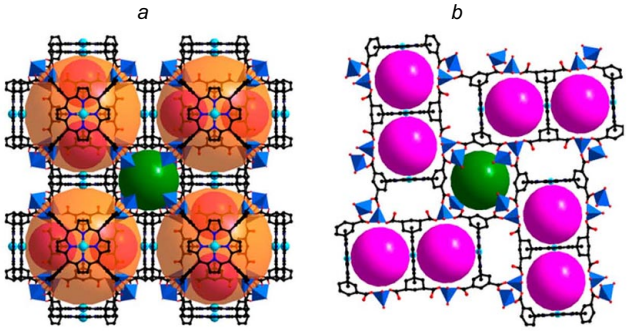


Figure 24. Structure of the SZJ-4 (*a*) MOF and its fragment (*b*) along the [001] direction.[76] The $Zn_2(CO_2)_4(H_2O)$ metal clusters are shown as blue tetrahedra; differently coloured spheres reflect the free space in cavities of different size. Published with permission from the American Chemical Society.

framework MMPF-5 of a similar structure, but containing $Cd(CO_2)_3$ clusters as the framework nodes (see Figs 21, 22).

The metal-organic framework SZJ-4 in which the porphyrin carboxyl groups act as either monodentate or bidentate ligands were obtained using the manganese(III) TDCPP complex and zinc(II) nitrate (Fig. 23).[76] As a result, $Zn_2(CO_2)_4(H_2O)$ metal clusters form the nodes, with participation of two types of porphyrin ligands and water molecules, which occupy free space in the coordination environment of zinc ions. This results in the formation of two types of cavities and open channels with diameters not exceeding 10 Å (Fig. 24). In the terms of its structure, the binding modes of building blocks and types of channels, this MOF resembles MMPF-2; however, they are not isostructural: the metal cluster of MMPF-2 includes three cobalt atoms, while SZJ-4 has two zinc atoms. Both types of clusters bind to four porphyrin molecules, *i.e.*, their connectedness is the same, and these structures can be considered to be topological analogues. The material SZJ-4 proved to be an efficient heterogeneous catalyst of olefin epoxidation.

The reaction of the same manganese(III) TDCPP complex with manganese(II) chloride gave the framework ZJU-18 formed by two types of metal clusters — $Mn_2(CO_2)_4$ and $Mn_3(CO_2)_4(\mu\text{-}H_2O)_2$.[77] This combination of structural components accounts for the presence of two types of cavities with diameters of 21.3 and 11.5 Å (Fig. 25), in which solvents are adsorbed and catalytic reactions involving the manganese porphyrin complex take place.

The reaction of nickel(II) TDCPP complex with copper(II) nitrate gave the ZJU-21 framework containing two types of pores 21 and 11 Å in diameter.[78] The use of

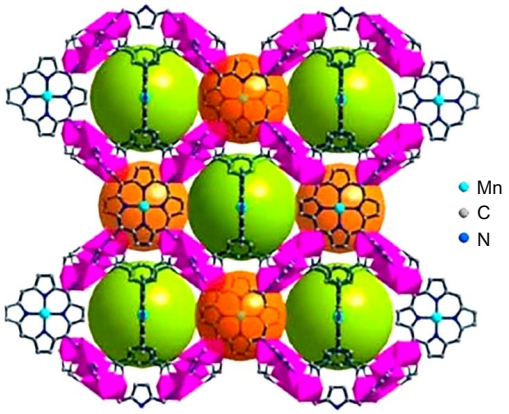


Figure 25. Structure of the ZJU-18 MOF.[77] The $Mn_2(CO_2)_4$ and $Mn_3(CO_2)_4(\mu\text{-}H_2O)_2$ clusters are shown as pink polyhedra; differently coloured spheres reflect the free space in cavities of different size. Published with permission from the American Chemical Society.

manganese(III) complex with the TDCPP ligand under the same conditions yielded porous ZJU-22 containing a system of 1D channels ~15 Å in diameter.

The synthesis of crystalline MOFs based on zinc(II) complex with porphyrin **4** and lanthanides proved to be possible only in the presence of either an alkali (NaOH) and/or or a strong acid (HNO_3) as modulators.[79] In the presence of NaOH, the reaction of Zn^{II}-TDCPP with some lanthanide nitrates $Ln(NO_3)_3$, where Ln = Sm, Eu, Gd, Pr, Tb, Dy, afforded isostructural MOFs, which were designated as LnMPF-1. The 1D chains formed by the metal clusters $\{NaLn(H_2O)(CO_2)_4\}_n$ were linked by porphyrin molecules, thus forming a polymer 3D framework pierced with zigzag-like 1D channels of 13.1×12.2 Å dimensions. An example of GdMPF-1 structure is shown in Fig. 26.

The use of a combination of modulators (HNO_3 and NaOH) in a definite order furnished also other 3D structures.[80] For example, the reaction of praseodymium(III) nitrate afforded the $\{PrNa_3(H_2O)_6(CO_2)_9\}^{3-}$ cluster, which was linked to porphyrin molecules to form a framework with hexagonal channels — PrMPF-2 (Fig. 27).

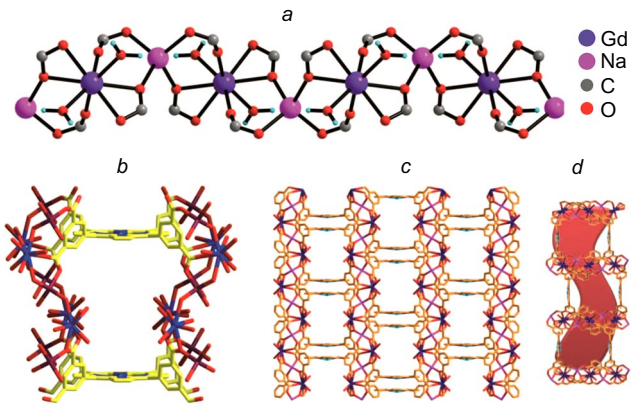


Figure 26. Structure of the $\{NaGd(H_2O)(CO_2)_4\}_n$ chain (*a*) and fragment of the GdMPF-1 framework, reflecting the type of binding of porphyrin molecules and metal clusters (*b*), and 3D structures of this MOF (*c*) and its zigzag-like 1D channels (*d*).[79] Published with permission from the Royal Society of Chemistry.

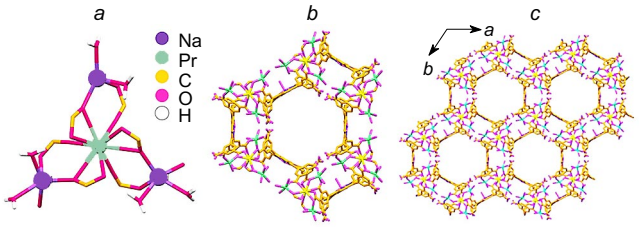


Figure 27. $\{PrNa_3(H_2O)_6(CO_2)_9\}^{3-}$ metal cluster (*a*), fragment of the structure (*b*) and 3D structure of the PrMPF-2 framework with hexagonal channels (*c*).[80] Published with permission from the American Chemical Society.

The same approach was also applied to other metal nitrates such as $In(NO_3)_3$, $Ga(NO_3)_3$, $Fe(NO_3)_3$ and $Mn(NO_3)_2$.[80] This gave various metal clusters and, correspondingly, frameworks (InMPF, GaMPF, FeMPF, MnMPF, respectively) with 1D channels variable in size and shape (Fig. 28).

Like in the case of TCPP, for porphyrin containing eight carboxyl groups, an additional linker can be introduced into the molecule, which results in increasing distance between the receptor groups and the macrocycle. This class of porphyrin ligands is exemplified by 5,10,15,20-tetrakis[4-(3,5-dicarboxy)biphenyl]porphyrin (TDCBPP, **10**) and 5,10,15,20-tetrakis[4-(3,5-dicarboxyphenoxy)phenyl]porphyrin (**11**), which served as the basis for the synthesis of few MOFs.

The use of sterically more bulky porphyrin ligands may give open-channel MOFs in which the channels are larger than those formed by porphyrin **4**. For instance, TDCBPP reacts with copper(II) nitrate to give the framework MMPF-9 formed by molecules of this porphyrin, copper(II)

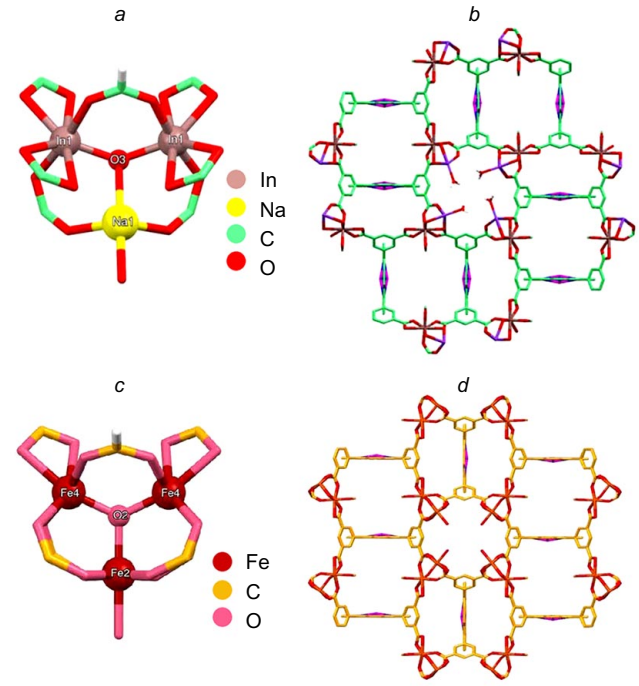
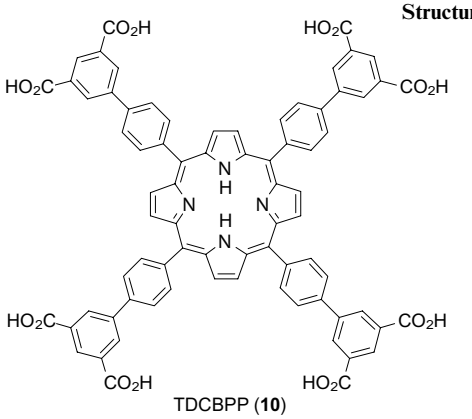
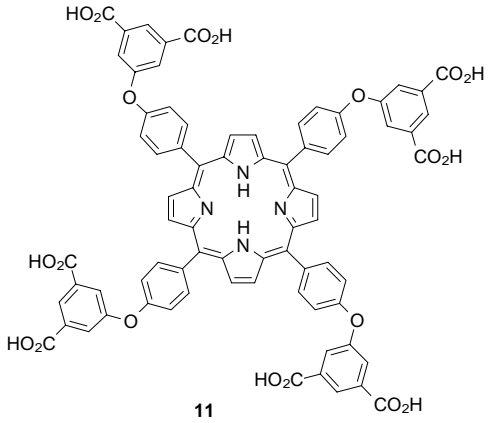


Figure 28. $In_2Na(CO_2)_7$ (*a*) and $Fe_3O(CO_2)_7$ (*c*) metal clusters and fragments of the frameworks InMPF-2 (*b*) and FeMPF-2 (*d*).[80] Published with permission from the American Chemical Society.

Structures 10, 11





ions and two sorts of $Cu_2(CO_2)_4$ metal clusters.[81] The framework MMPF-9 contains a system of 1D channels of two types, triangular ones with approximately 14 Å edge and hexagonal ones with 24.7 Å diagonal (Fig. 29).

meso-Tetrakis[4-(3,5-dicarboxyphenoxy)phenyl]porphyrin **11**, possessing a less rigid structure, was converted to a

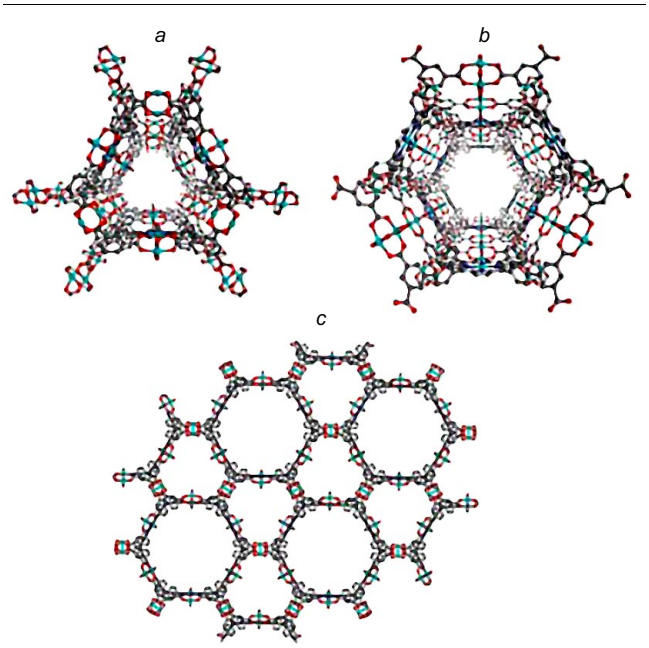


Figure 29. Structure of the triangular (*a*) and hexagonal (*b*) channels of the framework MMPF-9; channel view along the [001] direction (*c*).[81] Published with permission from the Royal Society of Chemistry.

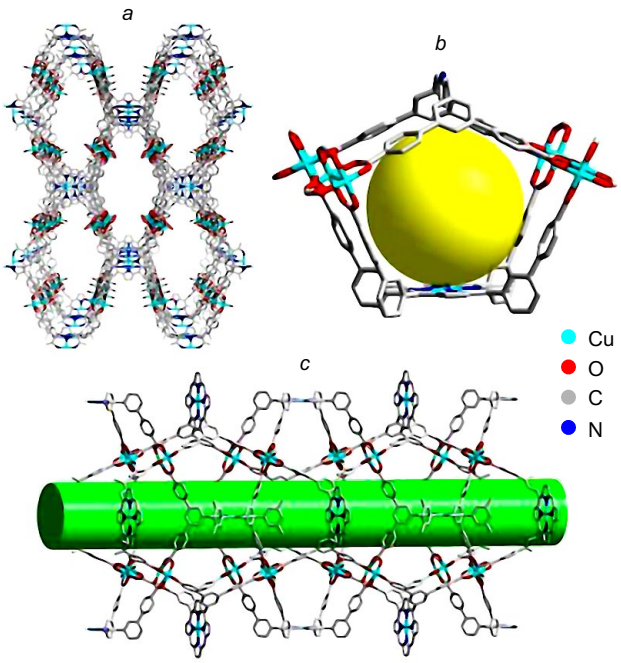


Figure 30. Hexagonal channels in MMPF-10: view along the *c* axis (*a*) and side view (*c*), and pentagonal cavity of this MOF (*b*).[84] Published with permission from the Royal Society of Chemistry.

MOF designated as 1·Mn.[82] This crystalline material has a system of open 1D channels of 16 × 7 Å size. Due to higher flexibility of substituents, the resulting structure has less free volume than MMPF-9.

Quite a few MOFs were prepared using 5,10,15,20-tetrakis{3,5-bis[(4-carboxy)phenyl]phenyl}porphyrin. Johnson *et al.*[83] allowed this ligand to react with zinc or cobalt nitrate and obtained UNLPF-1 and UNLPF-2 metal-organic frameworks, which formed isostructural networks. The reaction of this ligand with copper(II) nitrate afforded a new material, MMPF-10, which was topologically different from the above frameworks UNLPF-1 and UNLPF-2 due to difference in the torsion angles between the porphyrin ring and the *meso*-substituents formed through the binding of the carboxyl groups of the phenyl moieties to metal cations (Fig. 30).[84]

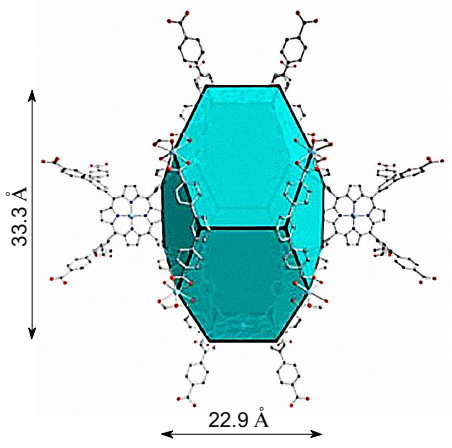


Figure 31. Structure of the framework UNLPF-10.[85] Turquoise colour designates the internal cage; its exact dimensions are indicated. Published with permission from the American Chemical Society.

The reaction of porphyrin **9** with indium(III) nitrate resulted in the synthesis of new MOF UNLPF-10 (Fig. 31).[85] This material had a high porosity, with the inner size of the internal cage being 33 × 23 × 23 Å and the sizes of the hexagonal and pentagonal windows being 19 × 16 and 17 × 13 Å, respectively. The indium cations are involved not only in the formation of the secondary building unit, but also in the metallation of the porphyrin ligand. The degree of metallation varies depending on the ratio of the starting reactants, which allows one to control the charge density of the framework.

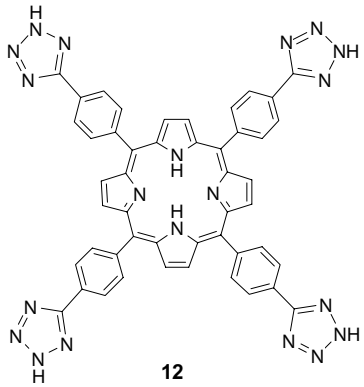
2.1.2. Metal-organic frameworks based on other A_4 type porphyrins

There are few reported examples of the synthesis of MOFs based on porphyrins with functional groups other than carboxyl groups.

Guo *et al.*[86] synthesized metal-organic framework UTSA-57 by the reaction of the manganese(III) chloride complex with 5,10,15,20-tetrakis[4-(2,3,4,5-tetrazol-1-yl)-phenyl]porphyrin ligand (TTZPP, **12**) and $MnCl_2 \cdot 4H_2O$. It was shown that the obtained framework has ellipsoid cavities of 11.9 Å size and large open 1D channels with a diameter of 20.3 Å (Fig. 32).

The first example of using 5,10,15,20-tetrakis(4-sulfonatophenyl)porphyrin (TPPS, **13**) as the organic ligand for the formation of MOF $[HSm\{VO(TPPS)\}]_n$ was reported[87] in 2011. The molecules of vanadyl complex with ligand **13** bind to one another *via* coordination of sulfonate oxygen atoms to samarium cations to give 2D layers. The intermo-

Structure 12



12

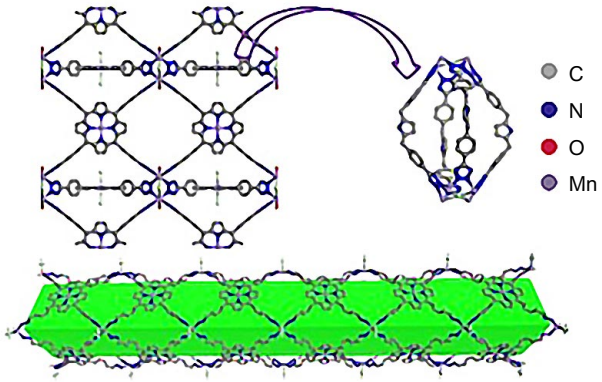
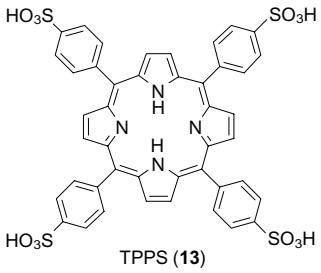


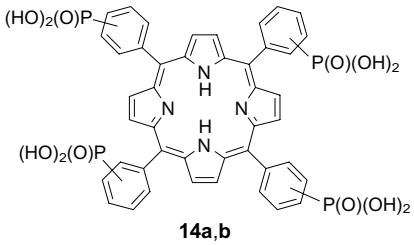
Figure 32. Crystal structure of the framework UTSA-57.[86] Published with permission from the American Chemical Society.

Structure 13



TPPS (**13**)

Structures 14



14a,**b**

Isomers: *para* (H_8TPPP, **a**), *meta* (H_8mTPPP, **b**)

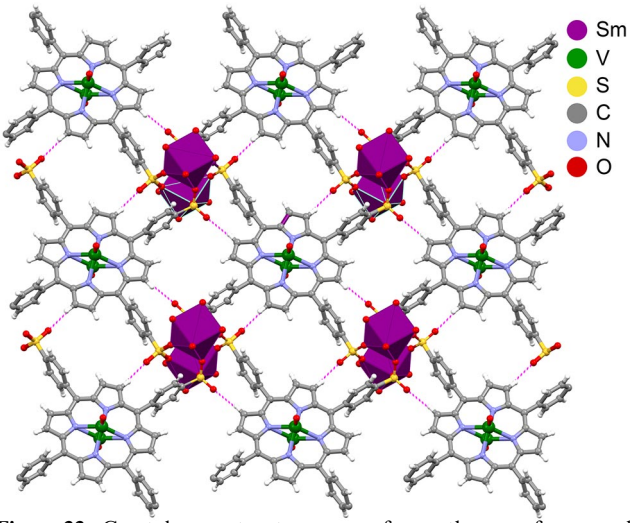


Figure 33. Crystal structure of the framework $[HSm\{VO(TPPS)\}]_n$.[87] The figure was created by the authors using the Cambridge Crystallographic Data Centre (Refcode RALZAH).

lecular interactions arising in the structure stabilize the framework and give 1D channels with a window of 5.5 × 3.0 Å (Fig. 33).

Subsequently, Chen's research group[87–95] published a series of studies describing MOFs based on 5,10,15,20-tetrakis(4-sulfonatophenyl)porphyrin (**13**); in the secondary building units, the authors always used Ln^{3+} cations (Ln = La, Sm, Eu, Dy, Tb, Er). This porphyrin was used to assemble MOFs both in the free state[89] and as complexes with zinc(II),[90–92] cobalt(II)[93–95] and vanadyl.[87,88] These MOFs showed relatively high thermal stability (up to 400 °C).

Another research group[96] prepared and characterized MOFs based on porphyrin **13** and europium(III) cations. According to X-ray diffraction data, the activation of the porous framework is accompanied by restructuring of the secondary building unit, which has a substantial effect on the photophysical properties of the material, in particular on the generation of singlet oxygen.

The introduction of a phosphonate group into periphery of the porphyrin ligand, which ensures enhanced thermal and chemical stability of the tetrapyrrole macrocycle, gives rise to a broad diversity of structures owing to the ability of three oxygen atoms of this group to form both strong coordination bonds with various metals and numerous additional intermolecular hydrogen bonds. However, published data on the synthesis and studies of MOFs based on phosphonate-substituted porphyrins are limited.

The synthesis of MOFs based on 4-phosphonatophenyl-substituted porphyrin H_8TPPP (**14a**)[§] was reported for the first time in 2018.[97]

The hydrothermal synthesis involving the reaction of nickel 5,10,15,20-tetrakis(4-phosphonatophenyl)porphyrin (Ni-H_8TPPP) with $MCl_2 \cdot 6H_2O$ ($M = Mn^{II}$, Co^{II}, Ni^{II}, Cd^{II}) yielded isostructural MOFs $[M(Ni\text{-}H_6TPPP)(H_2O)]$, which were called M-CAU-29 (Fig. 34). In relation to Ni-CAU-29, it was shown that this framework has two types of one-dimensional pores of 2.8 × 5.0 Å and 3.8 × 3.8 Å sizes (Fig. 35).

A similar reaction with application of $ZrOCl_2 \cdot 8H_2O$ or $HfCl_4$ in the presence of NaF and a 2 M solution of NaOH resulted in the formation of the frameworks Zr-CAU-30 or Hf-CAU-30, respectively.[98] The structure of these MOFs

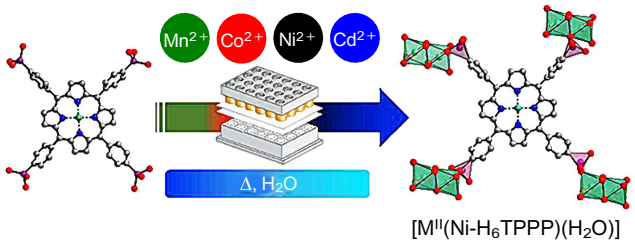


Figure 34. Scheme of the synthesis of the framework M-CAU-29.[97] Published with permission from the Royal Society of Chemistry.

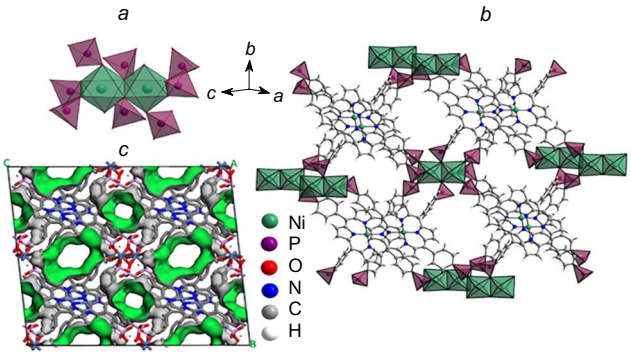


Figure 35. Inorganic unit consisting of NiO_6 polyhedra (*a*), fragment of the crystal structure of the framework Ni-CAU-29 (*b*), and Connolly pore surface (approximate radius of ~1.8 Å, view along the [101] direction) for this MOF (*c*).[97] Published with permission from the Royal Society of Chemistry.

§ The number of protons present in the designations of phosphonate-substituted porphyrins corresponds to the number of outer protons on phosphonate groups. This is important because the ligands in some frameworks are deprotonated to different extents.

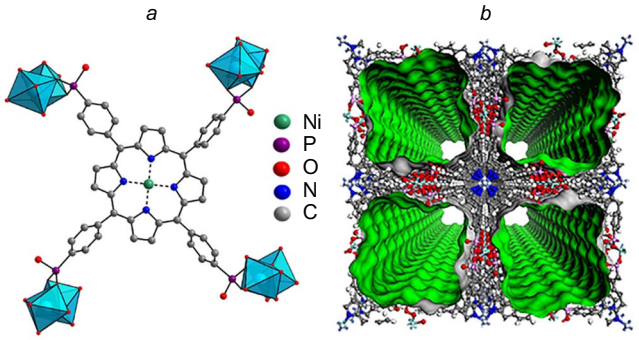


Figure 36. Coordination environment of the porphyrin molecule in the Zr-CAU-30 structure in which each nickel porphyrin molecule coordinates eight Zr^{4+} cations (*a*), and Connoly pore surface for this MOF along the [001] direction (*b*).[98] Published with permission from the Royal Society of Chemistry.

was determined by electron diffraction tomography (Fig. 36). Zr-CAU-30 was shown to be a 3D framework with 1D channels with pore width of 13 Å along the edge and 20 Å diameter along the diagonal. The channels are formed *via* binding of the porphyrin phosphonate groups to ZrO_6 or ZrO_4F_2 inorganic building units.

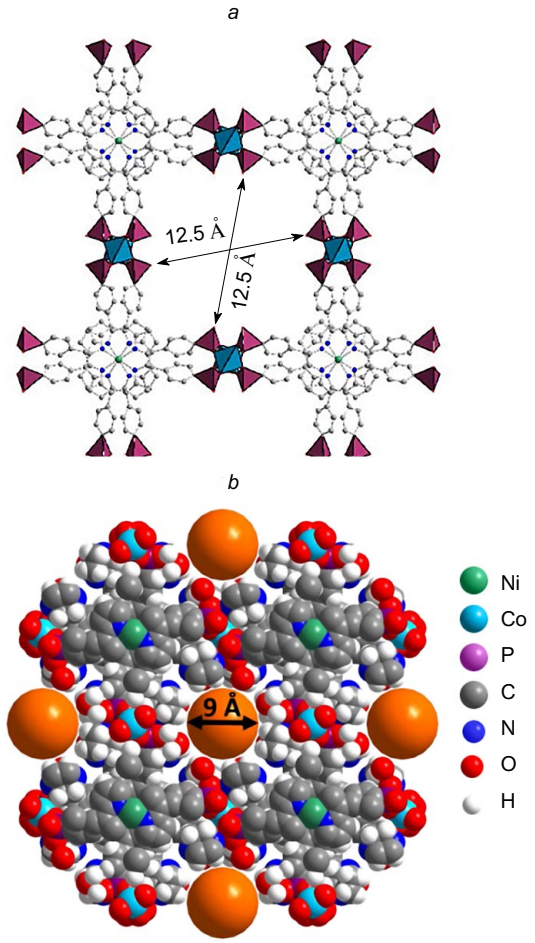


Figure 37. Free diameter of 1D channels in the framework Co-CAU-36 in the absence (*a*) and in the presence of DABCO and H_2O molecules; and view along the [001] direction (*b*).[99] Published with permission from Wiley.

Subsequently, the same authors[99] established that the presence of 1,4-diazabicyclo[2.2.2]octane (DABCO) and HCl in the reaction mixture is necessary to prepare the framework Co-CAU-36 based on this ligand, which contains cobalt cations in the nodes. In this MOF, the cobalt cation is coordinated by four oxygen atoms of four different phosphonate groups to give a 3D structure that contains one-dimensional channels along the [001] direction with a diameter of 9 Å (Fig. 37).

Pereira *et al.*[100] also applied the hydrothermal method to prepare MOFs $[(M\text{-}H_9TPPP)(H_2O)_x]Cl_2 \cdot y\,H_2O$ (where $x+y=7$; $M^{3+} = La^{3+}$, Yb^{3+}, Y^{3+}; H_9TPPP is porphyrin **14a** protonated at the centre of the macrocycle) by the reaction of free 5,10,15,20-tetrakis(4-phosphonatophenyl)-porphyrin (**14a**) with the corresponding lanthanide chlorides in the presence of HCl as the modulator. This material was studied by various physicochemical methods; however, no data on the structure of the resulting framework were presented.

The solvothermal reaction of free porphyrin **14a** with copper nitrate conducted under milder conditions afforded crystals of the metal-organic framework GTUB-1.[101] A specific feature of the crystal structure of this MOF is an unusual inorganic unit, which is a 1D polymer formed by rhombohedral Na–O chains connected by Na–O–Na and O–P–O bridges (Fig. 38). The formation of this inorganic building unit and the planarity of the organic ligand give rise to a 3D structure with 9.78×7.73 Å rectangular channels along the *a* axis in the framework GTUB-1.

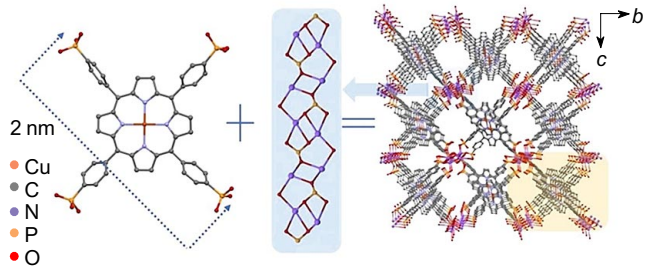


Figure 38. Crystal structure of the porphyrin ligand in the framework GTUB-1: porphyrin ligand (on the left), 1D Na–O–P chains of the inorganic building unit (at the centre) and MOF rectangular channels along the *a* axis (on the right).[101] Published with permission from Wiley.

We developed an approach to the preparation of MOFs based on phosphonate-substituted porphyrins that implies the use of phenylphosphonic (or phosphonic) acid as a modulator in the solvothermal reaction of phosphonatophenyl-substituted porphyrins with metal salts. For example, the reaction of Ni^{II} complex of porphyrin **14a** with zinc nitrate in the presence of excess phenylphosphonic acid in a DMF–water mixture under mild conditions afforded the 3D structure of the framework IPCE-1Ni — $[Zn_3(Ni\text{-}H_3TPPP)_3 \cdot 9\,Me_2NH_2 \cdot 3\,DMF \cdot 17\,H_2O]$.[102] It was shown that each molecule of nickel(II) complex with ligand **14a** is partially deprotonated, and all four phosphonate groups have different coordination environments (Fig. 39).

A unique feature of this MOF is that channels with a diameter of 8.36 Å accommodate dimethylammonium cations, resulting from DMF decomposition during the solvothermal synthesis, which counterbalance the negative charge of the framework. The IPCE-1Ni framework is the

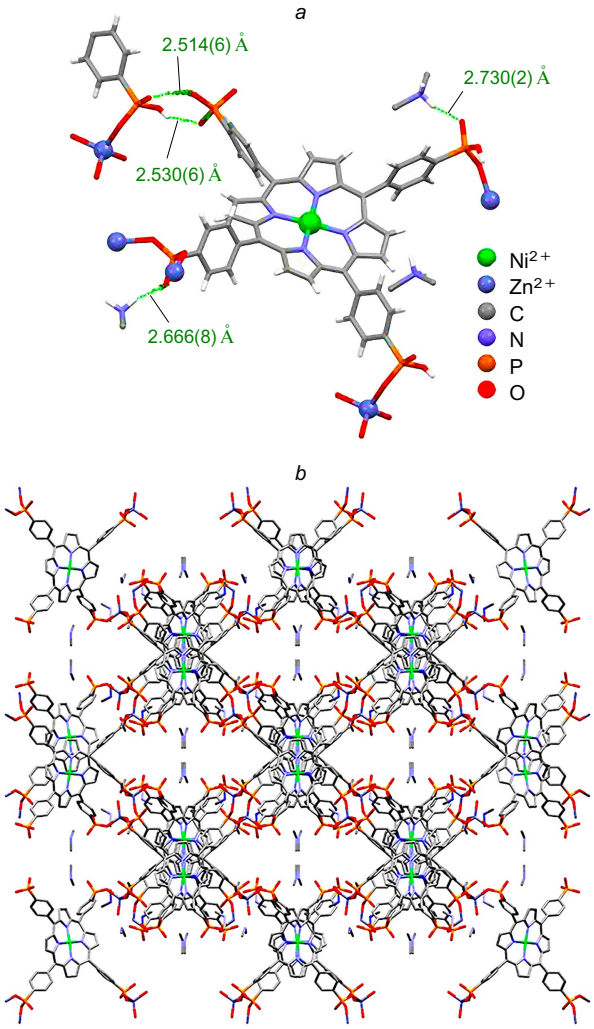


Figure 39. Coordination environment of the Ni-H_3TPPP molecule in the IPCE-1Ni framework (*a*) and fragment of this MOF (*b*).[102] Published with permission from Wiley.

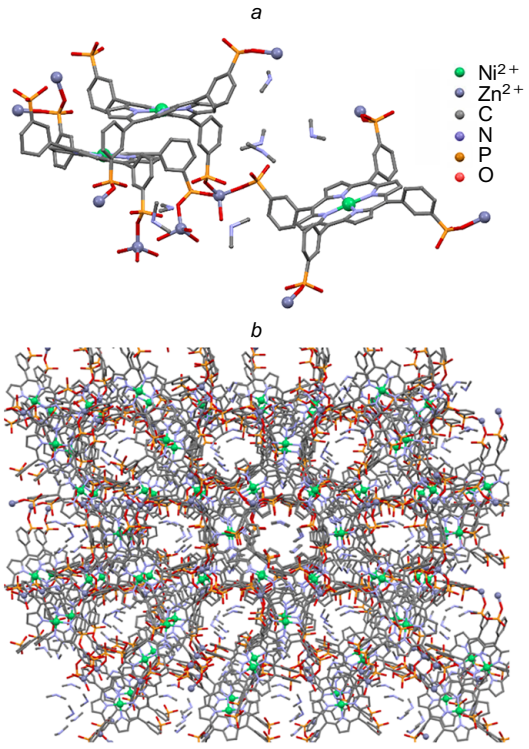


Figure 40. Coordination environment of the nickel(II) porphyrin molecule in the framework **IPCE-2Ni** (*a*) and fragment of this MOF (*b*).[103] Published with permission from Wiley.

first example of MOF with a discrete secondary building units based on zinc phosphonates.

The change of the position of the phosphonate functional groups from *para* to *meta* in the phenyl rings of porphyrin (compound **14b**) resulted in the formation of an unusual complicated 3D structure of IPCE-2Ni — $[Zn_3(Ni\text{-}H_2m\text{TPPP})(Ni\text{-}H_4m\text{TPPP})(Ni\text{-}H_5m\text{TPPP})\cdot 7\,Me_2NH_2\cdot \cdot DMF\cdot 7\,H_2O]$, where Ni-$H_x$mTPPP ($x$ = 2, 4, 5) are partially deprotonated nickel(II) 5,10,15,20-tetrakis(3-phosphonatophenyl)porphyrin (Fig. 40).[103]

The topology and, hence, the properties of the phosphonate-substituted porphyrin MOFs are also considerably affected by the nature of metal in the macrocycle. Indeed, the replacement of nickel(II) in the porphyrin ligand by palladium(II) in the solvothermal reaction described above gave IPCE-2Pd crystals $[Zn_2(Pd\text{-}H_2m\text{TPPP})\cdot 2\,Me_2NH_2\cdot 2\,H_2O]$.[104] The structure of this framework was determined by powder X-ray diffraction (Fig. 41).

The rigid planarity of palladium(II) porphyrin leads to the formation of a layered framework. A structural feature of this material is the inorganic building unit, which represents honeycomb-like 2D layers formed *via* coordination of the porphyrin phosphonate groups to zinc cations

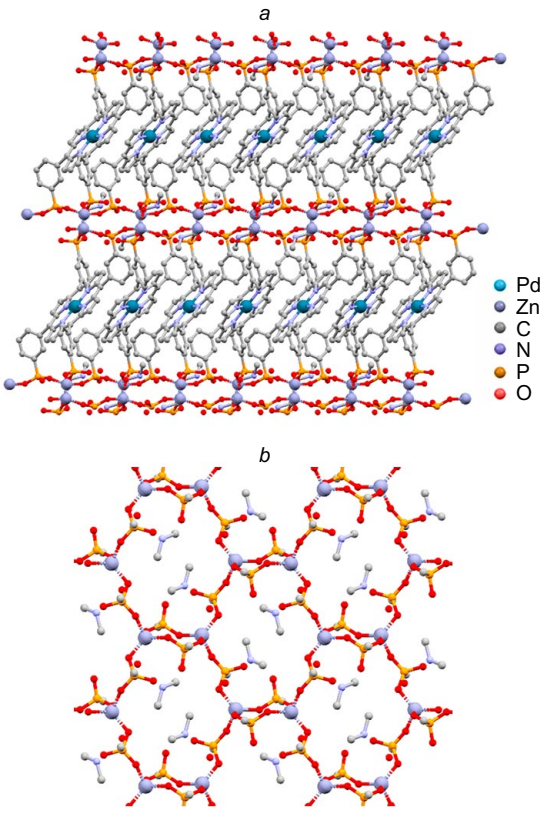


Figure 41. Crystal structure of IPCE-2Pd: image of this MOF along the *b* direction (*a*) and image of the secondary building unit containing dimethylammonium cations and water molecules along the *a* axis (*b*).[104] Published with permission from the Royal Society of Chemistry.

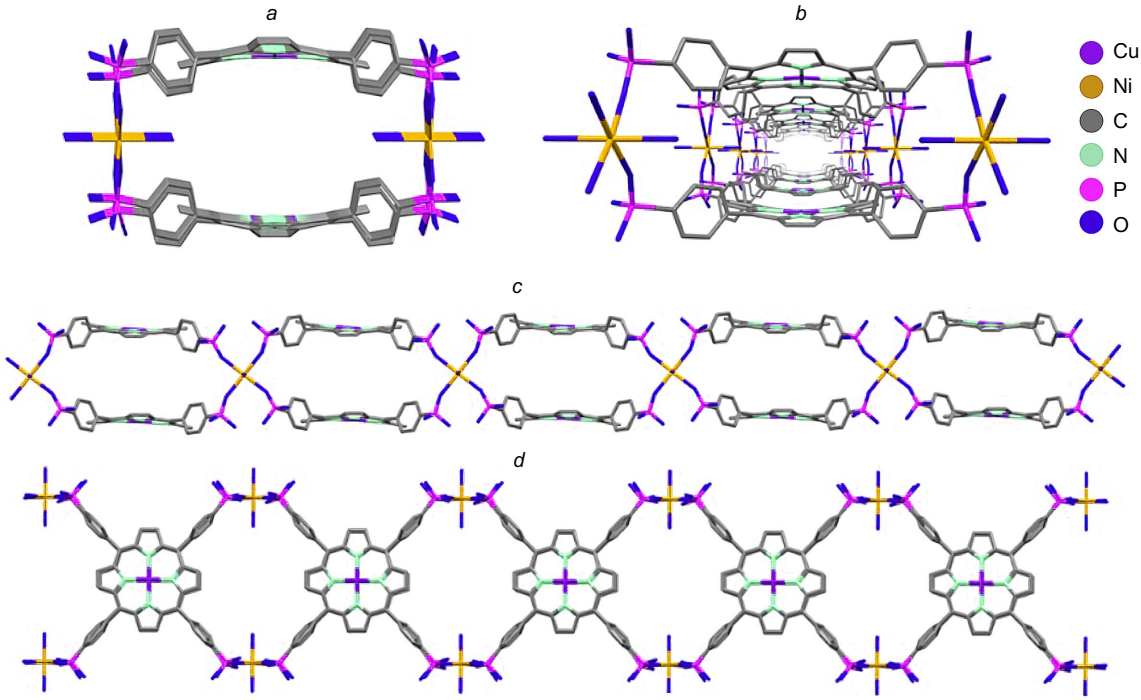


Figure 42. Structure of the rectangular channel (*a*) and its perspective view (*b*) for the framework GTUB-4, top view of the tubular structure and hexagonal lattice (*c*) and side view of the Cu-H_4TPPP^{4-} building unit with open square channels (*d*) for this MOF. The figure was created by the authors using data of Ref. 105.

(see Fig. 41). The honeycomb cavities incorporate dimethylammonium cations and water molecules that are linked to one another and to the framework by numerous hydrogen bonds. Owing to proximate positions of the porphyrin **14b** molecules, additional weak interactions occur between the hydrogen atoms of the phenyl substituents and the π-system of the neighbouring porphyrin molecule, which enhances the stability of this framework. The series of MOFs designated as IPCE possess promising proton-conducting properties (see Section 3.6).

Using a similar synthetic approach, Ayhan *et al.*[105] obtained the framework GTUB-4 by the reaction of copper(II) 5,10,15,20-tetrakis(4-phosphonatophenyl)porphyrin with nickel acetate in the presence of benzoic acid. The coordination of the phosphonate groups of porphyrin **14a** to nickel cations gave rise to a 1D tubular MOF with open channels (Fig. 42), which accommodate the dimethylammonium cations counterbalancing the framework charge. The apical positions of the octahedral nickel(II) cation in the GTUB-4 building units are occupied by two water molecules, which hold together the resulting 1D tubes *via* hydrogen bonds.

2.1.3. Metal-organic frameworks based on A_2 and A_2B_2 type carboxy-substituted porphyrins

Several examples of A_2 and A_2B_2 type porphyrins used to obtain MOFs have been reported. It is noteworthy that the range of such MOFs is rather narrow, since the approach used for the synthesis of porphyrins of this class is much more complicated.

For example, Gao *et al.*[20] prepared the framework MMPF-18 formed by 5,15-bis(4-carboxyphenyl)porphyrin (DBP, **15**) and the tetranuclear zinc cluster $[Zn_4(\mu_4\text{-}O)(CO_2)_6]$ (Fig. 43). The strong π–π stacking between the molecules of porphyrin **15** promotes the formation of 4-fold interpenetrating network. This structural feature leads to decreasing pore size, which may induce selective sorption of gases, in particular methane, and increases the framework stability.

A basically different MOF containing no interpenetrating lattice fragments was prepared on the basis of DBP. The reaction of ligand **15** with hafnium(IV) cation promotes the formation of the framework DBP-UiO.[43] This material had a porous framework structure with triangular channels of 16 Å size and octahedral and tetrahedral cavities of 28 and 20 Å size, respectively.

There are examples of MOFs formed with A_2 type porphyrins containing 3,5-dicarboxyphenyl groups (Fig. 44). Thus, the reaction of 5,15-bis(3,5-dicarboxyphenyl)porphyrin (**16**) with copper(II) nitrate gave the framework MMPF-1.[106] The structure of this MOF represented a 3D framework of identical polyhedral pores of 18.6×16.2 Å size with 3.4×3.5 Å windows; each pore being formed by eight porphyrin macrocycles and eight copper(II) clusters (see Fig. 44).

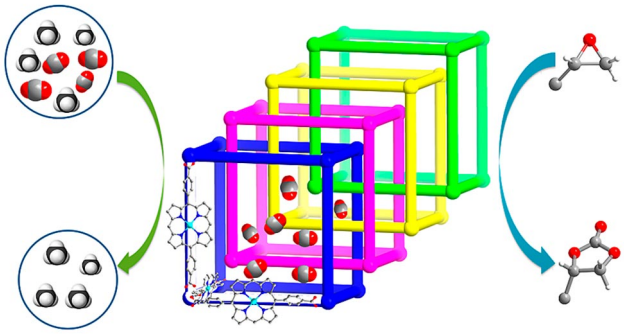


Figure 43. Structure of the framework MMPF-18. Different colours illustrate independent interpenetrating MOF fragments. The figure was created by the authors using data of Ref. 20.

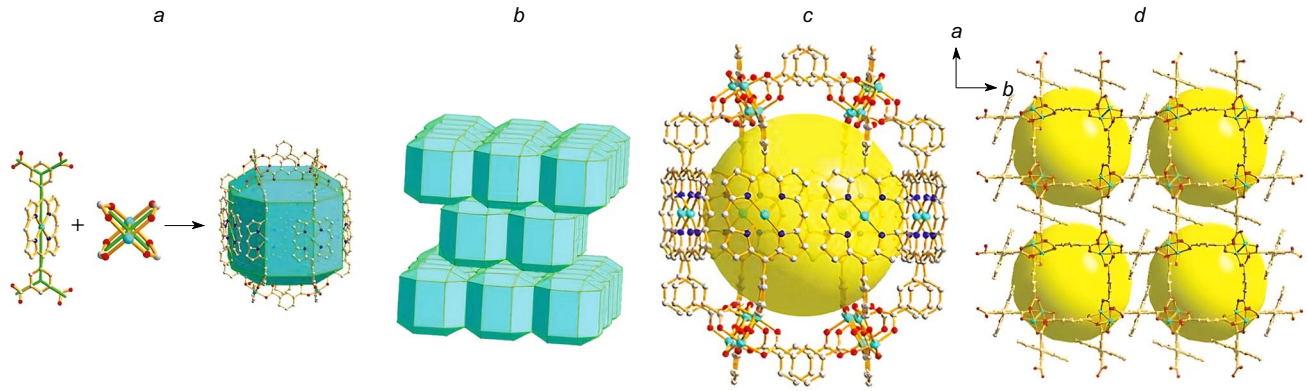
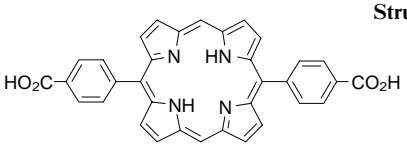
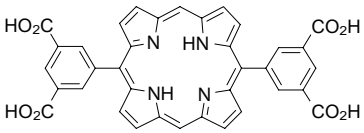


Figure 44. Schematic view of the formation of 3D porous MMPF-1 structure from ligand **16** and Cu metal cluster (*a*), packing of the layers into the framework (*b*), and images of a single cavity of this MOF (*c*) and in the *ab* plane (*d*).[106] Yellow spheres show free space of the pores; hydrogen atoms are omitted for clarity. Published with permission from the American Chemical Society.

Structures 15, 16



DBP (**15**)



16

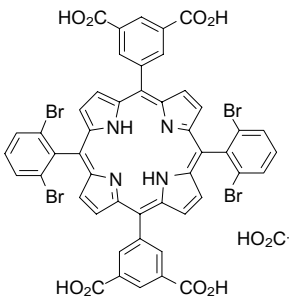
The replacement of 5,15-bis(3,5-dicarboxyphenyl)porphyrin (**16**) by an A_2B_2 type porphyrin, 5,15-bis(2,6-dibromophenyl)-10,20-bis(3,5-dicarboxyphenyl)porphyrin (DCDBP, **17**), gives the MMPF-3 structure composed of a network of pores that differ in shape in size.[107] This MOF contains cubohemioctahedral, truncated tetrahedral and truncated octahedral pores (Fig. 45).

The reaction of zinc(II) complex of hexadentate 5,15-bis(4-carboxyphenyl)-10,20-bis(3,5-dicarboxyphenyl)-porphyrin (H_6HCPP, **18**)¶ with various metal nitrates, including lanthanide nitrates — $Mn(NO_3)_2$, $Co(NO_3)_2$, $Zn(NO_3)_2$, $In(NO_3)_3$, $Pb(NO_3)_2$, $Gd(NO_3)_2$, $Pr(NO_3)_2$, $Yb(NO_3)_2$ — resulted in a series of materials M-hcMPF containing 53–64% free space in the crystal lattice (Fig. 46).[108]

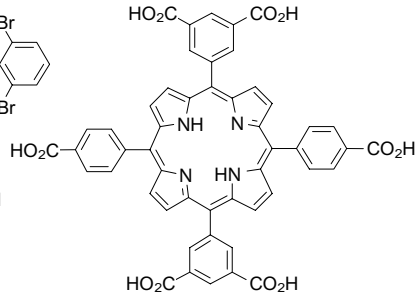
The use of cobalt(II) salt also affords MOF in which both porphyrin **18** and the metal cluster act as 6-connected nodes; however, cobalt cations form trinuclear clusters (Fig. 47).

Among MOFs containing p-elements in the binding units, there are frameworks In-*hc*MPF and Pb-*hc*MPF with indium(III) and lead(II) cations, respectively.[108] Previously unknown frameworks Ln-*hc*MPF containing lanthanides (Pr^{III}, Gd^{III} and Yb^{III}) were reported.[108] All new

Structures 17, 18



DCDBP (**17**)



H_6HCPP (**18**)

¶ The number 6 in the designation of porphyrin **18** corresponds to the number of outer protons of carboxyl groups, which is reflected in the framework composition.

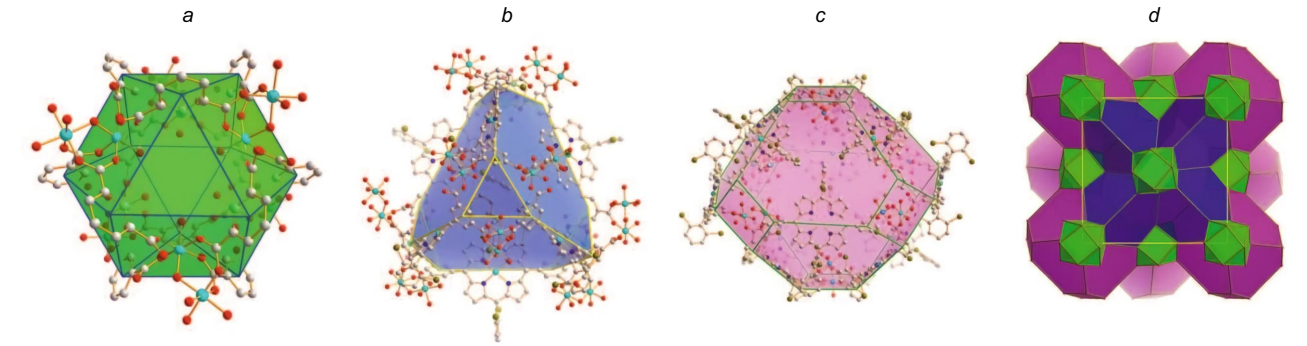


Figure 45. Three types of polyhedral pores formed by MMPF-3 (shown by coloured shapes): cubohemioctahedral (*a*), truncated tetrahedral (*b*) and truncated octahedral (*c*); and topological image of the 3D structure of this MOF illustrating the spatial arrangement of pores of different type (*d*).[107] Published with permission from Wiley.

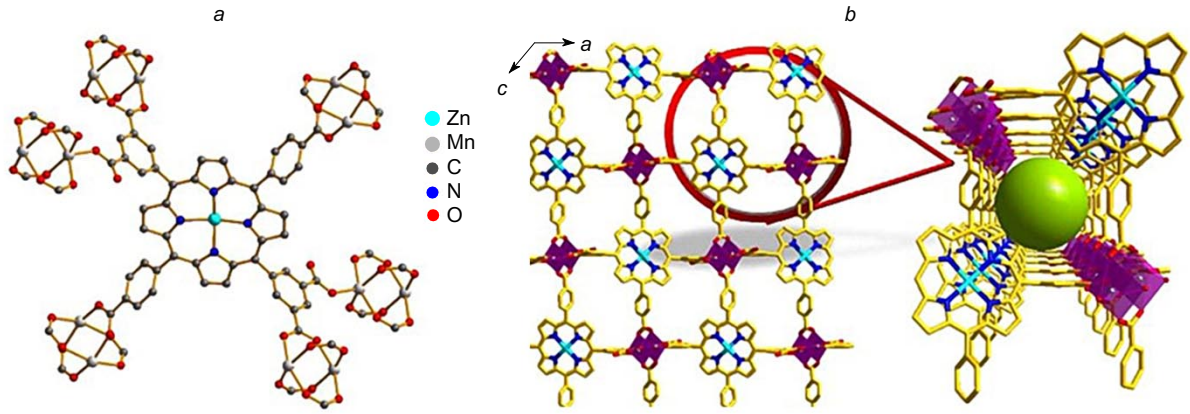


Figure 46. Fragment of 3D Mn-*hc*MPF structure formed by Zn^{II} complex of porphyrin **18** and $Mn_2(CO_2)_4(CO_2H)_2$ clusters (*a*) and 1D channels in this MOF (*b*).[108] Published with permission from the American Chemical Society.

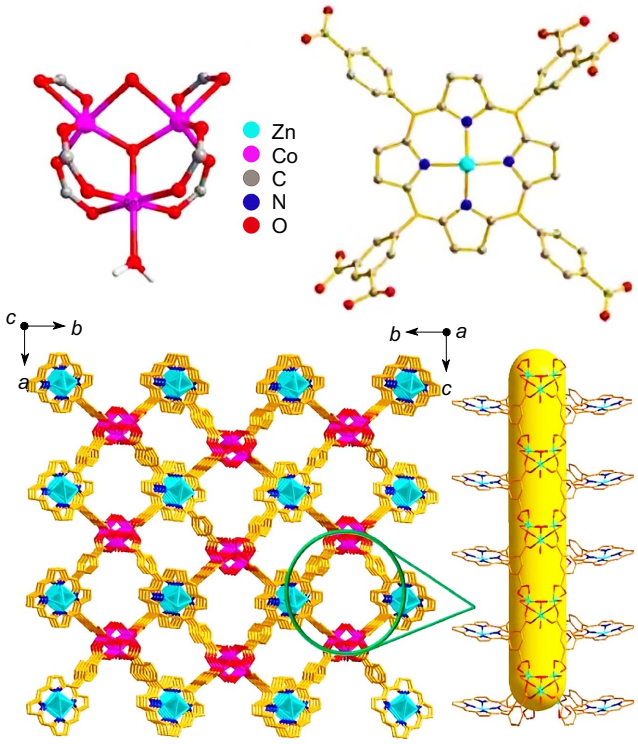


Figure 47. Components (*a*) and 3D structure of Co-*hc*MPF containing 1D channels (*b*).[108] Published with permission from the American Chemical Society.

MOFs were studied in detail regarding the crystal structure, formation mechanisms and types of topology.

2.2. Pillaring of two-dimensional layers by ditopic ligands

This strategy represents a rather simple and elegant method for the fabrication of 3D frameworks of crystalline materials. It includes binding of porphyrin-containing 2D layers *via* coordination bonds with additional ditopic ligands. By varying the length of such ligands, it is possible to control the geometric parameters of MOFs.

Choi *et al.*[109] prepared a number of frameworks PPF-*n* by the reactions of free porphyrin **3** or the corresponding palladium(II) TCPP complex with cobalt or zinc nitrate in the presence of 4,4′-bipyridine (bpy) (Fig. 48). It is noteworthy that when free porphyrin was used, metallation of the macrocycle with the metal cation (cobalt or zinc) took place during the solvothermal reaction. This approach is characterized by simultaneous formation of 2D MOFs and coordination of the ditopic organic ligand (4,4′-bipyridine) to metal cations in the already formed framework, which gives rise to porous 3D structures. The key role in the formation of target MOFs is played by the coordination properties of metal cations in porphyrin.

Layered 2D MOFs can be assembled with 4,4′-bipyridine in two ways: homogeneously and heterogeneously. The heterogeneous binding is implemented in PPF-3, in which 4,4′-bipyridine molecules connect the secondary building unit of the binuclear $[Co_2(CO_2)_4]$ cluster with the cobalt(II) cation in the porphyrin moiety, thus occupying all of the available coordination sites. In the PPF-4 structure $[Zn_2(Zn\text{-}TCPP)(bpy)_{1.5}]$, the 2D layers of porphyrins are linked by 4,4′-bipyridine molecules *via* alternating homogeneous and heterogeneous binding of the moieties. The zinc(II) cations in porphyrin are coordinatively unsaturated, with one axial position being vacant. In the framework PPF-5, the palladium(II) cation within porphyrin is incapable of additional axial binding; therefore, pillaring of 2D layers is due to homogeneous coordination of the ditopic bpy ligand to cobalt(II) cations in the nodes.

The presence of coordinatively unsaturated porphyrin metal centres in PPF-3 and PPF-5 mighj be significant for the development of porous materials for the storage of gases.

An increase in the pore size in these systems was attained by using 3,6-di(4-pyridyl)-1,2,4,5-tetrazine (DPT) and *N*,*N*′-di(4-pyridyl)naphthalene-1,4,5,8-tetracarboxydiimide (DPNI), which are 11.3 and 15.4 Å long, respectively, as the pillaring ditopic ligands.[110,111] The authors optimized conditions of synthesis, which resulted in the selective formation of porphyrin MOFs PPF-*n*. It was shown that the structures of PPF-18 and PPF-21 (Fig. 49) are formed upon binding of porphyrin 2D layers by ditopic N-donor ligands *via* axial coordination of ligand nitrogen atoms to the zinc cations in the porphyrin molecules and in the secondary building units, *i.e.*, due to heterogeneous binding. Hence, the use of molecules with different lengths as additional ligands leads to a targeted change in the parameter *c* of the crystallographic lattice, equal to twice the distance between

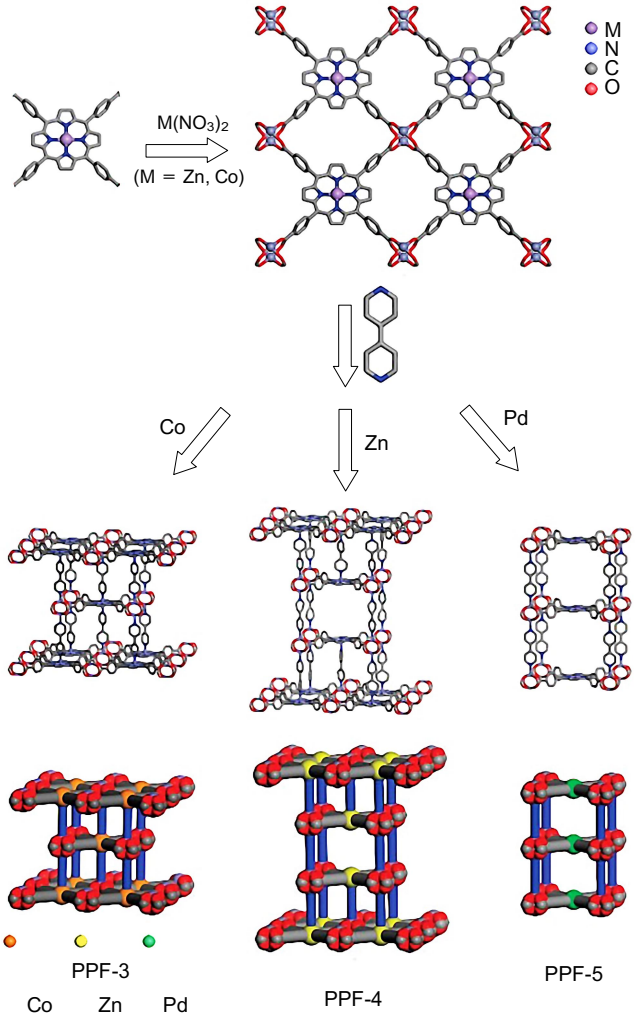


Figure 48. Scheme of the synthesis of metal-organic frameworks PPF-3, PPF-4 and PPF-5.[109] Published with permission from the American Chemical Society.

the porphyrin layers: 30.8966(6) Å for PPF-18 and 26.869(9) Å for PPF-21.

Interestingly, a change in the ratio of the building units used in the reaction and the simultaneous replacement of the solvent (DMF instead of diethylformamide) gave rise to new framework PPF-19, which significantly differed from PPF-18 described above (Fig. 50). The PPF-19 structure represented a 3D framework assembled from columns of DPNI ligands pillaring two two-dimensional porphyrin layers *via* coordination of the ligand nitrogen atoms to zinc cations in the nodes, *i.e.*, due to homogeneous coordination. This structure is further complicated by 2-fold interpenetration of the frameworks. It is noteworthy that the formation of interpenetrating frameworks is observed for MOFs with the longest pillars. This can, on the one hand, decrease the framework pore size and, on the other hand, increase its thermal and chemical stability.

When the reaction of ligand **3** with zinc nitrate was carried out in the presence of a relatively large amount of an additional ligand (DPNI or DPT), the authors obtained the metal-organic frameworks PPF-20 and PPF-22. These MOFs form structures similar to the porphyrin framework PPF-4 described above (see Fig. 48). However, the greater length of the ditopic ligands used in this case in comparison with the geometric size of 4,4′-bipyridine led to a considerable increase in the crystallographic parameters and, hence, targeted change in the framework density. Indeed, in the series of DPNI-based PPF-*n*, the calculated framework density increases in the following order, g cm^{-3}: 0.437 (PPF-20), 0.546 (PPF-18), 0.782 (PPF-19).

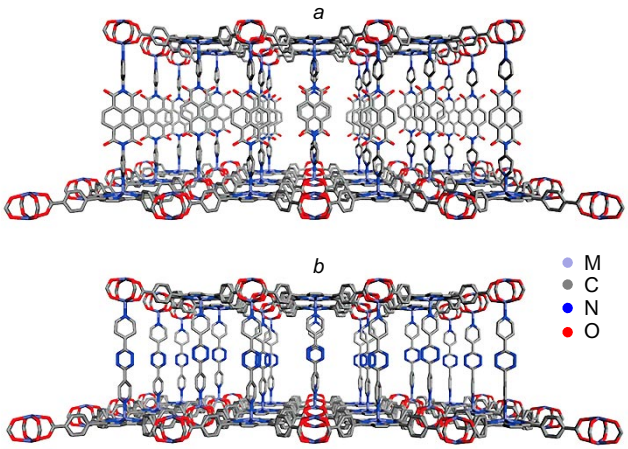


Figure 49. PPF-18 (*a*) and PPF-21 (*b*) structures.[110,111] Published with permission from the American Chemical Society.

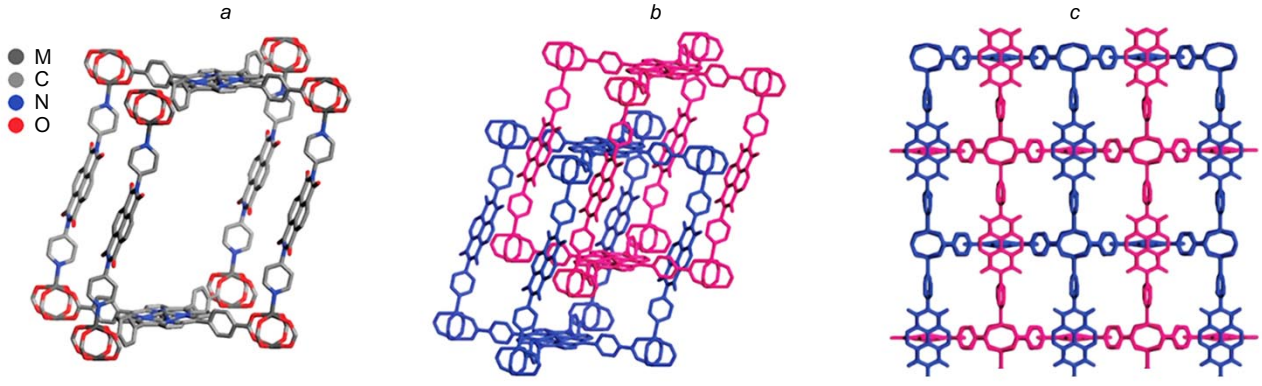


Figure 50. PPF-19 structure: one of the two interpenetrating networks (*a*), two interpenetrating networks (blue- and pink coloured) (*b*) and projection of 2-fold interpenetrating chains in the [001] direction.[110] Published with permission from the American Chemical Society.

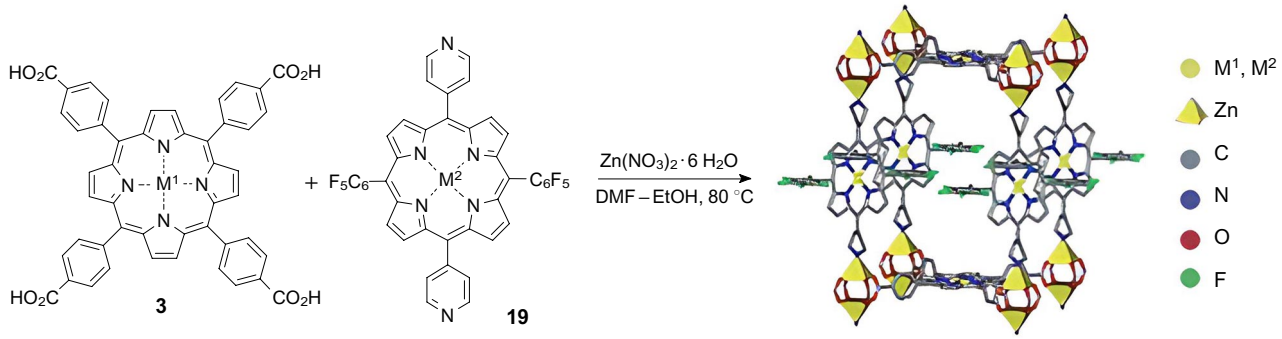


Figure 51. Scheme of synthesis of frameworks M^1M^2-RPM.[66] Published with permission from Wiley.

Burnett *et al.*[111,112] described one more unique method for the control of structural characteristics of MOFs using the PPF-18 and frameworks PPF-20 as examples. It was shown that the ditopic N-donor DPNI ligand can be replaced by 4,4′-bipyridine molecules without the loss of crystallinity of the formed MOF structures. It should be noted that no data on the sorption characteristics for this interesting class of porphyrin MOFs based on TCPP, divalent metal ions and ditopic organic ligands are available from the literature.

The parent porphyrins can also be used as ditopic N-donor ligands for the formation of MOFs. For example, with the goal to increase the number of coordinatively unsaturated metal centres able to act as efficient catalysts in various organic reactions, Keum *et al.*[66] developed an approach comprising the use of complex **19** based on 5,15-bis(pentafluorophenyl)-10,20-(4-pyridyl)porphyrin (dipy) as the pillaring ditopic N-donor ligand (Fig. 51). Highly important details of this approach are the order of reactant addition and the use of solubility differences between the carboxylate- and pyridyl-substituted porphyrins. Only the use of the DMF – EtOH solvent mixture (1 : 1 v/v ratio) did result in a faster reaction of the carboxyl groups of porphyrin **3** (L^1) with zinc cations to give layered 2D structures, which were then slowly pillared by dipyridylporphyrin **19** (L^2) to the target 3D framework *via* the coordination of the pyridyl nitrogen atoms to the MOF node units. This approach allowed the authors to obtain isostructural materials containing TCPP ligand either in the free state or as Al^{III}, Pd^{II} or Fe^{III} complex and either free porphyrin **19** or its complex with Mn^{III} as the ligand L^2.

2.3. Post-synthetic modification strategy

The strategy of post-synthetic modification of crystalline frameworks expands the possibilities of preparing MOFs with different metal centres or different organic linkers. For porphyrin-based MOFs, the most obvious way of modification is to introduce cations of various metals into the porphyrin cavity in order to attain definite properties, for example, the introduction of redox-active metals for the synthesis of catalysts. The metallation of the porphyrin macrocycle often takes place during the solvothermal reaction at an elevated temperature and an excess of metal salt.[75,81,85] However, there are examples in which the metal is introduced into the macrocycle cavity when the crystalline framework has already formed. The reaction of $ZrOCl_2 \cdot 8\,H_2O$ with TCPP free base in the presence of benzoic acid, which acts as modulator of the crystallization, gave MOF-525, which had the composition $Zr_6O_4(OH)_4(TCPP)_3$ and represented a 3D framework.[55,113,114] The isostructural frameworks MOF-525-Co and MOF-525-Zn containing cobalt(II) and zinc(II) complexes with TCPP as organic moieties were obtained by post-synthetic metallation of MOF-525 with cobalt(II) and zinc(II) nitrates, respectively.

The use of this post-synthetic procedure made it possible to introduce iron(III) cations into porphyrin in the preformed framework PCN-224,[115] structurally similar to MOF-525. It was shown that the modified material had a high peroxidase activity; therefore, it was used to develop a colorimetric method for facile and sensitive detection of hydrogen peroxide and glucose in combination with glucose oxidase.

The reaction of PCN-222, a hexagonal 3D MOF based on TCPP and 8-connected Zr_6 clusters (see Fig. 12), with an aqueous solution of H_2AuCl_4 in DMF resulted in the insertion of gold cations into the porphyrin cavity. This significantly improved the electrocatalytic performance of the resulting modified MOF (AuHPCN-222) and allowed the authors to develop an efficient electrochemical sensor for the analytical detection of estradiol.[116]

The approach mentioned above also proved to be effective for the insertion of rhodium cations into MOFs PCN-222 and NU-1102 based on TCPP and TCBPP, respectively.[117] The reaction was carried out for a suspension of the specified MOF in a degassed solution of $[Rh(CO)_2Cl]_2$ in CH_2Cl_2 for 24 h. The authors observed a gradual ageing of the crystals, that is, oxidative transformation of the initially formed Rh^I-MOFs into the corresponding Rh^{III}-MOFs with axially coordinated CO and Cl^- ligands, as was confirmed by single crystal X-ray diffraction.[117] The MOFs modified in this way proved to be efficient heterogeneous catalysts for hydrogenation of unsaturated hydrocarbons under mild conditions.

In some cases, direct synthesis of MOFs with the desired cations in the porphyrin ring is impossible. For example, the structure containing cobalt(II) cations in the porphyrin ring, topologically identical to MMPF-5,[75] containing the $Cd(CO_2)_3$ metal cluster and the Cd^{II}-TDCPP complex as secondary building units could be obtained only using post-synthetic treatment to replace the cadmium(II) cations by cobalt(II) cations in the porphyrin ring of MMPF-5.[118] Due to binding of cadmium(II) cations to the porphyrin macrocycle, the authors carried out the ion exchange reaction by keeping MMPF-5 in a solution of cobalt(II) nitrate in DMSO at 85 °C. This was accompanied by replacement of cadmium(II) cations in the inner cavity of the porphyrin macrocycle by cobalt(II) cations, with the crystal structure of the sample being retained. This targeted replacement of non-catalytic cadmium(II) cations

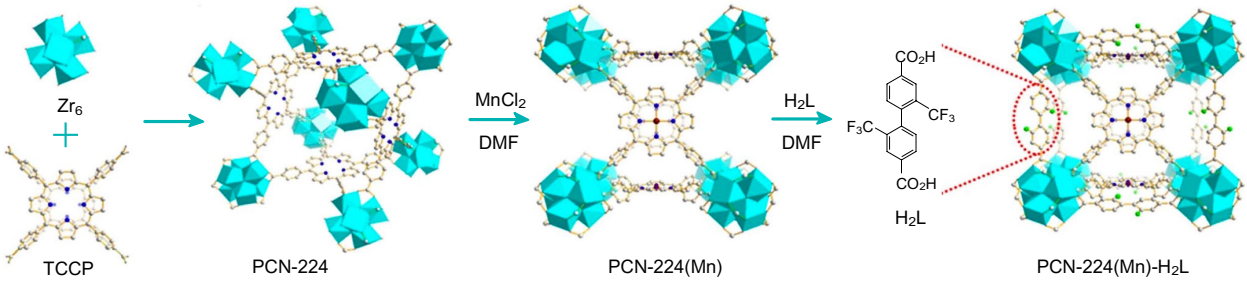


Figure 52. Scheme of synthesis of the framework PCN-224(Mn)-H_2L.[120] Published with permission from Wiley.

by cobalt(II) cations furnished a new catalytically active MOF.

The approach consisting in metal cation exchange in the framework nodes is also used to improve the functional properties of porphyrin MOFs. Gao *et al.*[119] reported the exchange of zirconium cations in the framework Zr-MOF-525 based on ligand **3** with titanium cations to give the structural isomer Ti/Zr-MOF-525. This modified material was found to be much more efficient than the initial MOF in the gas-phase photoreduction of CO_2 to CH_4 and CO under visible light irradiation and using water vapour.

The post-synthetic modification of porphyrin MOFs may also include the targeted insertion of secondary organic ligands into a metal-organic framework. Liu *et al.*[120] first heated the pre-synthesized framework PCN-224 in a solution of $MnCl_2$ in DMF at 120 °C for 12 h to give the derivative PCN-224(Mn). The solvothermal reaction of a suspension of this MOF with excess 2,2′-bis(trifluoromethyl)biphenyl-4,4′-dicarboxylic acid (H_2L) resulted in binding of the secondary organic ligand to the coordinatively unsaturated Zr_6 cluster in the framework nodes to give a new material — PCN-224(Mn)-H_2L (Fig. 52). The authors showed that this modification of the initial MOF increased the hydrophobicity and stability of the material and also markedly enhanced its catalytic performance in the oxidation of cyclohexane, which significantly exceeded the performance of PCN-224(Mn) and homogeneous catalysts based on metal porphyrins.[120]

The coordinative unsaturation of zirconium clusters in the secondary building units of porphyrin MOFs also provides the possibility of attaching small molecules inside the pores and channels. For example, by treating a series of frameworks PCN-22X (X = 2, 3, 4) with sulfuric acid solutions, Feng *et al.*[121] determined the optimal conditions for the insertion of sulfate ions within mesoporous frameworks and obtained sulfate analogues of PCN-22X-SO_4. The targeted modification of the pore content and enhanced cooperativity of properties make these materials efficient catalysts for the photochemical synthesis of artemisinin, the most efficient antimalarial drug. These catalysts show enhanced selectivity, reusability and stability compared to conventional homogeneous catalysts (Fig. 53).

In order to improve the antibacterial properties of TCPP-based MOFs containing zirconium clusters as the nodes, Mao *et al.*[122] inserted silver nanoparticles into the MOF pores by hydrothermal synthesis and thus obtained the hybrid material ZPM@Ag. The photocatalytic antibacterial efficiency of the MOFs doped with silver nanoparticles significantly increased due to the pronounced

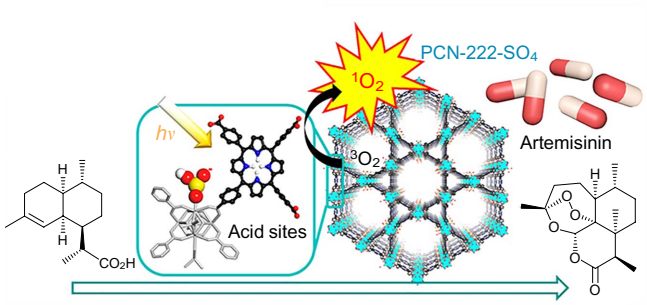


Figure 53. Scheme of the photochemical acid-catalyzed synthesis of artemisinin in the pores of modified PCN-222-SO_4.[121] Published with permission from the American Chemical Society.

synergistic effect and uniform distribution of active sites within the framework.

Hybrid porphyrin-containing nanocomposite NU-902 with zirconium clusters as secondary building units doped with silver nanoparticles is of interest as an electrocatalyst for the oxidation of nitrite ions.[123] A post-modification approach called solvent-assisted linker exchange (SALE), which consists in the replacement of the ligand in the MOF by another group, was employed to replace the hydroxy group of the zirconium cluster by functional sulfo group followed by partial potassium ion exchange with Ag^+ ions (Fig. 54). The authors noted partial reduction of silver cations, which resulted in the inclusion of silver nanoparticles into the pores of modified framework Ag-SO3-NU-902. It was shown that inclusion of electrocatalytically active silver nanoparticles and immobilized Ag^+ ions significantly enhances the electrocatalytic activity of the target material towards nitrite ions compared to the initial MOF NU-902.[123]

The targeted inclusion of nanoparticles (quantum dots) based on graphene into the pores of PCN-222 was reported by Chen and co-workers.[124, 125] The modified hybrid material GQD-PCN-222 demonstrated a 100 times higher electrical conductivity than the initial MOF due to considerable donor – acceptor charge transfer from the electron-donor quantum dots to porphyrin ligands in the MOF. The material also showed electrochemical activity towards nitrite ions in aqueous solutions.

The synthetic SALE approach is a facile strategy, which eliminates the problems of MOF synthesis related to the formation of undesirable topology, low solubility of the starting compounds or the absence of component functionality. The application of this approach has already resulted in the formation of various materials that could not be obtained previously by direct synthesis. In relation to the

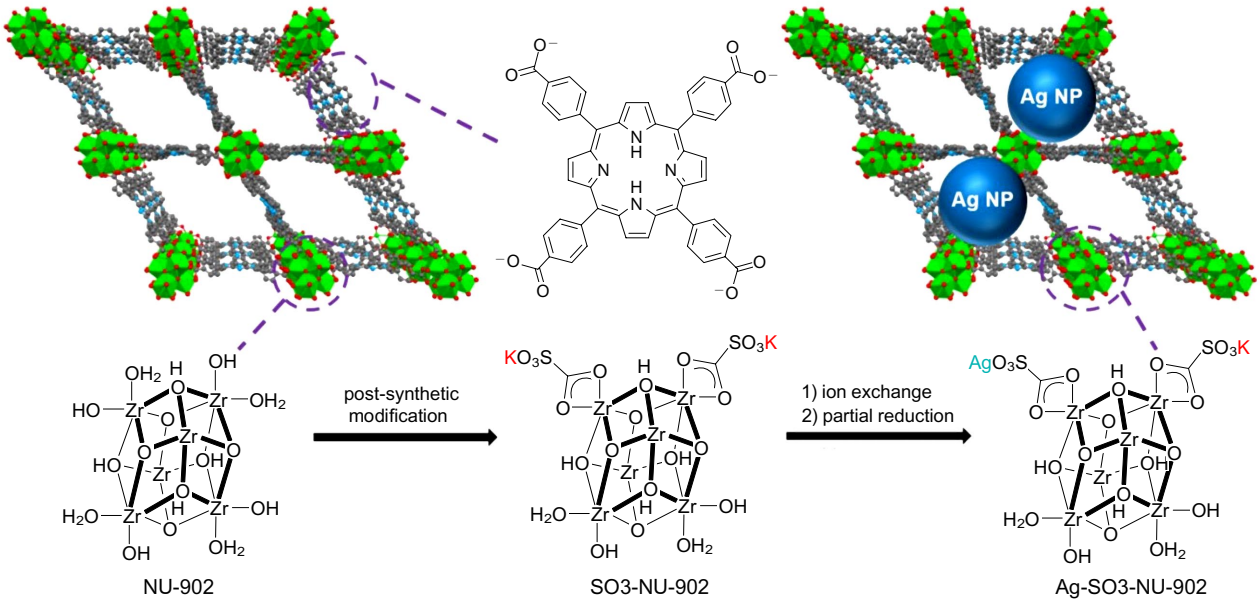


Figure 54. Scheme of two-stage post-synthetic approach for the preparation of Ag-SO_3-NU-902.[123] Published with permission from the American Chemical Society.

framework ZnZn-RPM, it was shown[126] that the zinc(II) complex with M-dipy (**19**) in the MOF can be replaced by free porphyrin and aluminium(III) or tin(IV) complex to give $Zn(Zn_{1-x}M_x)$-RPM ($x = 0.43$, 0.51 and 0.47 for M = 2H, Al^{III} and Sn^{IV}, respectively) (Fig. 55). The authors specially noted that Zn2H-RPM and ZnSn-RPM cannot be obtained by direct solvothermal synthesis, which emphasizes the unique character and efficiency of the SALE approach to fabricate new porphyrin-based MOFs.

A similar approach was used by Oh *et al.*[127] to insert carboxy-functionalized molecules of the iodinated boron

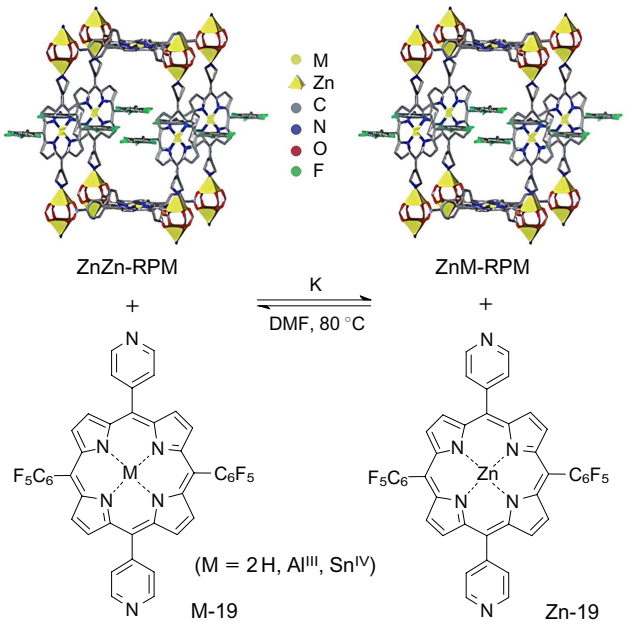


Figure 55. Ligand exchange in the framework ZnZn-RPM using the SALE method.[126] Published with permission from the Royal Society of Chemistry.

complex of dipyrromethene into the framework PCN-222(Nano). The reaction was carried out by heating a solution of I_2-BDP [I_2-BDP is 8-(4-carboxyphenyl)-4,4-difluoro-2,6-diiodo-1,3,5,7-tetramethyl-4-bora-3a,4a-diaza-*s*-indacene] in an acetonitrile–DMSO mixture (3 : 2 v/v) in the presence of this MOF at 60 °C for 24 h (Fig. 56). It was shown that PCN-I_2BDP(Nano) modified in this way was highly active in the photodynamic therapy of cancer due to synergistic properties of boradiazaindacene and porphyrin molecules: the quantum yield of singlet oxygen was approximately 30% higher for PCN-I_2BDP(Nano) than for the initial PCN-222(Nano). In addition, this material was approximately 10–20 times more cytotoxic for tumour cells owing to the improved light-harvesting properties and the effect of heavy atoms present in PCN-I_2BDP(Nano).

An unusual approach was used[128] to prepare a new MOF based on manganese(II) porphyrin: an framework IHEP of the composition $9[(UO_2)\cdot 4K_2(Mn\text{-}TCPP)_3(H_2O)_{10}]\cdot 5DMF\cdot 5H_2O$ containing uranyl ion as the secondary building unit. The addition of potassium cations, which are coordinated to the oxygen atoms of the porphyrin carboxyl groups and, together with the uranyl ion, form the multimetallic SBU clusters of the framework, give rise to a more stable structure of interpenetrating networks (Fig. 57). It was shown that IHEP-9 is a promising heterogeneous catalyst for the photocatalytic transformation of CO_2 into organic products under visible light irradiation at room temperature.

An interesting strategy for the controlled change of spectral properties of MOFs based on various porphyrins was proposed by Yang *et al.*[129] The hybrid MOFs with hierarchical core–shell structure were obtained by binding zirconium cations to ligand **3** or its N-confused analogue (NCP, **20**) by solvothermal synthesis in the presence of pre-synthesized seeds (Fig. 58). The targeted structural modification of the layers of these particles allowed the authors to tune the spectral characteristics (light absorption or emission) of the target frameworks $NCP_{MOF}@TPP_{MOF}$

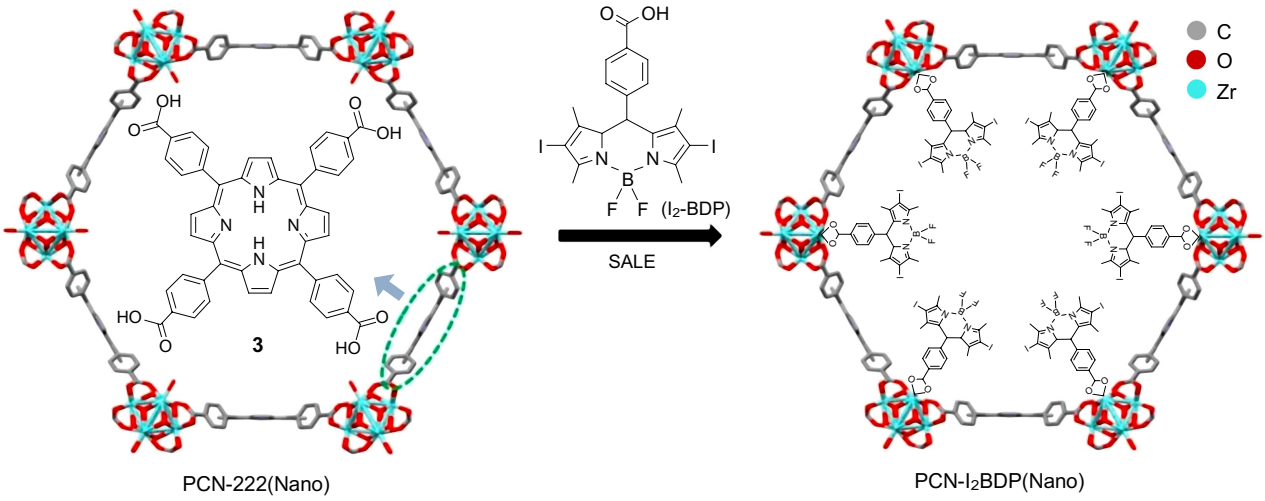


Figure 56. Scheme of synthesis of the framework PCN-I_2BDP(Nano) by the SALE method.[127] Published with permission from Elsevier.

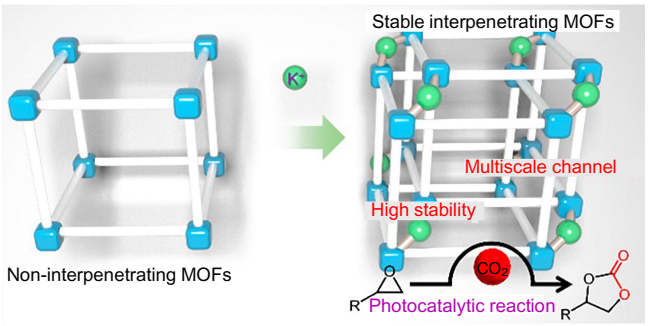


Figure 57. Scheme of synthesis of the framework IHEP-9.[128] Published with permission from the American Chemical Society.

and TPP_{MOF}@NCP_{MOF} in the visible and near-IR wavelength ranges, migration of the excited state energy and photosensitization of MOFs. The authors also noted that such controllable photoactive systems cannot be prepared by the interaction of the reaction mixture components under solvothermal conditions.

An alternative strategy of post-modification of MOFs is vapour-phase infiltration (VPI) of reactants. This method does not require solvents, and the deep diffusion of the substrate inside the porous material occurs at the vapour/solid interface; this makes it possible to avoid the competing adsorption of the solvent and complicated workup of reaction mixtures. It was shown[130] that microporous porphyrin-based MOF called MIL-173(Zr) is sufficiently stable to undergo VPI modification without destruction of the framework even when highly reactive compounds are used, such as trimethylaluminium and diethylzinc, which readily

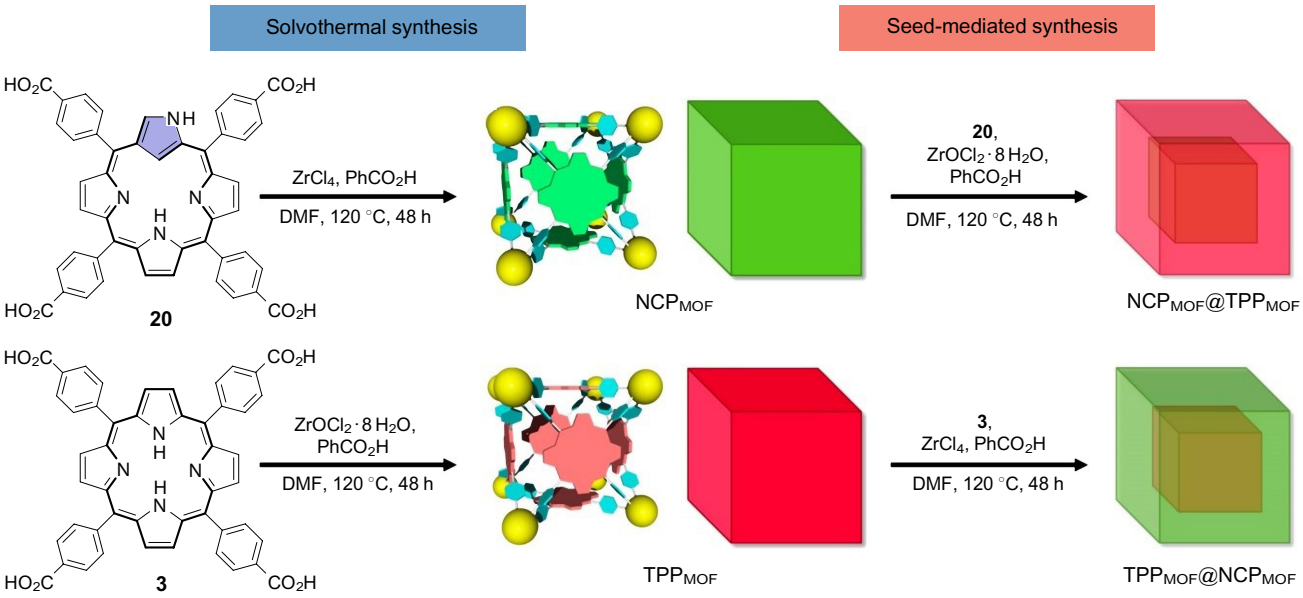


Figure 58. Synthetic strategy towards hierarchical hybrid MOFs.[129] Published with permission from the American Chemical Society.

react with phenolic and pyrrole moieties of the porphyrin macrocycle.

Metal-organic frameworks based on porphyrins and their metal complexes possessing tunable physicochemical parameters are promising precursors for the preparation of electrochemically active porous carbon materials with controlled structure and composition that can possess unique properties.[70,131] For MOFs based on TCBPP (**5**), it was shown that the framework ZrCPM-99(Fe) is excellent for use as a precursor to fabricate porous carbon materials. The material formed after carbonization at 700 °C showed high performance, comparable to that of 20% Pt/C catalyst, in the reduction of oxygen. This study demonstrated that the rational topological design of porous porphyrin-based MOFs can serve as an efficient strategy towards high performance characteristics in electrocatalysis. The authors also noted that the cubic crystal morphology and the porous structure of the initial framework are also retained after pyrolysis.

As noted above, a specific feature of the synthesis of MOFs based on tetratopic porphyrin ligands with zirconium clusters as the nodes is the possibility of simultaneous formation of frameworks of different topology (six topology types), which often complicates the preparation of a pure phase of a definite structure. This problem can be solved by using mechanochemical approach to the controlled and fast synthesis of pure polymorphs. Karadeniz *et al.*[132] investigated the effect of the structure of the zirconium cluster (Zr_6 or Zr_{12}) and role of the solvent (MeOH, DMF, diethylformamide) used in the mechanochemical reactions and the nature of the metal cation (Fe^{3+}, Mn^{2+}, Cu^{2+}) within the porphyrin ring on the topology of the resulting MOFs. They determined the optimal conditions for the fast and selective preparation of cubic (ftw-MOF-525) and hexagonal (shp-PCN-223) polymorphs during 20–60 min of grinding.

3. Practical application prospects

Porphyrin MOFs are a perfect platform for the development of materials for practical use in various fields of science. Unique physicochemical properties of porphyrins stimulate researchers to investigate diverse physicochemical functional characteristics of porphyrin-based metal-organic frameworks. This review is focused on the application of MOFs for the sorption and separation of gases, catalysis, medicine, luminescence and design of films and sensors; examples of these applications are presented below.

3.1. Sorption and separation of gases

In most of modern studies, gas sorption and calculation of the Brunauer–Emmett–Teller surface area are carried out to confirm the porous structure of MOFs. The linear dimensions of the porphyrin ligand allow the fabrication of porous frameworks with high surface areas and size of open channels. Table 1 summarizes the information on porphyrin MOFs discussed in this review; the Table gives their designations and compositions and sorption characteristics, that is, the absorbed gas volumes (*V*). The surface areas and pore volumes were determined by different authors using various gases. For clarity, MOFs are arranged in Table 1 in the order of decreasing gravimetric specific surface area measured in $m^2\ g^{-1}$.

Sorption characteristics of porphyrin-based metal-organic frameworks are highly variable. The BET surface areas vary from 200 to 5000 $m^2\ g^{-1}$. Large surface areas are very important for gas storage, and many porphyrin MOFs meet the requirements to materials promising for the hydrogen storage.[134,135] The highest specific surface areas were found for the materials FJI-H6 (Ref. 71) and PCN-229 (Refs 71, 72) based on tetracarboxyphenyl-substituted porphyrins **5** and **7** with long bridging groups at the periphery of the macrocycle and zirconium(IV) clusters. The sizes of open channels of porphyrin frameworks reach outstanding values of 35–37 Å in the MOFs PCN-222 (Ref. 50) and Hf-2 (Ref. 57) based on TCPP and zirconium(IV) and hafnium(IV) clusters; a value of 38 Å was found for the framework PCN-230,[72] composed of zirconium(IV) clusters and tetracarboxyphenyl-substituted porphyrin **8** with elongated periphery. In addition to unusually wide channels, porphyrin MOFs can also have small channels (3–9 Å), the size of which corresponds to the geometric parameters required for porous materials for methane storage[136] or for selective separation of gases.[137] Zhang *et al.*[36] showed that the porphyrin-based framework MMPF-20 can selectively adsorb CO_2 from a CO_2+CH_4 mixture, which is promising for natural gas purification.

Despite the efficiency of application of these MOFs in various fields, one should bear in mind high cost of the synthesis, purification and isolation of both the organic ligands and materials based on them. From this standpoint, it is most rational to use porphyrin MOFs as key components of high-tech processes, in which small amounts of substances are required and the material can be regenerated, *e.g.*, catalysis, photovoltaics, medical applications, sensorics, electrical conductivity, *etc.* These applications are considered below.

3.2. Catalysis of organic reactions

Catalysis of organic reactions is one of the most significant practical applications of porphyrin-based MOFs. Many-year studies of synthetic porphyrins showed that these macrocycles and their metal complexes are effective catalysts of some reactions taking place in solutions.[138–142] Owing to the specific optical and photophysical properties of porphyrins, the reaction conditions can vary significantly depending on the type of substrate and the nature of the catalyst. Nevertheless, it should be taken into account that even a minor content of the catalyst in the reaction products necessitates additional purification stages, which substantially complicate the purification of the target compounds. Thus, the industrial application of catalytic reactions under homogeneous conditions is restricted and brings about additional expenses for the purification and isolation of products.

An alternative is the use of heterogeneous catalytic systems.[143–147] The development of heterogeneous catalysts based on porphyrin-based MOFs brings about additional benefits. The porous structure of these materials can provide the access of substrate molecules to catalytic sites not only on the surface of catalyst particles, but also in the internal space of the material. High concentration of catalytic sites makes it possible to considerably reduce the catalyst loadings. The possibility of varying the type and size of pores during the design of MOFs allows the design of catalysts with optimal structure for a number of transformations, including stereoselective ones.[148] In addition, porphyrin MOFs possess enhanced thermal, hydrolytic and mechanical stability, which prevent degradation of their porous crystal structure during the reactions.

Table 1. Porphyrin-based metal-organic frameworks and their sorption characteristics.

Code	Composition	Pore or channel size, Å	BET surface area (according to Langmuir theory), $m^2\ g^{-1}$	V (gas), $cm^3\ g^{-1}$							Ref.
				CO_2	CO	H_2	N_2	CH_4	Ar	O_2	
FJI-H6	$[Zr_6O_4(OH)_4(TCBPP)_3]$	Pores, 25	5007	–	–	172,[a] 108[b]	1346[a]	–	–	–	71
FJI-H7	$[Hf_6O_4(OH)_4(TCBPP)_3]$	Pores, 25	3831	–	–	–	1029	–	–	–	71
FJI-H6(Cu)	$[Zr_6O_4(OH)_4(Cu\text{-}TCBPP)_3]$	–	3731	–	–	–	1128	–	–	–	17
FJI-H7(Cu)	$[Hf_6O_4(OH)_4(Cu\text{-}TCBPP)_3]$	–	3195	–	–	–	918	–	–	–	71
PCN-228	$[Zr_6(OH)_4O_4(TCP\text{-}1)_3]$	Pores, 25	4510	–	–	–	1245	–	–	–	72
PCN-229	$[Zr_6(OH)_4O_4(TCP\text{-}2)_3]$	Pores, 28	4619	–	–	–	1455	–	–	–	72
PCN-230	$[Zr_6(OH)_4O_4(TCP\text{-}3)_3]$	Pores, 38	4455	–	–	–	1085	–	–	–	72
MOF-526	$Zr_6O_4(OH)_4(Cu\text{-}TCBPP)_3$	Pores, 25.5	4260	–	–	–	1100	–	–	–	73
MOF-527	$Zr_6O_4(OH)_4(Cu\text{-}TCTPP)_3$	Pores, 31.4	2000	–	–	–	640	–	–	–	73
MOF-528	$Zr_6O_4(OH)_4(Cu\text{-}TCTTPP)_3$	Pores, 37.6	3550	–	–	–	920	–	–	–	73
Ir-PMOF · 1(Zr)	$[(Zr_6(\mu_3\text{-}O)_8(OH)_2(H_2O)_{10})_2(Ir\text{-}TCPP)Cl)_3]$	Square channels, 19	2637	–	1029[c]	–	705[a]	–	–	–	59
PCN-224-Ni	$Zr_6O_4(OH)_4(Ni\text{-}TCPP)_3$	3D channels, $d = 19$	2600	–	–	–	790[a]	–	–	–	58
MOF-525	$Zr_6O_4(OH)_4(TCPP)_3$	Pores 20	2620, 2127	25.3	–	–	–	–	~1200[b]	–	55, 113, 114
MOF-525-Co	$Zr_6O_4(OH)_4(Co\text{-}TCPP)_3$	–	1264	33.6	–	–	–	–	–	–	113, 114
MOF-525-Zn	$Zr_6O_4(OH)_4(Zn\text{-}TCPP)_3$	–	1317	28.1	–	–	–	–	–	–	113, 114
MOF-545	$Zr_6O_8(H_2O)_8(TCPP)_2$	Hexagonal channels, $d = 37$; triangular channels, $d = 8$	2260	–	–	–	–	–	~1250[b]	–	55
MOF-545-Fe	$Zr_6O_8(H_2O)_8(FeCl\text{-}TCPP)_2$	Hexagonal channels, $d = 37$; triangular channels, $d = 8$	2260	–	–	–	–	–	–	–	55
MOF-545-Cu	$Zr_6O_8(H_2O)_8(Cu\text{-}TCPP)_2$	Hexagonal channels, $d = 37$; triangular channels, $d = 8$	2260	–	–	–	–	–	–	–	55
PCN-222	$Zr_6(OH)_8(OH)_8(TCPP)_2$	1D channels, $d = 37$	2223	14,[d] 35,[e] 58[f]	–	–	846[a]	–	–	–	50 – 54
PCN-222(Fe)	$Zr_6O_8(H_2O)_8(FeCl\text{-}TCPP)_2$	1D channels, $d = 37$	2200	–	–	1009[a]	–	–	–	–	50 – 54
PCN-222(Mn)	$Zr_6O_8(H_2O)_8(MnCl\text{-}TCPP)_2$	1D channels, $d = 37$	2046	–	–	–	906[a]	–	–	–	50
PCN-222(Co)	$Zr_6O_8(H_2O)_8(Co\text{-}TCPP)_2$	1D channels, $d = 37$	1864	–	–	–	844[a]	–	–	–	50
PCN-222(Ni)	$Zr_6O_8(H_2O)_8(Ni\text{-}TCPP)_2$	1D channels, $d = 37$	2283	–	–	–	1067[a]	–	–	–	50
PCN-222(Cu)	$Zr_6O_8(H_2O)_8(Cu\text{-}TCPP)_2$	1D channels, $d = 37$	2312	–	–	–	899[a]	–	–	–	50
PCN-222(Zn)	$Zr_6O_8(H_2O)_8(Zn\text{-}TCPP)_2$	1D channels, $d = 37$	1906	–	–	–	764[a]	–	–	–	50
DGIST-1	$Ti_2(O)_2(TCPP)$	Pores 7.5	1957	195.3,[f] 110.1[e]	–	324[a]	–	–	–	–	66
PCN-134	$Zr_6O_4(OH)_6(H_2O)_2(BTB)_2(TCPP)$	–	1946	–	–	–	717	–	–	–	64
Hf-2	$Hf_6(OH)_8(OH)_8(TCPP)_2$	Hexagonal channels, ~35; triangular channels, ~12	1600	–	–	–	700[a]	–	–	–	57
MMPF-2	$[Co^{II}_3(OH)(H_2O)]_4(Co^{II}\text{-}TDCPP)_3$	Channels, 10.046 × 10.099 and 6.204 × 7.798	1400 (2037)	170,[f] 101[e]	–	–	–	–	545[b]	–	74
Al-PMOF	$(H_2TCPP)[AlOH]_2$	1D channels, 6 × 11	1400	77.9[e]	–	–	–	–	–	–	41, 42

Table 1 (continued).

Code	Composition	Pore or channel size, Å	BET surface area (according to Langmuir theory), $m^2\ g^{-1}$	V (gas), $cm^3\ g^{-1}$							Ref.
				CO_2	CO	H_2	N_2	CH_4	Ar	O_2	
Ga-PMOF	$[Ga_2(OH)_2(TCPP)]$	Channels, 5.0 × 11.8 and 3.4 × 11.8	1150 – 1400	7.7 [e]	–	–	–	–	–	–	43
In-PMOF	$[In_2(OH)_2(TCPP)]$	Channels, 5.0 × 11.8 and 4.0 × 12.6	1200 – 1250	6.6 [e]	–	–	–	–	–	–	43
PCN-22	Formed by TCPP and Ti_7O_6 clusters	Tetragonal channels, 15	1284	–	–	–	430 [a]	–	–	–	65
ZJU-21	$[Cu_4(Ni\text{-}TDCPP)(H_2O)_4]$	Pores, 11 and 21	1339	–	–	–	348 [a]	–	–	–	78
ZJU-22	$[Cu_{16}(Mn^{III}\text{-}TDCPP)_3(OH)_{11}(H_2O)_{17}]$	Channels 15	809	–	–	–	202 [a]	–	–	–	78
CPM-99(Fe)	$[Zr_6O_4(OH)_4(Fe\text{-}TCBPP)_3]$	Pores, 19 and 9	1030	76 [f]	–	–	450	–	–	–	70
CPM-99(H_2)	$[Zr_6O_4(OH)_4(TCBPP)_3]$	Pores, ~20	–	73 [f]	–	–	–	–	–	–	70
CPM-99(Zn)	$[Zr_6O_4(OH)_4(Zn\text{-}TCBPP)_3]$	Pores, ~20	–	60 [f]	–	–	–	–	–	–	70
CPM-99(Co)	$[Zr_6O_4(OH)_4(Co\text{-}TCBPP)_3]$	Pores, ~20	–	61 [f]	–	–	–	–	–	–	70
MMPF-4	$[Zn_{19}(TDCPP)_3][(NO_3)_8]$	Pores, d = 21.528; 'windows', 7.831 × 8.048; pores, d = 11.189; 'windows' 8.048 × 8.048	958 (1205)	124, [f] 67 [e]	–	–	3 [f]	–	376 [b]	–	75
MMPF-5	$[Cd_8(Cd\text{-}TDCPP)_3][(H_3O)_8]$	Pores, d = 22.521; 'windows', 8.004 × 8.195; pores, d = 11.589, 'windows' 8.195 × 8.195	–	67 [f]	–	–	–	–	–	–	75
MMPF-5(Co)	$[Cd_8(Co\text{-}TDCPP)_3][(H_3O)_8]$	Pores, d = 22.260; 'windows', 7.929 × 8.440	–	–	–	–	–	–	–	–	118
MMPF-9	$Cu_6(Cu\text{-}TDCBPP)(HCO_2)_4(H_2O)_6$	Triangular channels, edge length 14; hexagonal channels, diagonal 24.7	850 (1050)	–	–	–	245 [a]	–	–	–	81
NU-905	$Th_6(O)_2(HCO_2)_4(H_2O)_6(TCPP)_4$	Rhombic pores, 14 × 25, 4 × 5 and 6 × 8	800	–	–	–	–	190 [b]	–	–	68
MIL-141(A)	Fe(Ni-TCPP)A (A = Li, Na, K, Rb, Cs)	Channels, d = 4 and 6	510 – 860	–	–	–	160 – 240	–	–	–	45
MMPF-18	Formed by ZnDBP and the $[Zn_4(O)(CO_2)_6]$ cluster $[Zn_4(O)(CO_2)_6]$	Channels, d = 7 and 12; pores, d = 7 and 12	700	60, [f] 33.6 [e]	–	–	220 [a]	18, [f] 10 [e]	–	–	20
UNLPF-2	$[Co_2(CO_2)]_2'[(Co\text{-}TBCPPP)(H_2O)_2]$	–	623	280, [g] 250, [h] 11, [f] 85 [e]	–	200	700	–	–	–	83
PPF-1	$[Zn_2(Zn\text{-}TCPP)]$	1D channels, 11.8 × 11.8	622	–	–	115 [a]	–	–	–	–	33
DBP-UiO	$Hf_6(\mu_3\text{-}O)_4(\mu_3\text{-}OH)_4(DBP)_6$	Triangular channels, 16; octahedral pores, 20; tetrahedral pores, ~28	558	–	–	–	1150	–	–	–	21
MMPF-20	$Ni_3(Ni\text{-}TCPP)_2$	1D channels, 4.6 × 12.6	517	43 [f]	–	–	259	12 [f]	–	–	36

Table 1 (continued).

Code	Composition	Pore or channel size, Å	BET surface area (according to Langmuir theory), $m^2\ g^{-1}$	V (gas), $cm^3\ g^{-1}$							Ref.
				CO_2	CO	H_2	N_2	CH_4	Ar	O_2	
PMOF-1	$[Cd_{3.2}(TCPP)_2][Me_2NH_2]_{1.6}$	1D channels, 4.1 × 9.6 and 5.7 × 13.4	279 – 461 (407 – 672)	44 – 65,[f] 41 – 43[e]	–	–	98 – 160[a]	22 – 26,[f] 41 – 43[e] 13 – 16[e]	–	–	39
Th-IHEP-5	Formed by $Th_6(CO_2)_{20}(DMF)_4(H_2O)_2(O)_2$ clusters, TCPP and bpydc	Pores, 6 – 18	260	–	–	–	110	–	–	–	69
UTSA-57	$\{Mn^{II}_{0.5}[Mn^{II}_4Cl(Mn^{III}Cl\text{-}TTZPP)_2(H_2O)_4]\}$	Channels, 20.3; pores, 11.9	206.5	65[f]	–	–	137	15[f]	–	–	86
GdMPF-1	$[(Zn(H_2O)(TDCPP)Gd_2(H_2O)_4Na_2]$	Channels 13.1 × 12.2	(200)	–	–	101[a]	124[a]	–	–	–	79
UNLPF-10	Formed by TBCPPP and $[In(CO_2)_4]^-$	Hexagonal channels, 19 × 16; pentagonal channels, 17 × 13 pores, 33 × 23 × 23	–	–	–	–	–	–	–	–	85
MMPF-1	Cu_2(Cu-BDCPP)$(H_2O)_2$	Pores, 18.615 × 16.170; 'windows', 3.4 × 3.5	–	80[g]	–	50[a]	5[a]	18[g]	–	45	106
MMPF-3	$[Co_2(H_2O)_5]$(Co-DCDBP)	Three types of polyhedral pores	–	–	–	–	–	–	–	–	107
Isostructural Zn-*hc*MPF and Mn-*hc*MPF	$\{Zn_2[Zn(H_2O)\text{-}H_2HCPP]\}$ $\{Mn_2[Zn(H_2O)\text{-}H_2HCPP]\}$	Channels, 17.8 × 18.1	–	–	–	–	–	–	–	–	108
Co-*hc*MPF	$\{[Co_3(H_2O)_3](Zn(H_2O)\text{-}HCPP)\}$	Channels, 11	–	–	–	–	–	–	–	–	108
In-*hc*MPF	Formed by Zn-$HHCPP^{5-}$ and $\{InNa_2(CO_2)_5(H_2O)_3\}$ clusters	Channels, 15.9 × 20.2 and 16.0 × 20.3	–	–	–	–	–	–	–	–	108
Pb-*hc*MPF	$\{Pb_2[Zn(H_2O)\text{-}H_2HCPP]\}$	Two types of 1D channels	–	–	–	–	–	–	–	–	108
Isostructural Gd-*hc*MPF and Pr-*hc*MPF	Formed by Zn-$HHCPP^{5-}$ and $\{Ln(CO_2)_5Na_2(H_2O)_2(\mu_2\text{-}H_2O)_2\}_n$ clusters (Ln = Gd, Pr)	Channels, 10	–	–	–	–	–	–	–	–	108
Yb-*hc*MPF	Formed by Zn-HCPP and $Yb_2(CO_2)_6(H_2O)_3$ clusters	1D channels	–	–	–	–	–	–	–	–	108
1 · Mn	$[Mn_5L(H_2O)_6 \cdot (DMA)_2]$[i]	Channels 16 × 7	–	25.5[e]	–	–	–	–	–	–	82
CZJ-4	$[Zn_{16}(H_2O)_8$(MnCl-TDCPP)$_4]$	Two types of pores with $d \approx 10$ 'windows', ~10	–	–	–	–	–	–	–	–	76
ZJU-18, ZJU-19, ZJU-20	$[Mn_5Cl_2$(MnCl-TDCPP)$(DMF)_4(H_2O)_4]$, $[Mn_5Cl_2$(Ni-TDCPP)$(H_2O)_8]$, $[Cd_5Cl_2$(MnCl-TDCPP)$(H_2O)_6]$	Pores, 11.5 and 21.3	–	–	–	–	–	–	–	–	77

Table 1 (continued).

Code	Composition	Pore or channel size, Å	BET surface area (according to Langmuir theory), $m^2\ g^{-1}$	V (gas), $cm^3\ g^{-1}$							Ref.
				CO_2	CO	H_2	N_2	CH_4	Ar	O_2	
GaMPF	$[(Zn(H_2O)\text{-}TDCPP)Ga_2(H_2O)_4Na_2]$	Channels, 15	–	–	–	–	–	–	–	–	80
PrMPF-2	$Pr_2Na_6(H_2O)_{12}[Zn(H_2O)\text{-}TDCPP)]_3\cdot\cdot 6Me_2NH_2$	Hexagonal channels	–	–	–	–	–	–	–	–	80
InMPF	$\{In_2Na(H_2O)(\mu_3\text{-}H_2O)(\mu_2\text{-}HCO_2)\}_8\{Zn(H_2O)\text{-}TDCPP\}_6$	Channels, 11 × 11	–	–	–	–	–	–	–	–	80
FeMPF	$\{Fe_3(H_2O)(\mu_3\text{-}O)(\mu_2\text{-}HCO_2)\}_8\{Zn(H_2O)\text{-}TDCPP\}_6$	Two types of 1D channels	–	–	–	–	–	–	–	–	80
MnMPF	$\{Mn_3(\mu_3\text{-}O)(\mu_2\text{-}HCO_2)\}_8\{Zn(H_2O)\text{-}TDCPP\}_6$	Three types of 1D channels	–	–	–	–	–	–	–	–	80
PPF-3	$[Co_2(Co\text{-}TCPP)(bpy)_2](NO_3)$	–	–	–	–	–	–	–	–	–	109
PPF-4 (see [j])	$[Zn_2(Zn\text{-}TCPP)(bpy)_{1.5}]$	Channels, 7.2 × 7.3 and 8.9 × 10.3	–	–	–	–	–	–	–	–	109
PPF-18 (see [j])	$[Zn_2(Zn\text{-}TCPP)(DPNI)]$	Channels, 14.5 × 5.1	–	–	–	–	–	–	–	–	133
PPF-20 (see [j])	$[Zn_2(Zn\text{-}TCPP)(DPNI)_{1.5}]$	Channels, 14.5 × 5.1 and 17.3 × 10.3	–	–	–	–	–	–	–	–	133
PPF-27 (see [j])	$[Zn_2(ZnTCPP)(bpy)]$	Channels, 7.1 × 7.3	–	–	–	–	–	–	–	–	133

Notes. The solvent molecules present in MOFs are not indicated; *d* is diameter; dash means that no data are given in the original publication.
The data on gas sorption were obtained at 1 atm pressure of the gas and temperatures, K: [a] 77, [b] 87, [d] 308, [e] 298, [f] 273, [g] 195, [h] 212.
[c] The value for CO sorption was found at a gas pressure of 0.57 atm and a temperature of 77 K. [i] L is 1,5,10,15-tetrakis[4-(3,5-dicarboxyphenoxy)phenyl]porphyrin, DMA is *N*,*N* -dimethylacetamide.
[j] The channel dimensions were calculated using the Material Studio program.

As shown above, using effective methods for the preparation of porphyrin MOFs, it is possible to obtain materials formed by various metal complexes that exhibit catalytic activity under homogeneous conditions. Therefore, metal-organic frameworks were studied as heterogeneous catalysts for many types of reactions that are usually catalyzed by porphyrins in solutions. These catalytic processes can be divided into several types: oxidation reactions, CO_2 conversion and carbene insertion.

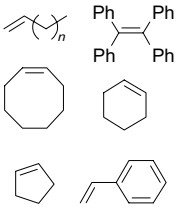
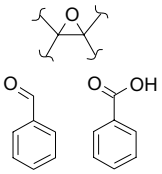
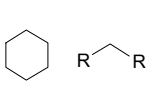
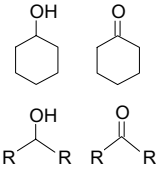
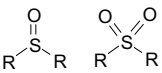
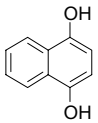
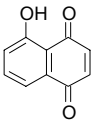
3.2.1. Oxidation reactions

The majority of studies addressing the catalytic properties of MOFs consider the use of these materials as catalysts for the oxidation of organic compounds giving rise to derivatives that are subsequently used to prepare polymers, biologically active compounds, agricultural chemicals, *etc*. There are dozens of such products, and their consumption amounts to 10^3 to 10^7 tons per year.

The best studied reactions are epoxidation of double bonds, oxidation of CH bonds in alkanes and cycloalkanes, oxidation of alcohols to carbonyl compounds, oxidation of sulfides to sulfoxides and sulfones and oxidation of phenols.[36, 38, 51, 76, 77, 149–156] As catalytically active compounds, porphyrin complexes of various metals, such as Mn^{III}, Fe^{III}, Cd^{II}, Ni^{II} and Pd^{II}, are used. The oxidants include molecular oxygen in the presence of aldehyde as activator, *tert*-butyl hydroperoxide and iodosobenzene. The reactions are carried out both at room temperature and on heating. The chemical oxidation of the above-indicated organic compounds is carried out using rather large catalyst loadings (1–10 mol.%), whereas photocatalytic reactions require an order of magnitude lower amounts of the catalyst.

Kosal *et al.*[157] developed catalysts for the oxidation of alcohols and alkanes using cobalt and manganese tetracarboxyphenylporphyrin complexes, PIZA frameworks, containing cobalt(III), manganese(III) or zinc(II) oxo-cluster fragments as the nodes. The first example of this type of MOFs used in catalysis is PIZA-3 with Mn^{III} ions as the nodes.[158] The authors note that this material has relatively small pores and, hence, reactions take place only on the catalyst surface. In this case, oxidation is accomplished by reactive oxygen species (superoxide anion, singlet oxygen), generated by means of photoactive porphyrin molecules under the irradiation with visible light. Porphyrin free

Table 2. Oxidation reactions catalyzed by metal-organic frameworks.

Substrates	Products	MOF name or composition	Metal cation in porphyrin	Ref.
		Co-PPF-1	Co^{II}	33, 118
		MMPF-20	Ni^{II}	36
		$[Cd_{1.25}(PdH_{1.5}TCPP)(H_2O)]\cdot 2\,DMF$	Pd^{II}	38
		CZJ-4	Mn^{III}	76
		MMPF-3	Co^{II}	107, 159
		$[Zn_2(HCO_2)_2(Mn\text{-}TCPP)][Me_2NH_2]\cdot 5\,DMF\cdot 2\,H_2O$	Mn^{III}	149
		MOF-525-Mn	Mn^{III}	150
		$[Ni_5(TCPP)_2O(H_2O)_4]$	Ni^{II}	154
		$[Zn_2(HCO_2)_2(Mn\text{-}TCPP)][Me_2NH_2]$	Mn^{III}	155
		PIZA-3	Mn^{III}	158
		CZJ-1	Mn^{III}	160
		ZnMn-RPM	Zn^{II}	161
		PCN-222(Fe)	Fe^{III}	51
		ZJU-18	Mn^{III}	75
		ZJU-19	Mn^{III}	75
		ZJU-20	Cd^{II}	75
		$[Zn_2(HCO_2)_2(Mn\text{-}TCPP)]\,[Me_2NH_2]\cdot 5\,DMF\cdot 2\,H_2O$	Mn^{III}	149
		PIZA-3	Mn^{III}	158
		CZJ-1, $[Zn_2(MnOH\text{-}TCPP)(DPNI)]\cdot 0.5\,DMF\cdot EtOH\cdot 5.5\,H_2O$	Mn^{III}	160
		MMPF-6	Fe^{II}	56, 162
		$[Ni_5(H_2TCPP)_2O(H_2O)_4]\cdot n\,Solv$	Ni^{II}	154
		Cr-PCN-600	Cr	163
		UNLPF-10	In^{III}	85
		PCN-222	—	156
		SO-PCN	Zn^{II}	153
Substituted phenols	Oxidative degradation products	TP-222(Zn)	Zn^{II}	164
		CuTNPP@MOF	Cu^{II}	165
		MnTNPP@MOF	Mn^{II}	165

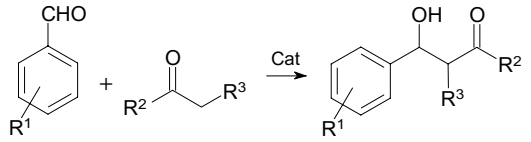
Note. R = Alk, Ar.

bases and porphyrin complexes with Zn^{II} and In^{III} or, in some cases, with Cu^{II}, Ni^{II} and Mn^{II} are used as photocatalysts.

Table 2 summarizes the structures of substrates, the possible oxidation products and the designations and compositions of MOFs that catalyze these reactions.

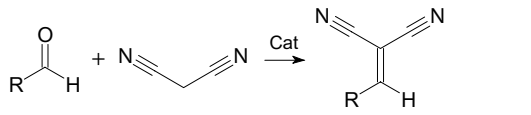
Interesting examples of reactions involving porphyrin MOFs are condensation reactions of aldehydes and ketones with compounds containing active methylene groups. The aldol condensation and Knoevenagel condensation [reactions (1) and (2) in Scheme 1] can be assigned to this type. These reactions are catalyzed by MOFs based on Mn^{III}, Fe^{III} and Ni^{II} porphyrin complexes.[149, 154]

Scheme 1



(1)

$R^1 - R^3$ = Alk; Cat = $[Zn_2(HCO_2)_2(Mn\text{-}TCPP)][Me_2NH_2] \cdot 5\,DMF \cdot 2\,H_2O$, $[Zn_2(HCO_2)_2(Cd\text{-}TCPP)][Me_2NH_2] \cdot 5\,DMF \cdot 3\,H_2O$, $[Zn_2(HCO_2)(Fe(H_2O)\text{-}TCPP)] \cdot 3\,DMF \cdot H_2O$, $[Cd_3(H_2O)_6(\mu_2\text{-}O)(Fe\text{-}HTCPP)_2] \cdot 5\,DMF$ (Ref. 74)

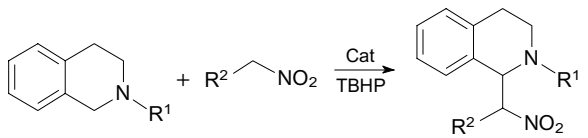


(2)

R = Alk, Cat = $[Ni_5(TCPP)_2O(H_2O)_4] \cdot n$ Solv (Ref. 78); Solv is solvent

Coupling of tertiary amines and nitroalkanes, which is preceded by dehydrogenation of the active methylene group of the nitro compound with *tert*-butyl hydroperoxide (TBHP), gives products in high yields and with high selectivity in the presence of MOFs ZJU-21 and ZJU-22 based on manganese(III) and nickel(II) porphyrin complexes, respectively, and $Cu_2(CO_2)_4(H_2O)_2$ clusters (Scheme 2).[78]

Scheme 2



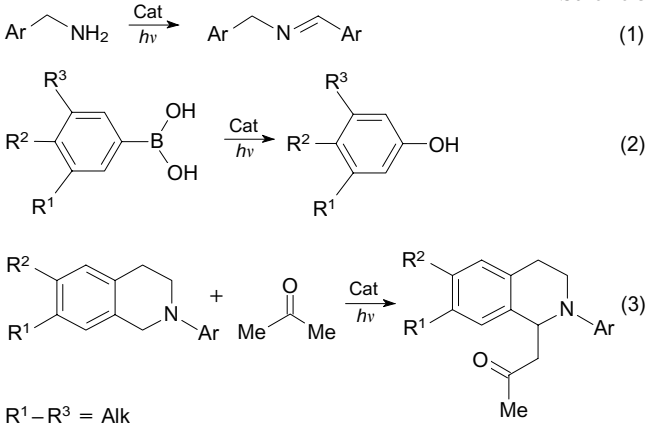
R^1, R^2 = Alk; Cat = ZJU-21, ZJU-22

In this case, Cu^{2+} cations serve as the catalytically active species. After six successive cycles of reaction of benzaldehyde with nitromethane, the catalytic activity of the material did not decrease and the crystal structure of the framework was retained.

There are reported examples of porphyrin MOFs that are used as catalysts for some light-induced oxidation reactions. They include oxidation of primary amines to imines, oxidative coupling of primary amines [reaction (1) in Scheme 3], oxidative hydroxylation of boronic acids [reaction (2)] and oxidative Mannich reaction [reaction (3)].[166]

It is known that porphyrins and their analogues are efficient catalysts of various biological processes taking

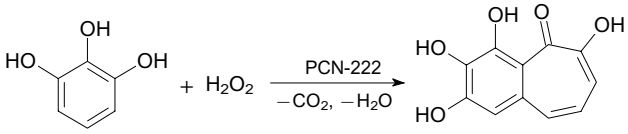
Scheme 3



$R^1 - R^3$ = Alk

place in living organisms. The development of synthetic analogues of hemin enzyme, not inferior in efficiency to natural compounds, is becoming one of the most significant applications of MOFs. A number of studies are devoted to the use of porphyrin porous materials close in their catalytic activity to enzymes containing haem as the prosthetic group.[50, 167] For example, PCN-222 showed a high catalytic activity in the pyrogallol oxidation (Scheme 4)[50] and in the oxidation of 3,3′,5,5′-tetramethylbenzidine and *o*-phenylenediamine in the presence of hydrogen peroxide.[162, 168]

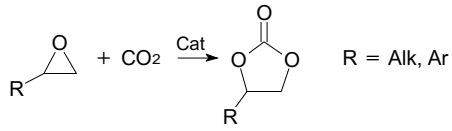
Scheme 4



3.2.2. CO_2 addition reactions

Porphyrin-based frameworks can be used as catalysts for chemical transformation of CO_2 to cyclic carbonates (Scheme 5).[20, 34, 35, 58, 81, 82, 84, 169]

Scheme 5



The zirconium-containing framework PCN-224(Co) obtained from the cobalt(II) TCPP complex was studied as a heterogeneous catalyst for the cycloaddition of carbon dioxide to propylene oxide to give propylene carbonate at a CO_2 pressure not more than 2 MPa at 100 °C for 4 h.[58] It was shown that this material retains its structure after three successive cycles of catalysis, which indicates the reusability of PCN-224(Co) as a heterogeneous catalyst. The authors noted high catalytic activity comparable to that observed for the homogeneous catalyst based on cobalt(II) TCPP complex.

The metal-organic framework MMPF-9,[81] formed upon the reaction of TDCPP with copper(II) nitrate and characterized by a high density of Cu^{II} cations, showed high efficiency as a heterogeneous catalyst of this reaction at room temperature and a CO_2 pressure of 1 atm. The reaction catalyzed by this MOF gives product in 87.4%

yield after 48 h at room temperature. This material surpasses in performance the reference MOF HKUST-1, which shows moderate activity towards the formation of propylene carbonate, which is formed 49.2% yield under similar conditions.

The best result for the cycloaddition to propylene oxide was found for the zinc MOF MMPF-18 based on 5,15-bis(4-carboxyphenyl)porphyrin.[20] The authors noted a unique catalytic efficiency of this framework, which allowed the synthesis of the target propylene carbonate in 96–97% yield at room temperature and CO_2 pressure of 1 atm in 48 h. The decrease in the product yields for the reactions of sterically hindered epoxides in the presence of various porphyrin MOFs as catalysts can be attributed to the restricted substrate diffusion in the pores of the materials; however, this drawback can be eliminated rather easily by the targeted design of the porphyrin molecule.

Jiang *et al.*[82] used 5,10,15,20-tetrakis[4-(3,5-dicarboxyphenoxy)phenyl]porphyrin (**11**) to elucidate the effect of the structure of the organic ligand on the ability of MOFs to catalyze cycloaddition reactions. The porous material $[Mn_5L(H_2O)_6(DMA)_2]\cdot 5\,DMA\cdot 4\,EtOH$ formed from this ligand (designated as 1·Mn; L is ligand **11**) catalyzes the reaction of epichlorohydrin or 1,2-epoxyhexane at a CO_2 pressure of 1 atm and a temperature of 80 °C to give the expected carbonate in 99% yield in 4 h.

The framework MMPF-10 based on *meso*-tetrakis[3,5-bis(4-carboxyphenyl)phenyl]porphyrin (**9**)[84] showed a high catalytic activity towards the CO_2 cycloaddition to 1-methylphenylaziridine, resulting in the formation of 3-methyl-5-phenyloxazolidin-2-one in 63% yield at room temperature and at an CO_2 pressure of 1 atm. The product yield was higher than that in the presence of the reference catalyst HKUST-1 under similar conditions. The authors noted that the yield of the corresponding 3-methyl-5-phenyloxazolidin-2-one substantially increased (up to 99%) as the temperature was raised to 100 °C and the CO_2 pressure was increased to ~2 atm.

A quantitative conversion of epichlorohydrin and shorter cycloaddition reaction time were observed when metal-organic framework MOF1 was used and the reaction solution was irradiated with high-power light-emitting diode lamps (30 W) at room temperature and at a CO_2 pressure of 1 atm.[34] In addition, the author found that the catalytic activity of this material in the CO_2 cycloaddition to epichlorohydrin carried out under mild conditions under visible light irradiation was higher than the activities of the most well-known MOFs.

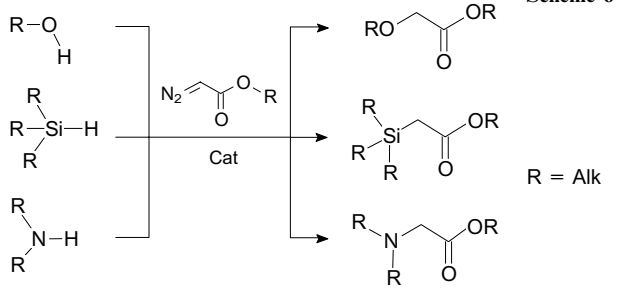
Liang *et al.*[170] described an example of using mixed-ligand zirconium-containing MOF based on TCPP and imidazolyl-substituted terephthalic acid — TCPP@Im-UiO-66. This catalyst provided reaction selectivity >90% and a high substrate conversion.

An efficient approach to CO_2 conversion is to involve it into various electrochemical reactions, particularly electrocatalytic reactions. These reactions can furnish a number of carbon-containing compounds such as methane, formic acid, methanol, *etc.*, for their subsequent use in industrial processes. Zhao *et al.*[171] repored MOF electrocatalysts that contained porphyrin molecular units based on TCPP grafted on an electrode coated by an alumina thin film. The authors estimated the electrochemical characteristics of thin films of MOFs based on porphyrin free base and complexes with catalytically active metals such as copper, zinc and cobalt under argon and CO_2 atmosphere. Each material demonstrated increasing current density in CO_2-saturated solutions; the most pronounced increase was observed for the cobalt-based system. A thorough analysis of the reaction products by gas chromatography and NMR spectroscopy allowed the authors to reveal the nature of chemical reactions occurring in MOF reactors and to determine the potential at which the selectivity of CO formation would reach 76%.

3.2.3. Carbene insertion

The catalytic properties of porphyrin MOFs in the reactions of carbene insertion into O–H, Si–H and N–H bonds were studied using frameworks Ir-PMOF-1(M) with the composition $[(M_6(\mu_3\text{-}O)_8(OH)_2(H_2O)_{10})_2(Ir(TCPP)Cl)_3]\cdot Solv$, where M = Zr, Hf, and frameworks Ru-PMOF-1(Hf) with the composition $[(Hf_6(\mu_3\text{-}O)_8(HO)_2(H_2O)_{10})_2(Ru(TCPP)CO)_3]\cdot Solv$ (Scheme 6).[59,61,172]

Scheme 6



The reactions performed out at room temperature in the presence of ~1 mol.% catalyst. The catalytic activity of the frameworks was shown to be comparable with that of the corresponding iridium and ruthenium complexes that catalyze analogous reactions under homogeneous conditions. Structurally diverse substrates were functionalized in the presence of MOFs under optimal conditions. Heterogeneous catalysts isolated from the reaction mixture retained their activity in the subsequent cycles.

It is of interest that the cyclopropanation reaction taking place as carbene addition to the C=C bond can be performed diastereoselectively in the presence of MOFs.[148] This stereochemical outcome can be attained by targeted control over the topology and pore shape of the material, as was demonstrated in relation to frameworks PCN-222(Rh) and PCN-224(Rh) comprising fragments of rhodium porphyrin complexes as linkers.

3.2.4. Photocatalytic reduction of CO_2

An example of successful use of the adsorption and catalytic properties of porphyrin MOFs is the photocatalytic reduction of CO_2 to formate anion and methanol.[42,52] The carbon dioxide reduction to the HCO_2^- ion was accomplished using the PCN-222 catalyst, formed by the TCPP ligand and the $Zr_6(\mu_3\text{-}O)_4(\mu_3\text{-}OH)_4(OH)_4(H_2O)_4(CO_2)_8$ cluster, in the presence of triethanolamine under irradiation with a 300 W xenon lamp (420–800 nm wavelength with a light filter).[52] The reaction carried out for 10 h gave 30 μmol of formate anions, which exceeded the amounts obtained using catalysts UiO-66-NH_2 and MIL-125-NH_2 under similar conditions.[173,174] The reaction did not give MeOH, CO, CH_4 or H_2 by-products. A study of the catalyst stability showed that the catalytic activity is retained in the subsequent cycles. The use of the MOF NH_2-MIL-125(Ti)

based on titanium oxo-clusters modified with zinc(II) tetracarboxyphenylporphyrin furnished a hybrid material for the selective photocatalytic reduction of CO_2 to CO.[175]

The photocatalytic reduction of CO_2 providing mainly methanol was carried out in the presence of MOF formed by the Cu^{II}-TCPP complex and $Al(OH)O_4$ clusters.[42] In this case, the reaction was carried out in the presence of triethylamine at 5 °C. The rate of methanol formation was 262.6 ppm g^{-1} h^{-1}, whereas the efficiency of analogous MOF containing no copper(II) ions was 7 times lower (37.5 ppm g^{-1} h^{-1}). The preparation of the analogue Al-PMOF based on free TCPP ligand in the presence of graphene oxide also afforded an efficient photocatalytic system meant for the reduction of CO_2 to the formate anion.[176]

The introduction of perovskite quantum dots into the cavity of iron porphyrin-based MOF [PCN-221(Fe_x)] afforded a hybrid photocatalyst capable of efficient reduction of CO_2 to CO and CH_4.[177] The preparation of this material can be regarded as a two-stage post-synthetic MOF modification, in which PbI_2 is first injected into the material cavities and then the reaction with methylammonium iodide is carried out to give the perovskite quantum dots $MeNH_3PbI_3$. The proximity of the quantum dots to the catalytic site facilitates the electron transfer from the quantum dot to the iron cation upon photoexcitation. This structural feature of the catalyst led to record-breaking CO_2 conversion (1559 mmol g^{-1}); this gave a 34 : 66 mixture of CO and CH_4. A similar material was produced by modification of MOF based on Co^{II}-TCPP complex with carbon nitride quantum dots;[178] however, it was markedly less efficient. Fine tuning of the metal coordination sphere in PCN-601 based on nickel(II) pyrazolylporphyrin complex provided the selective reduction of CO_2 to CO and CH_4;[179] the authors postulated a threefold increase in the efficiency of this MOF for CH_4 generation compared to the efficiency of PCN-222 type frameworks.

3.3. Photodynamic therapy of cancer and other biomedical applications

The photodynamic therapy (PDT) of cancer is a highly promising biomedical application of porphyrin-based MOFs. This method is based on activation of photoactive organic molecules with light at a definite wavelength, after which the excited molecules react with O_2 to give toxic reactive oxygen species (ROS) such as $^1O_2$, H_2O_2, OH^- and superoxide anion ($O_2^{\bullet-}$), which are able to kill cancer cells by inducing apoptosis and/or necrosis.[14, 100] In this respect, porphyrins are unique photosensitizers due to their photochemical activity, ability to absorb light in a wide wavelength range, stability, low toxicity, *etc*. The selective localization of the photoactive compound in the tumour is the crucial factor for the therapeutic efficacy of PDT. However, most porphyrins are hydrophobic; this leads not only to insufficient concentration of the sensitizers in the tumour, but also to their aggregation in the physiological medium, which deteriorates their photoactivity and thus significantly reduces the efficacy of the therapy.

The use of free porphyrins or metal porphyrin complexes as organic linkers for the assembly of MOFs makes it possible to prevent their aggregation and self-quenching and thus to retain the physicochemical characteristics. Moreover, owing to high porosity of porphyrin MOFs, it is possible to fabricate multimodal nanoplatforms by placing functional components for the treatment of cancer, such as vector molecules, photoactive therapeutic agents, chemotherapeutic drugs or various nanoparticles, into the pores or on the surface of the material.[180]

In 2014, Lu *et al*.[21] reported the first stable porous metal-organic framework for the PDT of cancer. The framework DBP-UiO, based on 5,15-bis(4-carboxyphenyl)porphyrin and hafnium(IV) ion, was used as an effective photosensitizer in the PDT of head and neck cancers. This MOF efficiently generated $^1O_2$ owing to isolation of porphyrin macrocycles in the structure, which prevented their aggregation and self-quenching of excited states. Moreover, the coordination of the porphyrin carboxyl groups to heavy metal hafnium centres in the nodes enhanced the intersystem crossing of molecules to the triplet state and, as a consequence, increased the probability of $^1O_2$ formation from $^3O_2$. The framework DBP-UiO showed high efficiency in the PDT both *in vitro* and *in vivo*, resulting in a significant growth retardation of the tumour weight and volume; in particular, the tumour decreased 50-fold in volume in half of mice and completely disappeared in the other half.

Liu *et al*.[181] reported multifunctional TCPP-based composite nanoparticles Hf-TCPP-NMOF-PEG. The authors showed that hafnium cations can serve not only as heavy atoms to enhance intersystem crossing, but also as ions able to absorb X-rays and emit photo/Auger electrons and free radicals. In addition, Hf-TCPP-NMOF-PEG nanoparticles were efficient in generation of singlet oxygen and had low toxicity, due to fast elimination from the body (in approximately 7 days).

In the development of multifunctional nanoplatforms for biomedical applications, it is important to take into account the size of the introduced particles, which should be in the $\sim 10-100$ nm range, because this influences accumulation of the photosensitizers in the tumour cells.[182] Park *et al*.[183] investigated the effect of the particle size of Zr^{IV}-containing porphyrin-based PCN-224 on the cellular uptake and efficiency of PDT. The predominant uptake by HeLa cells took place in the case of 90 nm PCN-224 nanoparticles; the cell apoptosis after PDT was 81%. Moreover, the Zr_6 clusters in this framework were selectively bound to folic acid, which was used as the vector molecule to increase the drug permeability and retention time. As compared with other MOFs or free TCPP, the functionalized framework PCN-224 with optimized particle size had enhanced efficiency in the PDT due to its high accumulation *in vivo*.

It deserves special mention that porphyrin MOFs can absorb photons only in a narrow spectral range (from ultraviolet to visible light), which markedly decreases the penetration depth and reduces the effect of PDT. In order to overcome the problem of low tissue penetration, Li *et al*.[184] obtained composite heterodimers UCMOF, which consisted of up-conversion nanoparticles doped with lanthanides (Yb^{3+} and Nd^{3+}) and the porphyrin-based framework PCN-224. These heterodimer systems can efficiently absorb light in the near-IR (NIR) range, since up-conversion particles are excited by laser radiation at 980 nm, which corresponds to the Yb^{3+} excitation wavelength. As a result of multiphoton process, up-conversion particles start to emit short-wavelength radiation, which activates the excited state of the framework PCN-224 due to the resonance energy transfer, which results in the generation of toxic $^1O_2$. Thus, the presented heterodimers demonstrated high antitumour efficacy upon excitation with long-wavelength light.

Liu *et al.*[185] improved the therapeutic efficacy of these heterodimers by fabricating Janus particles. These particles are highly specific to mitochondria and, owing to doping with Nd^{3+} ions, they can be activated by near-IR light at 808 nm wavelength, which is safer and more biocompatible because of the optimal penetration depth into the body tissues. On the other hand, owing to their luminescent properties, porphyrins can simultaneously act as molecular thermometers for intracellular measurements.[186]

He *et al.*[187] used a new approach to combining up-conversion particles with porphyrin MOFs, which consisted in the fabrication of core–shell composite structures UMOFs@Au-NPs (Fig. 59). The core composed of up-conversion particles served for the absorption of NIR photons and high-energy light emission for activation of porphyrin MOF layers. The authors noted that the efficiency of energy transfer from up-conversion particles to the metal-organic framework in the core–shell nanostructure proved to be markedly higher than in Janus particles. In addition, owing to greater surface area and porosity, ultrasmall gold nanoparticles are distributed in the MOF shell more appropriately for generation of H_2O_2 as a result of glucose decomposition in the intratumour microenvironment. In the presence of catalytically active Fe^{2+} porphyrin centres, some of H_2O_2 was converted to O_2, which generated cytotoxic $^1O_2$ for tumour degradation due to the PDT effect. The use of these structures in the therapy of mice not only led to a significant antitumour effect, but also increased the life span of mice for 50 days after the therapy.

A combination of PDT with chemotherapy is an efficient dual-mode treatment, which showed enhanced therapeutic efficacy and relatively low toxicity.[188] PDT leads to the generation of toxic ROS in tumour cells (tissues), which induce oxidative damage of cellular proteins and DNA; this leads to high sensitivity of tumour cells to toxic chemotherapeutic agents. Thus, the desired antiutumour effect can be attained using lower doses of chemotherapeutic agents, while the toxic effect on normal cells (tissues) decreases.

Liu *et al.*[189] described Zr^{IV} porphyrin-based system DOX@NPMOF possessing synergistic effect due to combination of chemotherapy and PDT. High loading of chemotherapeutic agent, doxorubicin (DOX), into the NPMOF was attained *via* noncovalent interactions (π–π stacking, hydrophobic and electrostatic interactions) between DOX molecules and MOF. Doxorubicin was slowly released in normal cells (tissues) (10.3% of the drug was released in 72 h at pH 7.0), while the release at the tumour site was faster (58.5% in 72 h at pH 5.0). Moreover, the synergistic therapy performed by laser irradiation of DOX@NPMOF particles at 655 nm led to apoptosis of 90% of tumour cells, indicating that porphyrin-based MOFs are fairly promising objects for the synergistic chemotherapy and PDT.

Zeng *et al.*[190] obtained a nanoplatform of triple therapeutic action [PDT, photothermal therapy (PTT) and chemotherapy]. The core–shell structure of AuNR@MOFs@CPT consisted of gold nanorods, which served as seed crystals for growing $Zr_6(TCPP)_{1.5}$ MOF on their surface. The molecules of the antitumour drug camptothecin (CPT) were placed into the nanopores of these composites. Laser irradiation of AuNR@MOF@CPT particles at 808 and 660 nm induced two types of phototherapeutic effect. The first one was the PTT effect, with the solution temperature increasing up to 54.8 ± 1.2 °C over a short period of time. Moreover, temperature rise promoted release of CPT. In the case of irradiation at 660 nm, considerable PDT effect was observed. Thus,

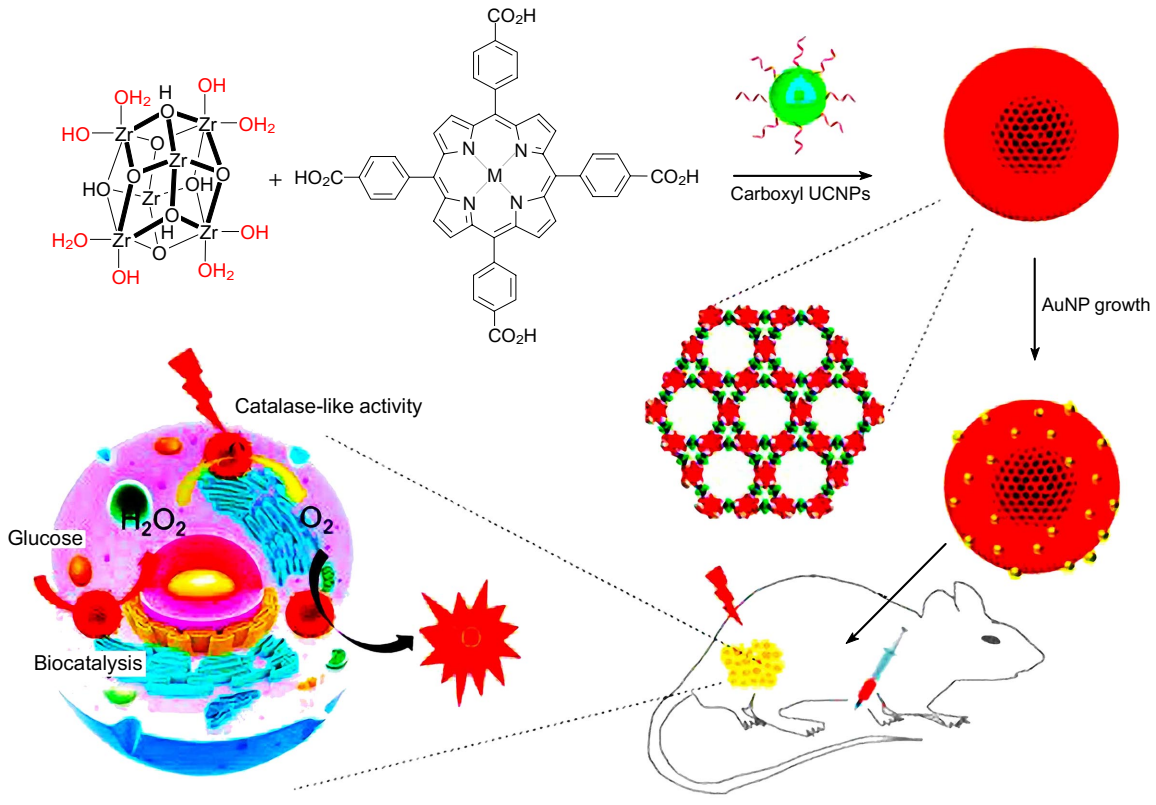


Figure 59. Preparation scheme of UMOFs@AuNPs nanoparticles.[187] Published with permission from the American Chemical Society.

AuNR@MOF@CPT particles proved to be a universal nanoplatform for cancer therapy, as they combined the synergistic antitumour effect of PDT and PTT with the chemotherapeutic action of camptothecin loaded into the MOF pores. During 50 days after treatment with AuNR@MOF@CPT particles, the authors observed almost complete destruction and disappearance of the tumour in mice.

Zhao *et al.*[191] obtained Fe-TCPP/Fe_2O_3 nanorice type nanocomposites based on porphyrin MOF and Fe_2O_3 nanoparticles. Encapsulation of these systems into erythrocyte membranes reduced phagocytosis of nanoparticles by macrophages and increased the nanoparticle stability and blood circulation time. The presence of iron cations in MOF nodes and Fe_2O_3 nanoparticles provided for processes similar to enzymatic catalysis, which result in generation of oxygen, thus overcoming the hypoxic environment in the tumour tissue. Owing to the high porosity, the FeTCPP/Fe_2O_3 nanorice had numerous active sites, which enhanced the PDT effect. Moreover, apart from the erythrocyte membrane, AS1411 aptamer vector molecules were introduced into the FeTCPP/Fe_2O_3 composite. In combination, this led to a high concentration of these particles in tumour cells. The resulting FeTCPP/Fe_2O_3 vector nanosystems demonstrated excellent therapeutic anticancer effect and also high biocompatibility and small number of side effects.

An interesting example of Mn^{III}-TCPP metal-organic framework was reported by Wan *et al.*[192] Initially, this system was inert for theranostics; however, as a result of endocytosis by tumour cells induced by intracellular glutathione (GSH), Mn^{III}-TCPP underwent a redox reaction to give manganese(II) and free TCPP. The resulting Mn^{II} cations acted as the contrast agent for magnetic resonance imaging (MRI), which allowed precise determination of the tumour position. Simultaneously, these cations participated in the nanocatalytic reaction with cellular H_2O_2, which gave O_2 and enhanced the PDT process involving free porphyrin **3**.

Chen *et al.*[193] described the multifunctional composite CHC-PZM@HA consisting of Zr^{IV}-containing MOF based on hyaluronic acid (HA)-coated TCPP, with inserted α-cyano-4-hydroxycinnamate, a monocarboxylate transporter affecting energy metabolism pathways in tumour cells. The system fabricated in this way was effective for PDT, as it mitigated the adverse consequences of hypoxia in tumour cells by changing cell metabolism and decreasing the tumour oxygen consumption. The presence of hyaluronic acid in CHC-PZM@HA particles facilitated the targeted delivery of photosensitizer molecules to tumour cells.

Ultrathin 2D nanosheets (approximately 5.1 nm thick) of the Cu-TCPP-MOF based on the copper TCPP complex were successfully used as a new class of theranostic material for PDT.[194] These sheets containing copper cations both in the porphyrin macrocycle and in the nodes showed synergistic effect for the PDT of cancer owing to their ability to generate ROS, together with the pronounced absorption in the near-IR range associated with d–d transitions in copper(II) complexes. The thermal effect observed upon 808 nm laser irradiation of Cu-TCPP-MOF sheets ensured the use of this MOF as an efficient agent for both MRI and PTT. The authors noted good biocompatibility of this material in *in vitro* and *in vivo* experiments.

Wang *et al.*[195] found peroxidase-like catalytic activity of ultrathin 2D Cu-TCPP nanosheets. Unlike other MOFs used for biological purposes, Cu-TCPP nanosheets, which were obtained using surfactants, have the optimal size for endocytosis and can be easily taken up by tumour cells. The Cu-TCPP particles caused destruction of excess GSH around the tumour by reducing the Cu^{II} cations in the chelate to Cu^{I}. The Cu^{I} cations thus formed catalyzed the Fenton reaction to give highly toxic hydroxyl radicals from endogenous H_2O_2 and generated superoxide anions from free O_2 in tumour cells, which subsequently generated $^1O_2$ *via* the Russell mechanism. It is noteworthy that 2D Cu-TCPP structures demonstrated high biocompatibility and the absence of side effects in *in vivo* experiments; therefore, they can be considered as a new therapeutic agent for the treatment of malignant neoplasms.

Two-dimensional nanoparticles of porphyrin-based MOF, $\{Cu_2(Zn\text{-}TCPP)\cdot H_2O\}_n$, obtained from Zn^{II}-TCPP complex and Cu^{II} cations, which can be activated by hydrogen sulfide signalling molecules, were proposed for targeted delivery of photosensitizer to tumour cells.[196] The paramagnetic Cu^{II} cations coordinate H_2S molecules, which are present in adenocarcinoma cells, thus performing the targeted delivery of porphyrin ligands and generation of ROS at the tumour site. The framework $\{Cu_2(Zn\text{-}TCPP)\cdot H_2O\}_n$ also proved to be a promising material for PDT.

Wan *et al.*[197] developed and presented the nanoplatform L-Arg@PCN@Mem based on Zr^{IV}- and porphyrin-based framework PCN-224, L-arginine (L-Arg) and cancer cell membranes (Mem). This platform demonstrated a synergistic therapeutic effect combining nitric oxide gas therapy and PDT. Nitric oxide performs an important connecting function in the body and participates in many physiological reactions, including cardiovascular homeostasis, immune response to infection and angiogenesis. In addition, at high concentrations (>1 μmol L^{-1}), NO exerts antitumour action by damaging mitochondria and DNA of tumour cells owing to high oxidative properties. L-Arginine placed into the pores of framework PCN-224 served as the source of NO. Under the action of NO synthase enzyme, L-arginine is converted to the target gas molecules.[197] Moreover, L-Arg can react with ROS, which are formed upon laser irradiation of the porphyrin metal-organic framework, to give an additional amount of NO. Owing to the coating by cancer cell membrane, L-Arg@PCN@Mem nanoparticles are specifically concentrated in the tumour. The synergistic therapeutic effect of the particles was confirmed by *in vivo* experiments, which suggest that the presented nanoplatform can serve as a potential antitumour agent in the hypoxic microenvironment.

It was shown[198] that tumour cells require large amounts of glucose for the growth and propagation; therefore, they are highly sensitive to the intracellular glucose level. In view of this fact, glucose starvation therapy was proposed.[199] This approach is based on the use of glucose oxidase (GOD) enzyme, which splits glucose in cancer cells and converts it to H_2O_2 and gluconic acid, thus controlling the tumour growth. The multifunctional nanosystems PCN-224(Cu)-GOD@MnO_2 based on copper-containing 3D framework PCN-224(Cu) and glucose oxidase coated by a MnO_2 layer demonstrated highly efficient antitumour action in both *in vitro* and *in vivo* experiments (Fig. 60).[199]

This system can consume glucose in the vicinity of the tumour to release hydrogen peroxide, which then reacts with Cu^{I} ions that are formed upon the redduction of Cu^{II} ions present in the metal-organic framework with endogenous glutathione. The reaction of Cu^{I} with H_2O_2 results in the generation of toxic OH^- ions. Meanwhile, the Russell

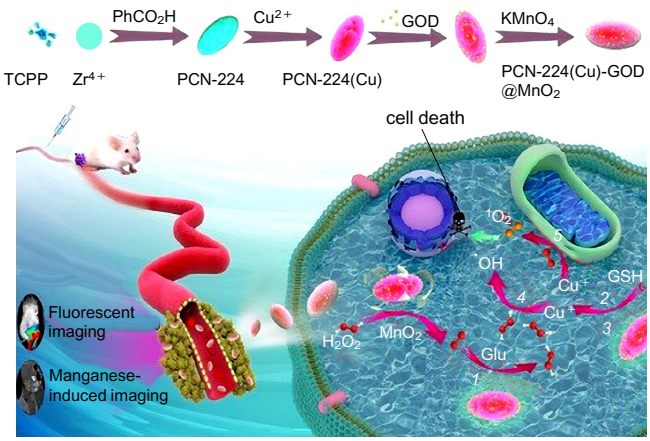


Figure 60. Main stages of the synthesis and mechanism of antitumour action of the PCN-224(Cu)-GOD@MnO_2 nanoplatform.[199] (*1*) Conjugated GOD; (*2*) GSH depletion; (*3*) chelated Cu^+; (*4*) Fenton reaction; (*5*) Russell mechanism. Published with permission from the American Chemical Society.

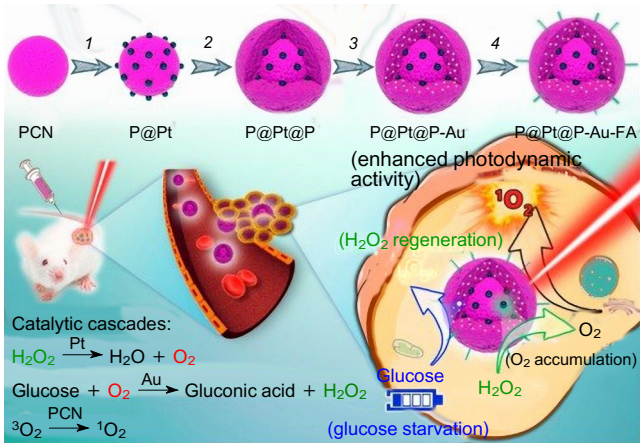


Figure 61. Preparation and mechanism of synergistic therapeutic action of P@Pt@P-Au-FA nanoreactors.[201] (*1*) Catalase mimicking Pt nanoparticles; (*2*) PCN; (*3*) glucose oxidase-mimicking Au nanoparticles obtained *in situ*; (*4*) folic acid. Published with permission from the American Chemical Society.

reaction of Cu^I, O_2 and H_2O leads to generation of singlet oxygen. The upper layer of the particles consisting of MnO_2 not only helps to avoid the conjugation of glucose oxidase to damage normal cells, but also catalyzes the generation of O_2 from H_2O_2, thus enhancing the glucose oxidation by the enzyme. The biocompatibility of the PCN-224(Cu)-GOD@-MnO_2 nanoplatform was confirmed by *in vivo* experiments.

Li *et al.*[200] developed a cascade nanobioreactor, Mem@catalase@GO_x@PCN-224 (mCGP), meant for the treatment of cancer due to the synergistic effect of the glucose starvation therapy and PDT. This system is formed by incorporation of the glucose oxidase and catalase enzymes into the membrane shell coating the porphyrin-based framework PCN-224. Due to biomimetic surface functionalization, mCGP particles are largely taken up and retained in cancer cells. In addition, after penetration into parts of the tumour, the enzymes present in mCGP start to catalyze the conversion of endogenous H_2O_2 to O_2, which subsequently facilitates decomposition of intracellular glucose and, upon irradiation with light, it is converted into cytotoxic singlet oxygen. Thus, the mCGP nanoreactor exhibited a potent synergistic therapeutic effect combining glucose starvation therapy and PDT, with the growth of cancer cells being inhibited even after a single injection.

According to the results of studies, the use of artificial nanoenzymes is often more favourable than the use of natural analogues, because the former are more chemically stable and are much less expensive for similar performance characteristics. A new type of nanoreactors P@Pt@P-Au-FA was developed using Zr^{IV}-containing porphyrin MOF (PCN) and nanoenzymes[201] (Fig. 61). Polyvinylpyrrolidone (PVP)-coated Pt nanoparticles mimicking the action of catalase were placed into the PCN framework (P@Pt) and then a layer of porphyrin-based MOF was again deposited to give the P@Pt@P sandwich structure. Then ultrasmall gold nanoparticles (Au-NPs) mimicking the action of glucose oxidase were inserted into the PCN shell where covalent binding to folic acid (FA) simultaneously takes place for increasing the physiological stability. It was shown that the integrated Pt nanoparticles catalyze the conversion of hydrogen peroxide to O_2, thus decreasing the hypoxia in the tumour microenvironment and simultaneously enhancing the effects of PDT (caused by the PCN framework) and glucose starvation therapy, which was provided by the embedded gold nanoparticles. Thus, the presented P@Pt@P-Au-FA nanoreactors have a pronounced antitumour action owing to combination of enzyme-catalyzed cascade reactions and the PDT effect.

In addition to the above examples, porphyrin-based MOFs can also be used in other fields of medicine, for example, for the development of antibacterial drugs. Thus, nanocomposites Ag/Cu-TCPP(Cu) were obtained from the spherical Cu-TCPP(Cu) particles containing copper(II) TCPP complex as the organic ligand with encapsulated silver nanoparticles.[202] These composites were found to promote wound healing *in vivo*; their antibacterial effect was higher than that of penicillin, while the cytotoxicity was lower compared to that of free Ag nanoparticles.

Liu *et al.*[203] obtained the composite nanocatalyst Cu-TCPP(Fe)/GOD with antibacterial action by physical adsorption of GO_x on the surface of ultrathin two-dimensional framework Cu-TCPP(Fe). This composite, together with glucose oxidase, can continuously convert non-toxic glucose to gluconic acid and H_2O_2, which decreases the pH of the medium from 7 to $\sim 3-4$ and sharply activates its peroxidase-like activity. Then the formed H_2O_2 is converted to toxic OH radicals *via* the Fenton reaction involving Cu and Fe cations. Experiments *in vitro* and *in vivo* demonstrated that the nanocatalyst Cu-TCPP(Fe)/GOD has low biotoxicity and fairly strong antibacterial effect.

Thus, it was shown that the application of porphyrin-based MOFs not only eliminates the drawbacks inherent in porphyrin molecules under physiological conditions (instability and self-quenching of excited states), but also produces a synergistic effect owing to combination of the benefits of MOFs and the properties of porphyrin derivatives. The materials corresponding to biomedical requirements are obtained using various approaches: insertion of heavy metal atoms, control over the particle size and modification with target molecules or their functional components to obtain composites. These approaches increase the efficacy of porphyrin-based MOFs in PDT. However, the application of only one therapeutic method often does not produce the optimal treatment efficacy, as

any approach has its own limitations and side effects such as drug resistance, poor tissue penetration, oxygen dependence, non-specific heating, *etc*. For this reason, considerable research efforts are directed towards the development of multifunctional nanoplatforms meant for the use in two or more therapeutic methods. In some cases, PDT is combined with other methods of treatment, including chemotherapy, PTT, gas therapy, radiotherapy, glucose starvation therapy.

3.4. Utilization of CO_2

The use of porphyrin MOFs as promising materials for the capture, storage and utilization of CO_2 is an important area of modern technology.

Nandi and Goldberg[204] synthesized the MOF $[(Zn\text{-}TCPP)_2(CO_2)(Pr_2Na_3(NO_3)(H_2O)_3)]_n \cdot Solv$, in which the two-layer coordination networks of zinc porphyrins are linked to one another by heterometallic praseodymium and sodium clusters (Fig. 62). The CO_2 molecules are arranged between two neighbouring five-coordinate zinc atoms. In the authors opinion, the conditions of synthesis of this MOF rule out the possibility of formation of CO_2 in the solvothermal reaction, and carbon dioxide molecules are of atmospheric origin.

According to calculations,[83] the geometric parameters of *meso*-tetrakis[3,5-bis[(4-carboxy)phenyl]phenylporphyrin (**10**) perfectly fit to MOF topology needed for capturing carbon dioxide. The structure of the framework based on this ligand has definite positively charged centres — metal atoms that are capable of bidentate binding of the linear CO_2 molecule. However, in this case, the formation of CO_2 molecules was explained particularly by decomposition of solvent molecules during the reaction.

It is noteworthy that the nature of the metal centre in this MOF plays the crucial role in CO_2 capturing, because porphyrin molecules in these frameworks have different conformations depending on the nature of the metal centre. In the case of zinc, peripheral substituents in porphyrin are arranged non-linearly as propeller blades; therefore, the metal clusters in the nodes are located too far from one another to bind CO_2 molecules. The introduction of a cobalt atom into the porphyrin ring gives rise to a saddle conformation of the ligand. This affords the UNLPF-2 structure, which is perfect for trapping CO_2 (Fig. 63). Satisfactory characteristics of this sample for the release and recapture of CO_2 molecules were noted.[81]

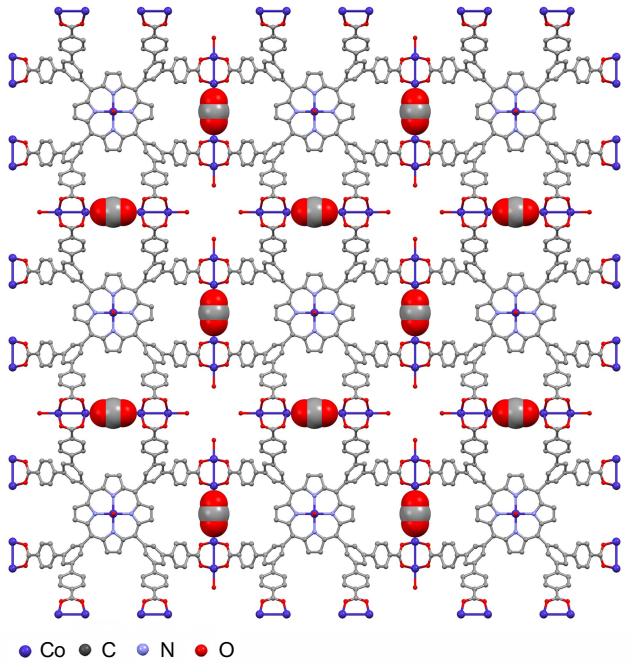


Figure 63. Structure of the framework UNLPF-2.[83] Published with permission from Wiley.

3.5. Photocatalytic production of hydrogen

The increasing energy demand of mankind and the search for alternative environmentally safe energy sources stimulated active development of new methods for production of molecular hydrogen in the beginning of the 21st century. One of such methods is photocatalytic water splitting,[205] which is similar to photosynthesis and includes similar steps: photoexcitation, charge separation and transfer and redox reaction.[178, 206, 207] The mechanisms of these processes attract particular research attention.[208] It is evident that implementation of these processes requires MOFs capable of most efficient absorption of solar radiation; high molar absorption coefficients of porphyrins help to solve this task.

The use of frameworks Al-TCPP and Al-TCPP-Zn containing TCPP or its zinc(II) complex and aluminium oxide hydroxide clusters as the nodes gave rise to a material capable of hydrogen photogeneration.[41] It is important that in this case, MOF is only a part of a complex catalytic

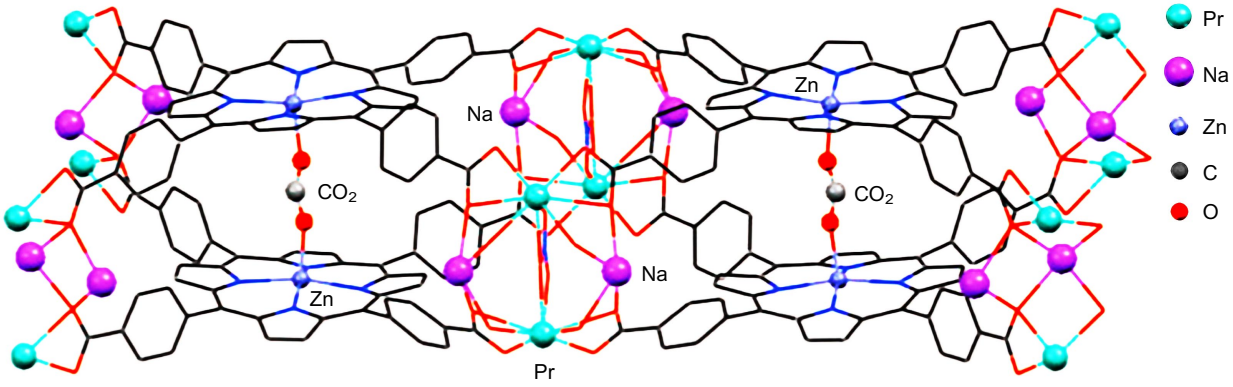


Figure 62. Fragment of the framework $[(Zn\text{-}TCPP)_2(CO_2)(Pr_2Na_3(NO_3)(H_2O)_3)]_n$ with the coordination of CO_2 molecule between two Zn^{2+} cations of neighbouring metal porphyrins.[204] Published with permission from the Royal Society of Chemistry.

system, which also includes a platinum catalyst, methylviologen and ethylenediaminetetraacetate (EDTA). The functions of porphyrin molecules **3** are to harvest solar light and generate electrons, which are accepted by methylviologen. Later, it was shown that platinum atoms can be inserted into the cavity of porphyrin **3** in Al-TCPP during post-modification, and thus the photocatalyst activity increases.[209] The amount of hydrogen generated in the presence of these catalytic systems reach up to 200 μmol g^{-1} h^{-1} for 3 h. In addition, there are examples of using MOF based on platinum porphyrin complex as a sensitizer and an active catalytic site.[210,211]

This trend was further developed by preparing similar MOFs based on indium(III) clusters[212] owing to specific electronic structure of indium cations.[213] The series of MOFs USTC-8 containing indium, cobalt, nickel and copper cations as porphyrin metal centres were synthesized. These structures proved to be active photocatalysts for water splitting. Leng *et al.*[212] proposed an unusual catalytic cycle mechanism involving USTC-8(In) framework in which the metal centre serves as the electron transporter. The authors suggested that photoactivation was accompanied by the reduction of indium, metal elimination from the porphyrin ring and the subsequent metal oxidation upon the electron transfer, which finally results in regeneration of USTC-8(In).

Special mention should be made of the two-dimensional framework PtSA-MNSs formed by platinum(II) tetracarboxyphenylporphyrin and nodal copper(II) carboxylate clusters.[214] It was found that the layered structure of this MOF promotes efficient generation of hydrogen, while the platinum atoms of the metal complex act as reducing centres for protons. An example of simultaneous non-stoichiometric introduction of platinum and iridium atoms into a PCN-222-related MOF is known. This provided unique efficiency of the photocatalytic generation of hydrogen by water splitting induced by visible light.[215]

Further enhancement of the photocatalyst performance for the generation of hydrogen is associated with the design of more complex hybrid materials based on porphyrin MOFs and inorganic compounds. The coordination of the disulfide complex of iron carbonyl [4-(i-SCH_2)$_2$$NC(O)C_5H_4N$]-[$Fe_2(CO)_6$] containing a terminal pyridine substituent to the metal centre of MOF based on zinc(II) tetracarboxyphenylporphyrin gave rise to an efficient photostable material.[17] The bond strength between the iron complex and zinc porphyrin was sufficient for this pair to act as a single electron mediator.

3.6. Proton and electronic conduction

Metal-organic frameworks, including porphyrin-based MOFs, are highly efficient as proton-conducting materials owing to unique set of geometric and chemical parameters of the framework that can be tuned by varying the coordination behaviour of binding metal cations and to stability and easy modification of the organic moiety. One more benefit of using these structures as proton conductors is their high crystallinity, which allows unambiguous determination and modelling of interaction of framework components or functional groups with one another or with potential proton carriers, which is necessary for detailed study of the conduction mechanisms, using X-ray diffraction methods.

In 2013, Kitagawa and co-workers[216] showed that a nanofilm of a Cu^{II}-TCPP-based MOF containing copper cations as the nodes deposited layer-by-layer on a patterned Cr/Au electrode has a proton conductivity of 3.9×10^{-3} S cm^{-1} at 98% a relative humidity (RH) and room temperature. In the authors' opinion, this high proton conductivity is due to the pore size of pre-synthesized 2D layers of the framework, highly oriented thin film morphology of the MOF on the electrode and the presence of numerous axial groups on the nanosheets (water molecules coordinated to copper(II) cations and uncoordinated carboxy groups) (Fig. 64).

The metal-organic framework BUT-83 obtained from cobalt 5,15-bis(4-carboxyphenyl)-10,20-di(4-pyridyl)porphyrin complex was fabricated *via* the axial coordination of pyridine N-donor groups to the cobalt cation of the neighbouring macrocyclic molecule.[217] This material had a outstanding proton conductivity of 3.9×10^{-2} S cm^{-1} at a temperature of 80 °C and RH of 97%. In this case, high conductivity was ensured by free carboxyl groups not involved in the MOF formation (Fig. 65).

Modification of the porphyrin periphery by pyrogallol moieties, each containing three hydroxy groups, allowed Wu *et al.*[217] to obtain new MOFs ZrPP-*n* [*n* = 1, 5,10,15,20-tetrakis(3,4,5-trihydroxyphenyl)porphyrin; *n* = 2, 5,10,15,20-tetrakis(3′,4′,5′-trihydroxybiphenyl-4-yl)porphyrin] (Fig. 66).

The inorganic nodes of the 3D framework were formed by zirconium(IV) coordination chains connected through porphyrin macrocycles. This structure, together with partially protonated 1,2,3-trihydroxybenzene moieties, water molecules and dimethylammonium cations, which counterbalanced the lattice charge, accounted for high proton conductivity at 25 °C and 98% RH: 8.0×10^{-3} and 4.2×10^{-3} S cm^{-1} for the ZrPP-1 and frameworks ZrPP-2, respectively. The authors noted high chemical stability of these materials in comparison with known MOFs formed by the interaction of the carboxyl groups of the organic ligand with zirconium cations.[218]

The stability of MOFs can be increased by using phosphonate-substituted porphyrins organic moiety. Their advantage is the presence of three oxygen atoms capable of coordination to metal cations and, hence, formation of more diverse MOF structures. Moreover, phosphonate groups can form hydrogen bonds with proton carrier molecules and participate in proton transfer during conduction. In addition, metal phosphonates are known to be more stable than carboxylates in aqueous media and at

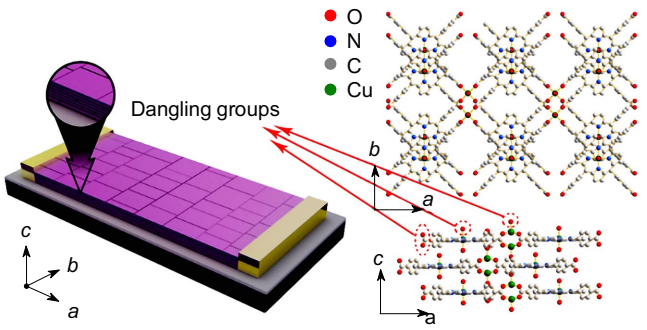


Figure 64. Illustration of electrode-deposited MOF nanosheet based on Cu^{II}-TCPP (*a*) and modelled crystal structure of this nanosheet in two projections (*b*).[215] Published with permission from the American Chemical Society.

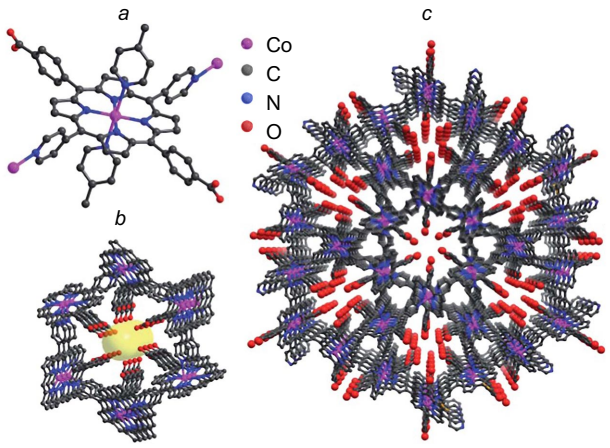


Figure 65. Structure of the framework BUT-83: coordination environment of cobalt 5,15-bis(4-carboxyphenyl)-10,20-di(4-pyridyl)porphyrin (*a*) and images of 1D channel (*b*) and 3D framework along the *c* axis (*c*).[217] Published with permission from the Royal Society of Chemistry.

elevated temperatures, which is also promising for using them as proton conductors.

The MOF Ni-CAU-29 based on 5,10,15,20-tetrakis(4-phosphonatophenyl)porphyrinate of nickel containing nickel cations in the framework nodes described by Rhauderwiek *et al.*[97] had a moderate proton conductivity of 5.62×10^{-6} S cm^{-1} at 80 °C and 90% RH.

We developed a synthetic approach, which was used to obtain the unique MOF IPCE-1Ni containing dimethylammonium cations in the framework pores and coordinatively unsaturated phosphonate groups.[102] Its structure determines the detected high proton conductivity of 1.55×10^{-3} S cm^{-1} observed at 75 °C and a of 80% RH. A directed change in the position of functional phosphonate groups in the nickel(II) porphyrin molecule from the *para*- to *meta*-position, with other reaction conditions being the same, resulted in the formation of the framework IPCE-2Ni with expectedly smaller pore size. In combination with the presence of uncoordinated phosphonate groups directed inside the channels and the presence of dimethylammonium cations, this gave a high proton conductivity of 1.0×10^{-2} S cm^{-1} at 75 °C and of 95% RH.[103] This value is comparable the highest values within all MOFs described previously. The replacement of nickel(II) cation in the porphyrin molecule by palladium(II) cation, resulting in the formation of the dense layered IPCE-2Pd structure, considerably changes the MOF stability and proton-conducting characteristics compared to those of the nickel analogue IPCE-2Ni.[104] More rigid structure of IPCE-2Pd ensures higher thermal and hydrolytic stability of the sample up to 95 °C; this results in proton conductivity comparable to that of IPCE-2Ni: 8.11×10^{-3} S cm^{-1} at 95 °C and 95% RH.

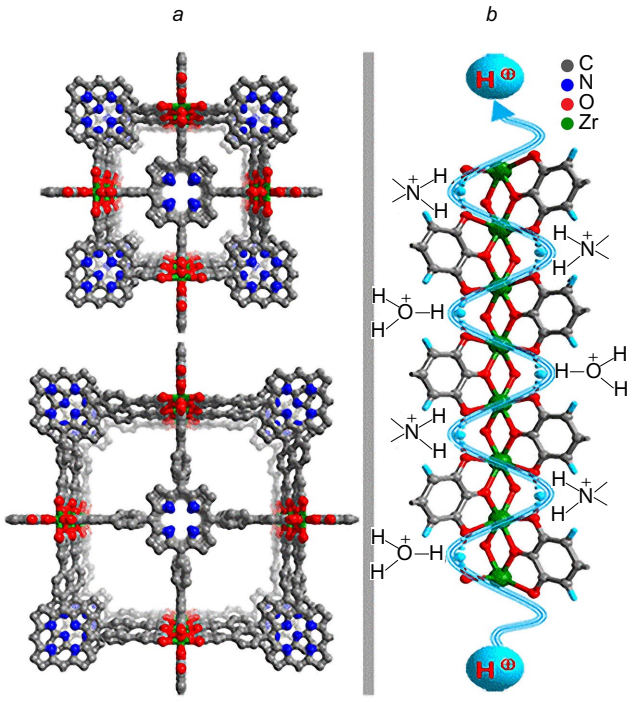


Figure 66. Structure of the frameworks ZrPP-1 and ZrPP-2 (*a*) and possible proton transfer mechanism in these materials (*b*).[218] Published with permission from the American Chemical Society.

Apart from proton conductivity, some publications[105,219] note semiconductor properties and electronic conductivity for porphyrin-based MOFs. Indeed, porphyrin-based frameworks absorb light in the range of 600–800 nm, which corresponds to a band gap (E_g) of 1.55–2.07 eV typical of semiconductors.

Often, electronic conductivity appears in a material only after visible light irradiation as a result of photoexcitation of porphyrin ligands. Tian *et al.*[220] reported high photoconductivity of an oriented thin film based on indium-oxo chains and TCPP. It was found[221,222] that the conductive properties are improved after modification of MOF using dopants such as fullerenes. In a theoretical study published in 2020, Pratik *et al.*[221] showed that the crystal structure of PCN-222 and PCN-222-Zn makes it possible to generate a charge-separated state as a result of electron localization on one porphyrin moiety and hole localization on the other one. The band gap in the isostructural frameworks depends on the presence or absence of a transition metal cation in the porphyrin cavity. The same publication gives calculations of E_g for frameworks with guest molecules, in particular fullerene C_{60} molecules, in the pores. According to calculations, in this situation, the frameworks become conductive and the band gap considerably decreases. Indeed, it was shown[222] that the photocurrent markedly increases when C_{60} molecules are introduced into PCN-222.

A combination of the oriented film of zinc porphyrin-based MOF and C_{60} guest molecules also increased the material photoconductivity owing to better charge separation.[223] The mechanisms of energy transfer and charge separation and transfer in porphyrin-containing MOFs are considered in detail in a review[219] published in 2021.

3.7. Films based on metal-organic frameworks

The unique structure and application potential of porphyrin-based MOFs affect the modern chemistry of materials, the main goal of which is to design and fabricate functional layered systems on the surfaces; moreover, these structures could be controlled on a nanoscale.[31,224–226] These materials have gained popularity in recent years and are called SURMOF (surface-supported metal-organic frameworks). However, the control of their size at the

nanolevel and their deliberate positioning on the surface are still challenging problems.

The Langmuir–Blodgett method is one of the most convenient approaches for fabricating ordered monolayers on a liquid surface. Makiura and Kitagawa [227] reported the preparation of oriented nanofilm NAFS1 based on the Co-TCPP complex on the surface of an aqueous solution of copper chloride, which was then transferred on a solid silicon surface. Two-dimensional structures of TCPP and binuclear clusters of divalent metals (Zn^{2+}, Cu^{2+}, Co^{2+}) are of particular interest for the fabrication of films owing to weak bonds between the layers and strong bonds within the layers. Powder X-ray diffraction data for such film attested to highly ordered positions of molecules; and the authors carried out structure calculations for the formed MOF (Fig. 67).

Using TCPP free base as the organic ligand, Soichiro *et al.*[228] succeeded in preparing NAFS-2 film (Fig. 68). In the reaction between porphyrin solutions and a solution of copper chloride, no metallation of the porphyrin cavity took place. According to powder X-ray diffraction data, this film contained water molecules axially coordinated to the binuclear copper complex in the MOF nodes.

Later, the same authors [229] proposed a modular approach to the formation of ordered thin films on solid substrates, consisting of two stages. The modularization stage included the synthesis of porphyrin-based MOF by any known method and the second stage included fast assembly of the MOF modules into a highly oriented thin film (Fig. 69). In this study, the initial MOF nanoplates were synthesized by the reaction of TCPP with copper nitrate under solvothermal conditions. Subsequently, the material was dispersed in ethanol or water under sonication to give a colloidal suspension. The suspension was deposited dropwise on a water surface, which is a perfectly planar substrate; due to their hydrophobic properties, nanosheets of porphyrin MOFs were spontaneously distributed over the surface and thus formed a thin film. This process was repeated for a definite number of times, and then the thin film was transferred on a solid substrate by stamping (Fig. 70). Using powder X-ray diffraction, the authors determined the film structure (Fig. 71), which contained

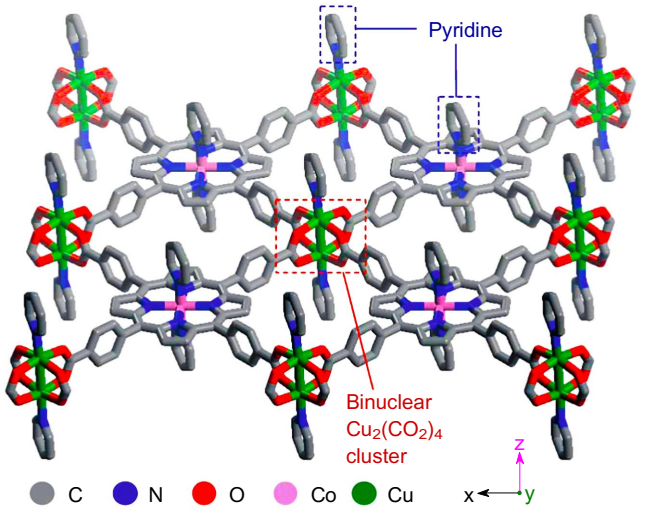


Figure 67. Calculated structure of the NAFS-1 film.[227] Published with permission from Wiley.

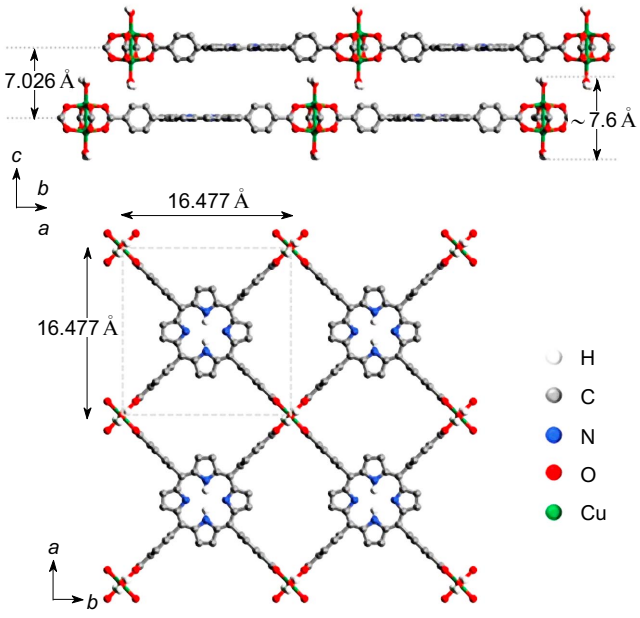


Figure 68. Calculated model structure of the NAFS-2 film along two directions.[228] Published with permission from the American Chemical Society.

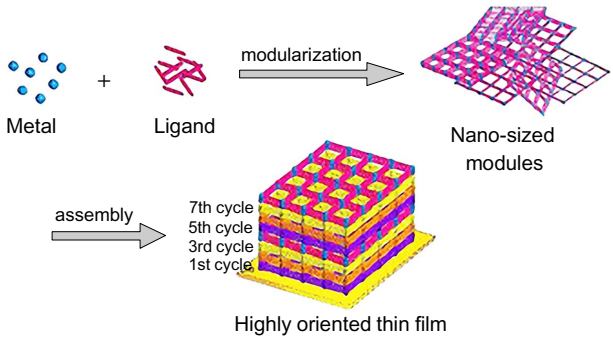


Figure 69. Modular design of porphyrin-based thin films.[229] Published with permission from the American Chemical Society.

water molecules coordinated to copper cations both in the porphyrin cavity and in the framework nodes.[229]

The presence of ordered water molecules in this material allowed the authors to study for the first time the proton conductivity of a film based on porphyrin-containing MOF.[216] The modular approach was also used in other studies [167, 230] to prepare a series of 2D films based on M^1-TCPP(M^2) frameworks ($M^1 = Co^{II}$, Cu^{II}, Zn^{II}; $M^2 = Zn^{II}$, $Fe^{III}Cl$). The films were <10 nm thick as a result of addition of a surfactant, *e.g.*, polyvinylpyrrolidone, capable of selective coordination to metal cations in the porphyrin cavity, during the synthesis (Fig. 72). In relation to the Cu-TCPP(Cu) thin film, the authors demonstrated benefits of using this material as a fluorescent sensor platform for detection of DNA.

Two-dimensional Zn-TCPP(Zn) nanosheets were obtained in a similar way in the presence of PVP surfactant;[231] they were shown to be applicable for the design of a synaptic transistor. In this case, a layer of 2D MOF acts as a

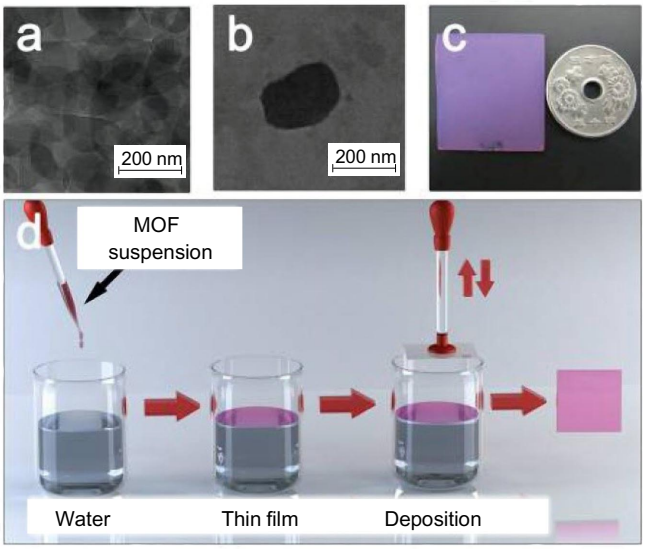


Figure 70. Modular design of a thin film of MOF based on Cu-TCPP and Cu^{2+} cations on a solid surface: TEM images of Cu-TCPP nanosheets (*a*, *b*), photograph of the thin film after 15 deposition cycles on a quartz substrate (*c*) and illustration of assembly process (*d*).[229] Published with permission from the American Chemical Society.

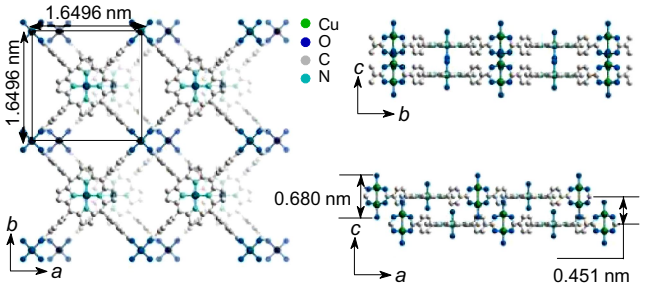


Figure 71. Structure of the Cu-TCPP- and Cu^{2+}-based film in three projections.[229] Published with permission from the American Chemical Society.

charge carrier trap; moreover, these nanosheets can trap both electrons and holes depending on the operation mode of the transistor.

Jian *et al.*[232] employed a modular approach to obtain a monolayer of a TCPP- and aluminium(III)-based MOF. A dispersion of single MOF nanosheets obtained by ultrasonic treatment of the suspension was deposited on a porous alumina layer. This gave a nanoporous membrane with an oriented MOF thin layer. Stability in water of the MOF based on TCPP and trivalent metal ions (Al^{3+}) made it possible to use this membrane for separation of ions in aqueous solutions.

According to one more efficient method for the preparation of oriented thin films with a controllable thickness, alternating solutions of structural components were deposited layer-by-layer onto functional substrates, with film thickness increasing with increasing number of growth cycles. So *et al.*[233] used this approach to prepare DA-MOF and L2-MOF films of porphyrin-based MOFs on a 3-aminopropyltrimethoxysilane (3-APTMS)-functionalized silicon substrate *via* binding to zinc cations (Fig. 73 *a*).

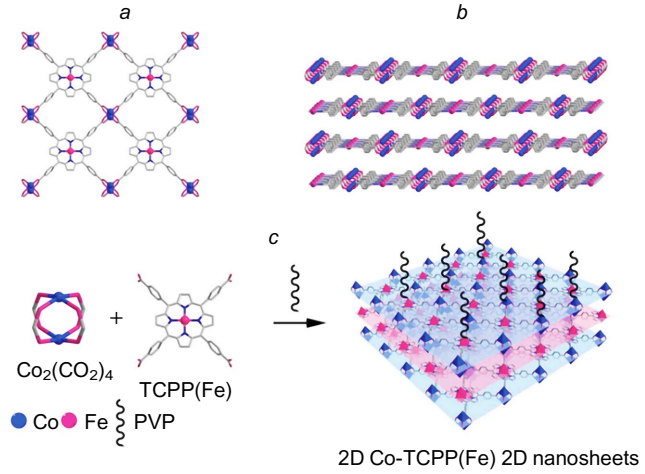


Figure 72. Structure of the Zn-TCPP(Zn) nanosheets along two directions (*a*, *b*) and synthesis of 2D layers of porphyrin MOF in the presence of a surfactant (*c*).[167, 230] Published with permission from Wiley.

Binding of the layers to one another to form 3D structures was accomplished by coordination of ditopic P1 and P2 ligands to metal cations (see Fig. 73 *b*,*c*). The authors controlled the number of growth cycles of films to obtain a material of a specified thickness. The strictly ordered arrangement of chromophores in these films was confirmed by the intensity of their fluorescence. It was shown that energy transfer towards the film periphery takes place due to the optical excitation of porphyrin molecules, which thus provides a basis for studying and using porphyrin-based films in solar energy conversion devices.

Subsequently, Liu *et al.*[234] designed operating solid-state photoelectric materials containing thin films of porphyrin-based MOFs. These films exhibited excellent photophysical properties, including high mobility of charge carriers and unusually high efficiency of charge carrier generation.

Similar layer-by-layer assembly on a functionalized silicon substrate was used to obtain an oriented thin film based on indium-oxo chains and TCPP (Fig. 74 *a*).[220] It was shown that this film can be used as a highly sensitive photodetector. The geometry of the inorganic building units is the key factor for the formation of SURMOF, determining the organization of porphyrin macrocycles and, as a consequence, the photodetector efficiency. The film virtually did not conduct current in the dark, while optical excitation of porphyrins in the light gave rise to a photocurrent. This photodetector showed a stable and reproducible on/off photocurrent when irradiated with a periodic light pulses (see Fig. 74 *b*).

The photoconductivity of films of porphyrin MOFs can also be increased by introducing guest molecules into the pores of SURMOF. It was shown[223] that combining an oriented MOF film based on zinc porphyrin with C_{60} guest molecules results in charge separation in the material and, as a consequence, markedly increases the material photoconductivity. Upon light absorption, porphyrin macrocycles are transferred to the excited state, which is followed by fast charge separation due to high electron affinity of fullerene species. This behaviour was confirmed by density functional theory calculations.

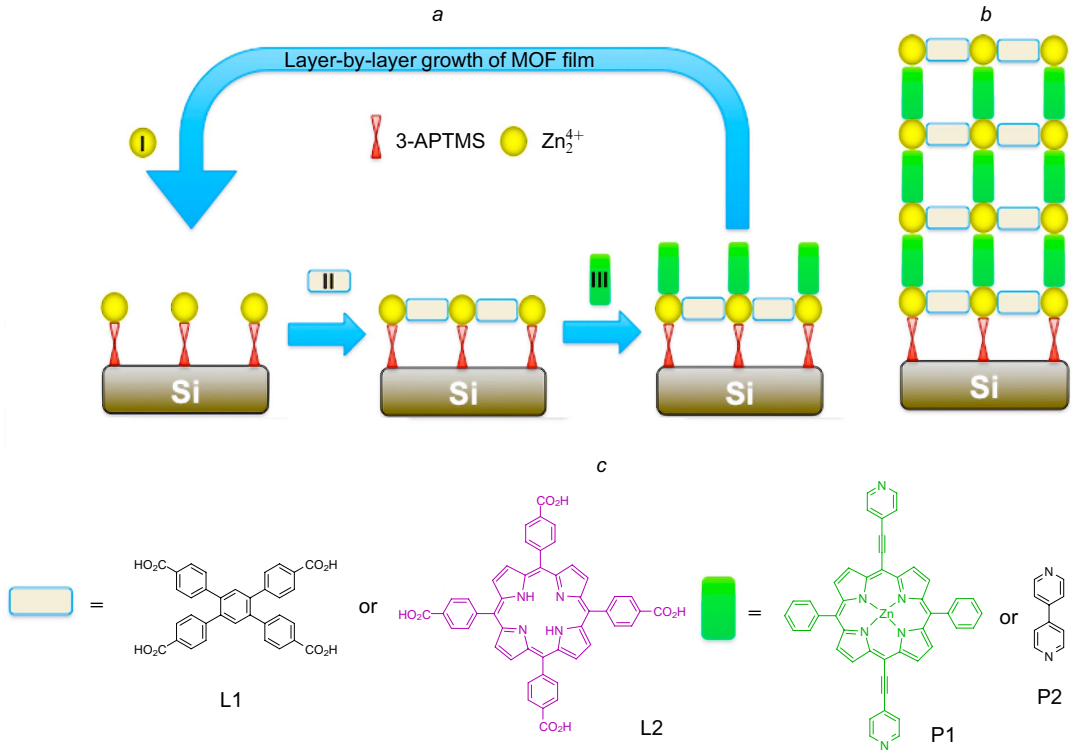


Figure 73. Layer-by-layer fabrication of DA-MOF and L2-MOF films on the silicon surface (*a*), film after three growth cycles (*b*) and building units used for the formation of films (*c*).[233] Published with permission from the American Chemical Society.

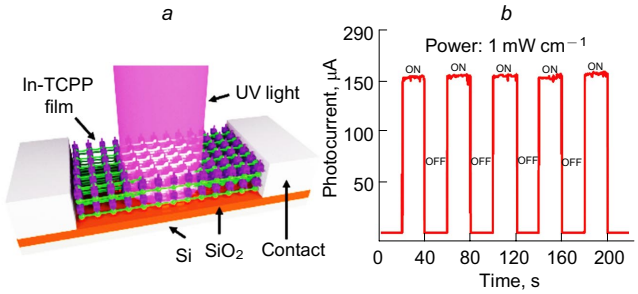


Figure 74. Scheme of a photodetector based on In-TCPP film (*a*) and time dependence of the photocurrent under periodic light pulse irradiation at 420 nm at a 10 V voltage (*b*).[220] Published with permission from Wiley.

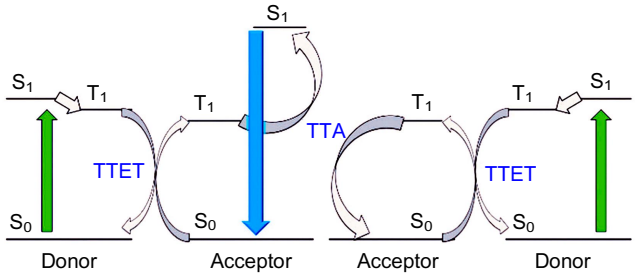


Figure 75. Mechanism of up-conversion based on triplet – triplet annihilation (see text).[235] S is singlet state, T is triplet state. Published with permission from the Royal Society of Chemistry.

The unique photophysical properties of porphyrins draw enhanced interest also in relation to their potential use as a new class of materials capable of efficient conversion of low-energy photons to higher energy photons in up-conversion processes *via* triplet – triplet annihilation.[235] The up-conversion consists in the transfer of photon energy absorbed by sensitizer (porphyrin) molecules to give triplet excited states to the emitter molecule *via* the triplet – triplet energy transfer (TTET). Then a pair of generated emitter triplets interact *via* triplet – triplet annihilation (TTA) and emit a photon with an energy higher than the energy of initially absorbed photons (Fig. 75). The efficiency of this process opens up broad prospects for its numerous applications ranging from solar energy conversion to chemical biology. Currently, highly efficient up-conversion of photon energy has been implemented for a broad range of chromophores such as non-solvent liquids, ionic liquids, amorphous solids, gels, supramolecular assemblies, molecular crystals, *etc.*[236–241]

The possibility of targeted design and, correspondingly, control over physicochemical and geometric properties of porphyrin MOFs is responsible for high attention to this class of compounds as sensitizers for up-conversion processes to control the molecular environment that is favourable for elucidation of the structure – property relationships. Oldenburg *et al.*[242] obtained for the first time a film consisting of three layers of different MOFs on a silicon substrate (Fig. 76). The upper and lower layers were structures based on 4,4′-(anthracene-9,10-diyl)dibenzoate with zinc cations in the nodes (layers A) acting as emitters. Sensitizer layer B was a MOF based on palladium(II) 5,15-bis(4-carboxyphenyl)-10,20-diphenylporphyrin with zinc

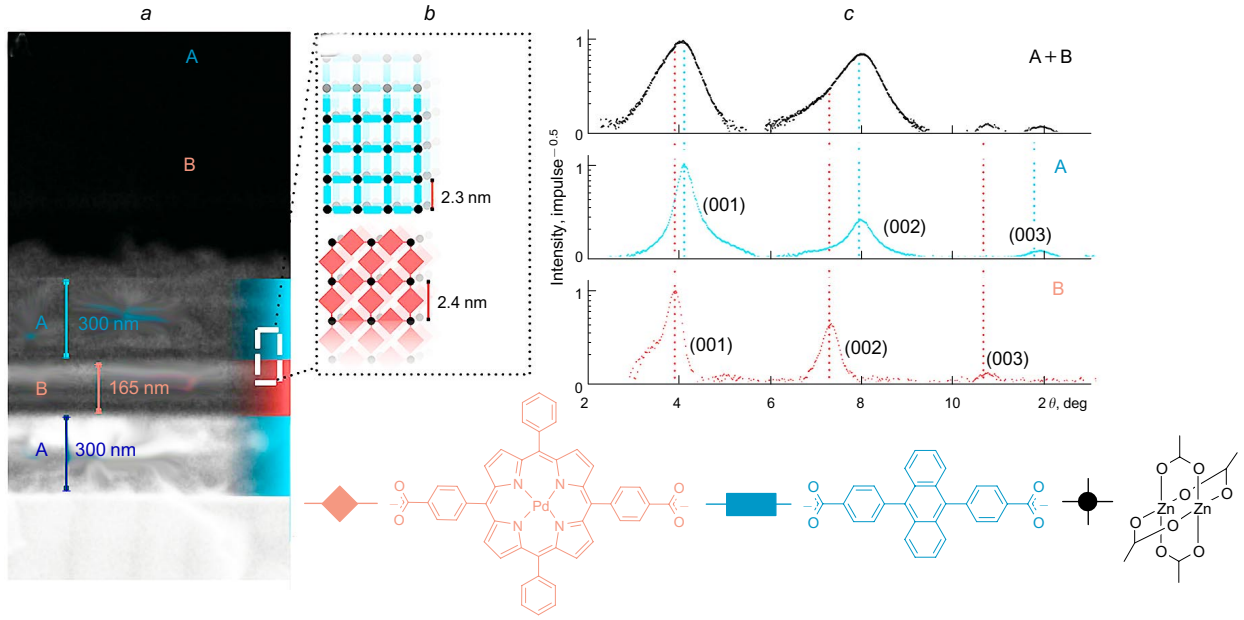


Figure 76. SEM images of the A – B – A three-layer film on a silicon substrate (*a*), diagram of the layers (*b*) and X-ray diffraction patterns in the (001) crystallographic direction: A – B – A films (on the top) and A (in the middle) and B (at the bottom) (*c*).[242] Published with permission from Wiley.

cations in the nodes. Despite low quantum yields of up-conversion (< 0.1%), the possibility of formation of emitter and sensitizer layers demonstrated in this study opens up prospects for improving the photophysical properties of such materials by changing the thickness of deposited layers, for overcoming sensitizer aggregation problem and for fabrication of controlled phase-separated structures in the heterostructures on various surfaces.

The same authors [243] studied the triplet exciton structure in an oriented film based on palladium(II) 15-bis(4-carboxyphenyl)-10,20-diphenylporphyrin and zinc cations, similar to layer A. They showed high rate of exciton transfer, which makes it possible to predict the theoretical diffusion of an exciton to a depth of several micrometres inside the material. In the film obtained by the authors, the exciton diffusion was restricted by the domain boundaries in the polycrystalline sample; therefore, the theoretical transport characteristics were not attained.

The exciton diffusion in the film was also studied in detail by Gu *et al.*[244] The authors obtained an oriented film of TCPP-based MOF with cobalt(II) ions in the nodes. Owing to the ordered proximate positions of porphyrin molecules in the film, the excitons efficiently hop between the macrocycles, which makes these films promising candidates for the manufacture of semiconductor materials.

Special mention should be made of numerous publications devoted to 2D nanoplates of porphyrin MOFs, which were obtained as amorphous nanoparticles without any substrate. These materials often have promising catalytic properties;[245, 246] they can be used simultaneously as MRI contrast agents and for generation of singlet oxygen [247] and as sensors for H_2S.[248] However, discussion of these issues is beyond the scope of this Section, which addresses only oriented crystalline SURMOF films deposited on various substrates.

In recent years, composite materials based on porphyrin MOFs have been actively studied. Thus 2D sheets of porphyrin-based MOF can be parts of hybrid materials with copper,[249] gold,[250, 251] and silver [252] nanoparticles, reduced graphene oxide,[253 – 255] other types of MOF [256 – 258] and textile fibres,[259] and can be parts of layered hydroxides,[260] which results in synergistic properties of materials of different classes and in new functional characteristics.

A separate task is to obtain electrochemically active thin films of porphyrin MOFs. Ahrenholtz *et al.*[261] were the first to grow a thin film directly on a conducting fluorinated tin oxide substrate using an alternative approach called solvothermal deposition. This method consists in adsorption of a self-assembled porphyrin layer on a substrate surface; the substrate is then kept in a solution of $CoCl_2 \cdot 6\,H_2O$, TCPP, pyridine and KOH under solvothermal conditions, which leads to MOF formation on the surface of tin oxide. The authors showed that this material is electrochemically active and stable for several hours. In addition, the mechanism of charge transfer was established and the catalytic activity of this material was successfully demonstrated in relation to the electrocatalytic reduction of CCl_4.

A similar approach was used [18] to obtain a thin film of TCPP-based MOF with zirconium cations in the nodes. Since porphyrin is not complexed with zirconium cations under these conditions, MOF formed in this way can serve as a platform for transmetallation of porphyrin molecules with other metals, in particular zinc and cobalt. The authors estimated the electrochemical activity of this material and demonstrated that a considerable redox signal appeared in all cases and could be tuned by introducing various metal cations, which provides for the use of this material in electrochemical processes.

For example, metal-organic materials based on TCPP complexes of catalytically active metals (Cu^{II}, Zn^{II}, Co^{II}) grafted to an electrode coated by a thin film of alumina were studied [19] as catalysts for electrochemical reduction of CO_2. The authors evaluated the electrochemical characteristics of these materials and found that the current density increased in all cases in CO_2-saturated solutions. Moreover, detailed analysis of the products by gas chromatography and NMR

spectroscopy made it possible to identify the types of chemical processes taking place in a nanoreactor based on the Co-TCPP complex and to determine the potential at which the selectivity to CO reached 76%.

A MOF film based on nickel(II) TCPP complex containing zirconium cations in the framework nodes obtained by solvothermal deposition on conductive tin oxide substrates was used for the first time for electrochemical oxidation of water.[262] This material was shown to possess unique ability to catalyze water oxidation owing to the presence of nickel cations in the porphyrin cavity, on the one hand, and to act as an efficient acceptor of the released protons by the nodal zirconium clusters, on the other hand.

4. Conclusion

The data analyzed in this review demonstrated that porphyrin MOFs are the most promising molecular platforms for targeted design of materials. The presented diversity of functional MOFs and their properties attests to unique potential for their application in heterogeneous catalysis and medicine, in energy transfer-related technologies, in sensorics and for traditional applications of porous frameworks: sorption and separation of gases and small molecules. It is clear that application prospects of MOFs based on substituted porphyrins will be markedly expanded in the near future with further development of synthetic chemistry of this class of compounds. Despite high yields of porphyrin MOFs in the described procedures (60–80%), there are difficulties regarding the industrial implementation of these processes, first of all, due to high cost. For this reason, development of approaches reducing the cost of MOF synthesis is a primary task. Meanwhile, it is shown in the review that porphyrin MOFs are versatile systems for the use in modern high-tech applications requiring small amounts of substances. Therefore, particular attention should be paid to advancement of methods for the preparation of thin-film MOFs (SURMOF) based on modified porphyrins, which, according to published data, are convenient building blocks for the fabrication of two-dimensional materials. A separate promising trend in the development of this area is the design of hybrid materials in which combination of porphyrin MOFs with various nano-objects gives rise to new application prospects in modern technologies. As indicated by numerous studies, this research area includes quite a few trends, and we are sure that this review will stimulate researchers specializing in various fields of chemistry and materials science to engage in this promising and fascinating subject.

Acknowledgments: The reported study was funded by RFBR, project number 20-13-50308.

5. List of abbreviations

The following abbreviations are used in the review:

abz — 4-aminobenzoate;

3-APTMS — 3-aminopropyltrimethoxysilane;

t-BA — *tert*-butyl acetate;

BDCPP — 5,15-bis(3,5-dicarboxyphenyl)porphyrin;

I_2-BDP — 8-(4-carboxyphenyl)-4,4-difluoro-2,6-diiodo-1,3,5,7-tetramethyl-4-bora-3a,4a-diaza-*s*-indacene;

BET — Bruanauer–Emmett–Teller;

BPDC — biphenyl-4,4-dicarboxylate;

bpy — 4,4′-bipyridine;

BTB — 1,3,5-tris(4-carboxyphenyl)benzene;

CPT — camptothecin;

DABCO — 1,4-diazabicylo[2.2.2]octane;

DBP — 5,15-bis(4-carboxyphenyl)porphyrin;

DCDBP — 5,15-bis(2,6-dibromphenyl)-10,20-bis(3,5-dicarboxyphenyl)porphyrin;

DCDPS — 4,4′-dicarboxydiphenyl sulfone;

dipy — 5,15-bis(pentafluorophenyl)-10,20-di(4-pyridyl)-porphyrin;

DMA — *N*,*N*′-dimethylacetamide;

DOX — doxorubicin;

DPNI — *N*,*N*′-di(4-pyridyl)naphthalene-1,4,5,8-tetracarboxydiimide;

DPT — 3,6-di(4-pyridyl)-1,2,4,5-tetrazine;

FA — folic acid;

EDTA — ethylenediaminetetraacetate.

E_g — band gap;

GOD — glucose oxidase;

GSH — glutathione;

HA — hyaluronic acid;

H_2bpydc — 2,2′-bipyridine-5,5′-dicarboxylic acid;

H_8TPPP — 5,10,15,20-tetrakis(4-phosphonatophenyl)-porphyrin;

H_8*m*TPPP — 5,10,15,20-tetrakis(3-phosphonatophenyl)porphyrin;

HCPP — 5,15-bis(4-carboxyphenyl)-10,20-bis(3,5-dicarboxyphenyl)porphyrin;

Mem — cell membrane;

MOF — metal-organic framework;

MRI — magnetic resonance imaging;

NIR — near-IR range;

PDT — photodynamic therapy;

PTT — photothermal therapy;

PVP — polyvinylpyrrolidone

RE — rare earth element;

RH — relative humidity;

ROS — reactive oxygen species;

SALE — solvent-assisted linker exchange;

SBU — secondary building unit;

sc — supercritical;

Solv — solvent;

SURMOF —surface-supported metal-organic framework;

TBHP — *tert*-butyl hydroperoxide;

TBCPPP — 5,10,15,20-tetrakis[3,5-bis(4-carboxyphenyl)phenyl]porphyrin;

TCBPP — 5,10,15,20-tetrakis(4-carboxybiphenyl)porphyrin;

TCPP — 5,10,15,20-tetrakis(4-carboxyphenyl)porphyrin;

TCP-1 — 5,10,15,20-tetrakis(4'-carboxybiphenyl-4-yl)-octaethylporphyrin;

TCP-2 — 5,10,15,20-tetrakis[4-(4-carboxyphenylethynyl)phenyl]octaethylporphyrin;

TCP-3 — 5,10,15,20-tetrakis(4-{[4-(2,5-dimethyl-4-(4-carboxyphenylethynyl)phenyl]ethynyl}phenyl)octaethylporphyrin;

TCTPP — 5,10,15,20-tetrakis(4-carboxytriphenyl)porphyrin;

TCTTPP — 5,10,15,20-tetrakis(4-carboxytetraphenyl)-porphyrin;

TCYP — 5,10,15,20-tetrakis(4-cyanophenyl)porphyrin;

TDCBPP — 5,10,15,20-tetrakis(4-(3,5-dicarboxy)biphenyl)porphyrin;

TDCPP — 5,10,15,20-tetrakis(3,5-dicarboxyphenyl)porphyrin;

TPP — 5,10,15,20-tetra(4-pyridyl)porphyrin;
TPPS — 5,10,15,20-tetrakis(4-sulfonatophenyl)porphyrin;
TTA — triplet–triplet annihilation;
TTET — triplet–triplet energy transfer;
TTZPP — 5,10,15,20-tetrakis[4-(2,3,4,5-tetrazol-1-yl)-phenyl]porphyrin;
VPI — vapour-phase infiltration.

Names of 3D-MOFs:
1·Mn — based on Mn^{II} 5,10,15,20-tetrakis[4-(3,5-dicarboxyphenoxy)phenyl]porphyrin and Mn^{2+} cations;
Al-TCPP — based on TCPP and Al^{3+} cations;
CPM-99 — based on TCBPP and Zr^{4+} cations;
DBP-UiO — based on DBP and Hf^{4+} cations;
FeMPF — based on Zn^{II}-TDCPP complex and Fe^{3+} and Na^{+} cations;
FJI-H6 — based on TCBPP and Zr^{4+} cations;
FJI-H7 — based on TCBPP and Hf^{4+} cations;
GdMPF-1 — based on Zn^{II}-TDCPP complex and Gd^{3+} and Na^{+} cations;
GTUB-1 — based on Cu^{II}-H_8TPPP complex and Na^{+} cations;
GTUB-4 — based on Cu^{II}-H_8TPPP complex and Ni^{2+} cations;
InMPF — based on Zn^{II} -TDCPP complex and In^{3+} and Na^{+} cations;
IPCE-1Ni — based on Ni^{II}-H_8TPPP complex and Zn^{2+} cations;
IPCE-2Ni — based on Ni^{II}-H_8*m*TPPP complex and Zn^{2+} cations;
IPCE-2Pd — based on Pd^{II}-H_8*m*TPPP complex and Zn^{2+} cations;
Ir-PMOF-1(Zr) — based on Ir^{III}-TCPP complex and Zr^{4+} cations;
MMPF-1 — based on Cu^{II}-BDCPP complex and Cu^{2+} cations;
MMPF-2 — based on TDCPP and Co^{2+} cations;
MMPF-3 — based on Co^{II}-DCDBP complex and Co^{2+} cations;
MMPF-4 — based on TDCPP and Zn^{2+} cations;
MMPF-5 — based on TDCPP and Cd^{2+} cations;
MMPF-9 — based on Cu^{II}-TDCBPP complex and Cu^{2+} cations;
MMPF-10 — based on Cu^{II} 5,10,15,20-tetrakis[3,5-bis(4-carboxyphenyl)phenyl]porphyrin and Cu^{2+} cations;
MMPF-18 — based on DBP and Zn^{2+} cations;
MOF1 — based on TCPP and Mn^{2+} cations;
MOF1(Mn) † — based on Mn-TCPP and Mn^{2+} cations;
MOF-525 — cubic framework based on TCPP and Zr^{4+} isostructural to PCN-224;
MOF-526 — mesoporous framework based on Cu-TCBPP and Zr^{4+} cations;
MOF-527 — mesoporous framework based on Cu-TCTPP and Zr^{4+} cations;
MOF-528 — mesoporous framework based on Cu-TCTTPP and Zr^{4+} cations;
MOF-545 — hexagonal framework based on TCPP and Zr^{4+} isostructural to PCN-222;
M-PMOF-3(Fe) — based on MTCPP and Fe^{3+} cations;
Ni-CAU-29 — based on Ni^{II}-H_8TPPP and Ni^{2+} cations;
NU-905 — based on TCPP and Th^{4+} cations;
PCN-134 — based on TCPP, BTB and Zr_6 clusters;
PCN-22 — based on TCPP and Ti^{4+} cations;
PCN-222 — hexagonal framework based on TCPP and 8-connected Zr_6 clusters;
PCN-223 — hexagonal framework based on TCPP and 12-connected Zr_6 clusters;
PCN-224 — cubic framework based on TCPP and 6-connected Zr_6 clusters;
PCN-228 — mesoporous framework based on TCP-1 and Zr^{4+} cations;
PCN-229 — mesoporous framework based on TCP-2 and Zr^{4+} cations;
PCN-230 — mesoporous framework based on TCP-3 and Zr^{4+} cations;
PCN-900(Eu) — based on TCPP, DCDPS and Eu^{3+} cations;
SZJ-4 — based on Mn^{III}-TDCPP complex and Zn^{2+} cations;
Th-IHEP-5 — based on TCPP, H_2bpydc and Th^{4+} cations;
U-IHEP-4 — based on CoTCPP and the UO_2^{2+} uranyl ion;
UNLPF-1 — based on Zn^{II}-TBCPPP complex and Zn^{2+} cations;
UNLPF-2 — based on Co^{II}-TBCPPP complex and Co^{2+} cations;
USTC-8 — based on TCPP and In^{3+} cations;
UTSA-57 — based on Mn^{III}-TTZPP complex and Mn^{2+} cations;
ZJU-18 — based on Mn^{III}-TDCPP complex and Mn^{2+} cations;
ZJU-21 — based on Ni^{II}-TDCPP complex and Cu^{2+} cations;
ZJU-22 — based on Mn^{III}-TDCPP complex and Cu^{2+} cations;
Zr-CAU-30 — based on Ni^{II}-H_8TPPP complex and Zr^{4+} cations.

Designations of composites and films:
AuNR@MOFs@CPT — core–shell nanoplatform consisting of gold nanorods, TCPP- and Zr^{4+}-based MOF and the antitumour agent camptothecin;
FeTCPP/Fe_2O_3 — nanocomposites based on Fe-TCPP framework and Fe_2O_3 nanoparticles;
L-Arg@PCN@Mem — nanoplatform based on PCN-224, L-arginine and cancer cell membranes;
mCGP — nanobioreactor based on PCN-224, membrane shell, glucose oxidase and catalase;
NAFS1 — oriented MOF nanofilm based on Co-TCPP and Cu^{2+};
P@Pt@P-Au-FA — nanoreactor based on Pt nanoparticles, MOF of the PCN series, Au nanoparticles and folic acid;
PCN-224(Cu)-GOD@MnO_2 — nanoplatform based on PCN-224(Cu) and glucose oxidase coated by MnO_2 layer;
PCN-I_2BDP(Nano) — PCN-222 MOF modified with iodinated boron complex of dipyrromethene.

† We changed the designation of this MOF for convenience of perception, while in the original publication,[34] it is designated by MOF1.

6. References

1. K.A.Kovalenko, A.S.Potapov, V.P.Fedin. *Russ. Chem. Rev.*, **91**, RCR5026 (2022) (in the press)
2. I.S.Antipin, M.V.Alfimov, V.V.Arslanov, V.A.Burilov, S.Z.Vatsadze, Y.Z.Voloshin, K.P.Volcho, V.V.Gorbatchuk, Y.G.Gorbunova, S.P.Gromov, S.V.Dudkin, S.Y.Zaitsev, L.Y.Zakharova, M.A.Ziganshin, A.V.Zolotukhina, M.A.Kalinina, E.A.Karakhanov, R.R.Kashapov, O.I.Koifman, A.I.Konovalov, V.S.Korenev, A.L.Maksimov,

N.Z.Mamardashvili, G.M.Mamardashvili, A.G.Martynov, A.R.Mustafina, R.I.Nugmanov, A.S.Ovsyannikov, P.L.Padnya, A.S.Potapov, S.L.Selektor, M.N.Sokolov, S.E.Solovieva, I.I.Stoikov, P.A.Stuzhin, E.V.Suslov, E.N.Ushakov, V.P.Fedin, S.V.Fedorenko, O.A.Fedorova, Y.V.Fedorov, S.N.Chvalun, A.Y.Tsivadze, S.N.Shtykov, D.N.Shurpik, M.A.Shcherbina, L.S.Yakimova. *Russ. Chem. Rev.*, **90**, 895 (2021)

3. A.A.Lysova, D.G.Samsonenko, K.A.Kovalenko, A.S.Nizovtsev, D.N.Dybtsev, V.P.Fedin. *Angew. Chem., Int. Ed.*, **59**, 20561 (2020)
4. T.A.Makal, J.R.Li, W.Lu, H.C.Zhou. *Chem. Soc. Rev.*, **41**, 7761 (2012)
5. Y.He, W.Zhou, G.Qian, B.Chen. *Chem. Soc. Rev.*, **43**, 5657 (2014)
6. Y.Cui, Y.Yue, G.Qian, B.Chen. *Chem. Rev.*, **112**, 1126 (2012)
7. W.P.Lustig, S.Mukherjee, N.D.Rudd, A.V.Desai, J.Li, S.K.Ghosh. *Chem. Soc. Rev.*, **46**, 3242 (2017)
8. M.P.Yutkin, D.N.Dybtsev, V.P.Fedin. *Russ. Chem. Rev.*, **80**, 1009 (2011)
9. L.Ye, Y.Gao, S.Cao, H.Chen, Y.Yao, J.Hou, L.Sun. *Appl. Catal., B: Environ.*, **227**, 54 (2018)
10. M.Zhao, S.Ou, C.De Wu. *Acc. Chem. Res.*, **47**, 1199 (2014)
11. Y.B.Huang, J.Liang, X.S.Wang, R.Cao. *Chem. Soc. Rev.*, **46**, 126 (2017)
12. H.Cai, Y.-L.L.Huang, D.Li. *Coord. Chem. Rev.*, **378**, 207 (2019)
13. M.Lismont, L.Dreesen, S.Wuttke. *Adv. Funct. Mater.*, **27**, 1606314 (2017)
14. H.S.Wang. *Coord. Chem. Rev.*, **349**, 139 (2017)
15. O.I.Koifman, T.A.Ageeva, I.P.Beletskaya, A.D.Averin, A.A.Yakushev, L.G.Tomilova, T.V.Dubinina, A.Y.Tsivadze, Y.G.Gorbunova, A.G.Martynov, D.V.Konarev, S.S.Khasanov, R.N.Lyubovskaya, T.N.Lomova, V.V.Korolev, E.I.Zenkevich, T.Blaudeck, C.von Borczyskowski, D.R.T.Zahn, A.F.Mironov, N.A.Bragina, A.V.Ezhov, K.A.Zhdanova, P.A.Stuzhin, G.L.Pakhomov, N.V.Rusakova, N.N.Semenishyn, S.S.Smola, V.I.Parfenyuk, A.S.Vashurin, S.V.Makarov, I.A.Dereven'kov, N.Z.Mamardashvili, T.S.Kurtikyan, G.G.Martirosyan, V.Burmistrov, V.V.Aleksandriiskii, I.V.Novikov, D.A.Pritmov, M.A.Grin, N.V.Suvorov, A.A.Tsygankov, A.Y.Fedorov, N.S.Kuzmina, A.V.Nyuchev, V.F.Otvagin, A.V.Kustov, D.V.Belykh, D.B.Berezin, A.B.Solovieva, P.S.Timashev, E.R.Milaeva, Y.A.Gracheva, M.A.Dodokhova, A.V.Safronenko, D.B.Shpakovsky, S.A.Syrbu, Y.A.Gubarev, A.N.Kiselev, M.O.Koifman, N.S.Lebedeva, E.S.Yurina. *Macroheterocycles*, **13**, 311 (2020)
16. O.I.Koifman, D.B.Berezin, M.I.Bazanov, T.A.Ageeva. In *Funktsional'nye Materialy na Osnove Tetrapirrol'nykh Makrogeterotsiklicheskikh Soedinenii. (Functional Materials Based on Tetrapyrrole Macroheterocyclic Compounds)*. (Ed. O.I.Koifman). (Moscow: Lenand, 2019). P. 848
17. K.Sasan, Q.Lin, C.Mao, P.Feng. *Chem. Commun.*, **50**, 10390 (2014)
18. C.W.Kung, T.H.Chang, L.Y.Chou, J.T.Hupp, O.K.Farha, K.C.Ho. *Chem. Commun.*, **51**, 2414 (2015)
19. N.Kornienko, Y.Zhao, C.S.Kley, C.Zhu, D.Kim, S.Lin, C.J.Chang, O.M.Yaghi, P.Yang. *J. Am. Chem. Soc.*, **137**, 14129 (2015)
20. W.-Y.Y.Gao, C.-Y.Y.Tsai, L.Wojtas, T.Thiounn, C.-C.C.Lin, S.Ma. *Inorg. Chem.*, **55**, 7291 (2016)
21. K.Lu, C.He, W.Lin. *J. Am. Chem. Soc.*, **136**, 16712 (2014)
22. L.Zhang, J.Lei, F.Ma, P.Ling, J.Liu, H.Ju. *Chem. Commun.*, **20**, 10831 (2016)
23. B.F.Abrahams, B.F.Hoskins, D.M.Michail, R.Robson. *Nature (London)*, **369**, 727 (1994)
24. H.Nagatomi, N.Yanai, T.Yamada, K.Shiraishi, N.Kimizuka. *Chem. – Eur. J.*, **24**, 1806 (2018)
25. Z.Meng, J.Luo, W.Li, K.A.Mirica. *J. Am. Chem. Soc.*, **142**, 21656 (2020)
26. R.Matheu, E.Gutierrez-Puebla, M.Â.Monge, C.S.Diercks, J.Kang, M.S.Prävot, X.Pei, N.Hanikel, B.Zhang, P.Yang, O.M.Yaghi. *J. Am. Chem. Soc.*, **141**, 17081 (2019)
27. E.S.Golovashova, Y.S.Mengel, T.A.Ageeva, E.V.Kudrik, O.I.Koifman. *Russ. J. Phys. Chem. A*, **91**, 2437 (2017)
28. E.S.Golovashova, V.A.Kulev, E.V.Kudrik, K.E.Moiseeva, T.A.Ageeva, O.I.Koifman. *Russ. J. Phys. Chem. A*, **94**, 638 (2020)
29. K.E.Moiseeva, E.S.Golovashova, T.A.Ageeva, O.I.Koifman. *Ross. Khim. Zh.*, **65** (2), 55 (2021)
30. S.Huh, S.-J.Kim, Y.Kim. *CrystEngComm*, **18**, 345 (2016)
31. W.-Y.Y.Gao, M.Chrzanowski, S.Ma. *Chem. Soc. Rev.*, **43**, 5841 (2014)
32. L.D.Devries, W.Choe. *J. Chem. Crystallogr.*, **39**, 229 (2009)
33. E.-Y.Choi, C.A.Wray, C.Hu, W.Choe. *CrystEngComm*, **11**, 553 (2009)
34. N.Sharma, S.S.Dhankhar, C.M.Nagaraja. *Microporous Mesoporous Mater.*, **280**, 372 (2019)
35. N.Sharma, S.S.Dhankhar, S.Kumar, T.J.D.D.Kumar, C.M.Nagaraja. *Chem. – Eur. J.*, **24**, 16662 (2018)
36. W.Zhang, W.Gao, T.Pham, P.Jiang, S.Ma. *Cryst. Growth Des.*, **16**, 1005 (2016)
37. N.L.Rosi, J.Kim, M.Eddaoudi, B.Chen, M.O Keeffe, O.M.Yaghi. *J. Am. Chem. Soc.*, **127**, 1504 (2005)
38. M.-H.Xie, X.-L.Yang, C.-D.Wu. *Chem. Commun.*, **47**, 5521 (2011)
39. Q.Li, Y.Luo, Y.Ding, Yi.Wang, Yu.Wang, H.Du, R.Yuan, J.Bao, M.Fang, Y.Wu. *Dalton Trans.*, **48**, 8678 (2019)
40. C.Zou, M.-H.Xie, G.-Q.Kong, C.-D.Wu. *CrystEngComm*, **14**, 4850 (2012)
41. A.Fateeva, P.A.Chater, C.P.Ireland, A.A.Tahir, Y.Z.Khimyak, P.V.Wiper, J.R.Darwent, M.J.Rosseinsky. *Angew. Chem., Int. Ed.*, **51**, 7440 (2012)
42. Y.Liu, Y.Yang, Q.Sun, Z.Wang, B.Huang, Y.Dai, X.Qin, X.Zhang. *ACS Appl. Mater. Interfaces*, **5**, 7654 (2013)
43. T.Rhauderwiek, S.Waitschat, S.Wuttke, H.Reinsch, T.Bein, N.Stock. *Inorg. Chem.*, **55**, 5312 (2016)
44. J.Luo, J.Wang, Y.Cao, S.Yao, L.Zhang, Q.Huo, Y.Liu. *Inorg. Chem. Front.*, **4**, 139 (2017)
45. A.Fateeva, S.Devautour-Vinot, N.Heymans, T.Devic, J.-M.Grenèche, S.Wuttke, S.Miller, A.Lago, C.Serre, G.De Weireld, G.Maurin, A.Vimont, G.Férey. *Chem. Mater.*, **23**, 4641 (2011)
46. G.Liu, H.Cui, S.Wang, L.Zhang, C.Y.Su. *J. Mater. Chem. A*, **8**, 8376 (2020)
47. L.Zhang, S.Yuan, L.Feng, B.Guo, J.Qin, B.Xu, C.Lollar, D.Sun, H.Zhou. *Angew. Chem., Int. Ed.*, **57**, 5095 (2018)
48. X.Wang, C.Chu, Y.Wu, Y.Deng, J.Zhou, M.Yang, S.Zhang, D.Huo, C.Hou. *Sens. Actuators, B: Chem.*, **321**, 128455 (2020)
49. C.Fu, X.Sun, G.Zhang, P.Shi, P.Cui. *Inorg. Chem.*, **60**, 1116 (2021)
50. D.Feng, Z.-Y.Y.Gu, J.-R.R.Li, H.-L.L.Jiang, Z.Wei, H.-C.C.Zhou. *Angew. Chem., Int. Ed.*, **51**, 10307 (2012)
51. L.Li, Q.Yang, S.Chen, X.Hou, B.Liu, J.Lu, H.-L.L.Jiang. *Chem. Commun.*, **53**, 10026 (2017)
52. H.-Q.Xu, J.Hu, D.Wang, Z.Li, Q.Zhang, Y.Luo, S.-H.Yu, H.-L.Jiang. *J. Am. Chem. Soc.*, **137**, 13440 (2015)
53. J.H.Park, S.Lach, K.Polev, S.Granick, B.A.Grzybowski. *ACS Nano*, **11**, 10914 (2017)
54. A.-N.Meng, L.-X.Chaihu, H.-H.Chen, Z.-Y.Gu. *Sci. Rep.*, **7**, 1 (2017)
55. W.Morris, B.Volosskiy, S.Demir, F.Gándara, P.L.McGrier, H.Furukawa, D.Cascio, J.F.Stoddart, O.M.Yaghi. *Inorg. Chem.*, **51**, 6443 (2012)

56. Y.Chen, T.Hoang, S.Ma. *Inorg. Chem.*, **51**, 12600 (2012)
57. M.H.Beyzavi, N.A.Vermeulen, A.J.Howarth, S.Tussupbayev, A.B.League, N.M.Schweitzer, J.R.Gallagher, A.E.Platero-Prats, N.Hafezi, A.A.Sarjeant, J.T.Miller, K.W.Chapman, J.F.Stoddart, C.J.Cramer, J.T.Hupp, O.K.Farha. *J. Am. Chem. Soc.*, **137**, 13624 (2015)
58. D.Feng, W.Chung, Z.Wei, Z.Gu, H.Jiang, Y.-P.Chen, D.J.Darensbourg, H.-C.Zhou. *J. Am. Chem. Soc.*, **135**, 17105 (2013)
59. H.Cui, Yi.Wang, Ya.Wang, Y.-Z.Fan, L.Zhang, C.-Y.Su. *CrystEngComm*, **18**, 2203 (2016)
60. Y.Wang, H.Cui, Z.-W.Wei, H.-P.Wang, L.Zhang, C.-Y.Su. *Chem. Sci.*, **8**, 775 (2016)
61. L.Chen, H.Cui, Y.Wang, X.Liang, L.Zhang, C.-Y.Su. *Dalton Trans.*, **47**, 3940 (2018)
62. J.Liu, Y.Z.Fan, X.Li, Z.Wei, Y.W.Xu, L.Zhang, C.Y.Su. *Appl. Catal., B: Environ.*, **231**, 173 (2018)
63. D.Feng, Z.-Y.Gu, Y.-P.Chen, J.Park, Z.Wei, Y.Sun, M.Bosch, S.Yuan, H.-C.Zhou. *J. Am. Chem. Soc.*, **136**, 17714 (2014)
64. S.Yuan, J.-S.Qin, L.Zou, Y.-P.Chen, X.Wang, Q.Zhang, H.-C.Zhou. *J. Am. Chem. Soc.*, **138**, 6636 (2016)
65. S.Yuan, T.-F.Liu, D.Feng, J.Tian, K.Wang, J.Qin, Q.Zhang, Y.-P.Chen, M.Bosch, L.Zou, S.J.Teat, S.J.Dalgarno, H.-C.Zhou. *Chem. Sci.*, **6**, 3926 (2015)
66. Y.Keum, S.Park, Y.-P.Chen, J.Park. *Angew. Chem., Int. Ed.*, **57**, 14852 (2018)
67. K.Q.Hu, Z.W.Huang, Z.H.Zhang, L.Mei, B.B.Qian, J.P.Yu, Z.F.Chai, W.Q.Shi. *Chem. – Eur. J.*, **24**, 16766 (2018)
68. P.Li, S.Goswami, K.I.Otake, X.Wang, Z.Chen, S.L.Hanna, O.K.Farha. *Inorg. Chem.*, **58**, 3586 (2019)
69. Z.Huang, K.Hu, L.Mei, X.Kong, J.Yu, K.Liu, L.Zeng, Z.-F.Chai, W.-Q.Shi. *Dalton Trans.*, **49**, 983 (2020)
70. Q.Lin, X.Bu, A.Kong, C.Mao, X.Zhao, F.Bu, P.Feng. *J. Am. Chem. Soc.*, **137**, 2235 (2015)
71. J.Zheng, M.Wu, F.Jiang, W.Su, M.Hong. *Chem. Sci.*, **6**, 3466 (2015)
72. T.Liu, D.Feng, Y.Chen, L.Zou, M.Bosch, S.Yuan, Z.Wei, S.Fordham, K.Wang, H.-C.Zhou. *J. Am. Chem. Soc.*, **137**, 413 (2015)
73. X.Xu, S.Li, Q.Liu, Z.Liu, W.Yan, L.Zhao, W.Zhang, L.Zhang, F.Deng, H.Cong, H.Deng. *ACS Appl. Mater. Interfaces*, **11**, 973 (2019)
74. X.-S.Wang, M.Chrzanowski, C.Kim, W.-Y.Gao, L.Wojtas, Y.-S.Chen, X.Peter Zhang, S.Ma. *Chem. Commun.*, **48**, 7173 (2012)
75. X.-S.Wang, M.Chrzanowski, W.-Y.Gao, L.Wojtas, Y.-S.Chen, M.J.Zaworotko, S.Ma. *Chem. Sci.*, **3**, 2823 (2012)
76. X.L.Yang, C.De Wu. *Inorg. Chem.*, **53**, 4797 (2014)
77. X.-L.Yang, M.-H.Xie, C.Zou, Y.He, B.Chen, M.O Keeffe, C.-D.Wu. *J. Am. Chem. Soc.*, **134**, 10638 (2012)
78. X.-L.Yang, C.Zou, Y.He, M.Zhao, B.Chen, S.Xiang, M.O'Keeffe, C.-D.Wu. *Chem. – Eur. J.*, **20**, 1447 (2014)
79. B.K.Tripuramallu, H.M.Titi, S.Roy, R.Verma, I.Goldberg. *CrystEngComm*, **18**, 515 (2016)
80. B.K.Tripuramallu, I.Goldberg. *Cryst. Growth Des.*, **16**, 1751 (2016)
81. W.Y.Gao, L.Wojtas, S.Ma. *Chem. Commun.*, **50**, 5316 (2014)
82. W.Jiang, J.Yang, Y.-Y.Liu, S.-Y.Song, J.-F.Ma. *Chem. – Eur. J.*, **22**, 16991 (2016)
83. J.A.Johnson, S.Chen, T.C.Reeson, Y.-S.Chen, X.C.Zeng, J.Zhang. *Chem. – Eur. J.*, **20**, 7632 (2014)
84. X.Wang, W.-Y.Gao, Z.Niu, L.Wojtas, J.A.Perman, Y.-S.Chen, Z.Li, B.Aguila, S.Ma. *Chem. Commun.*, **54**, 1170 (2018)
85. J.A.Johnson, X.Zhang, T.C.Reeson, Y.-S.Chen, J.Zhang. *J. Am. Chem. Soc.*, **136**, 15881 (2014)
86. Z.Guo, D.Yan, H.Wang, D.Tesfagaber, X.Li, Y.Chen, W.Huang, B.Chen. *Inorg. Chem.*, **54**, 200 (2015)
87. W.-T.Chen, Y.Yamada, G.-N.Liu, A.Kubota, T.Ichikawa, Y.Kojima, G.-C.Guo, S.Fukuzumi. *Dalton Trans.*, **40**, 12826 (2011)
88. Y.Pei, J.Huang, R.Hu, Y.Yang, J.Zhou, W.-T.Chen. *J. Porphyrins Phthalocyanines*, **19**, 1 (2015)
89. W.Chen, Q.Luo, Y.Xu, Y.Dai, S.Huang, P.Guo. *Inorg. Chem. Commun.*, **49**, 16 (2014)
90. W.Chen, Z.Luo, Y.Wang, X.Zhang, H.Fu. *Inorg. Chim. Acta*, 414, 1 (2014)
91. W.Chen, R.Hu, Y.Wang, X.Zhang, J.Liu. *J. Solid State Chem.*, **213**, 218 (2014)
92. W.Chen, D.Liu, Y.Xu, Q.Luo, Y.-P.Pei. *Luminescence*, **31**, 158 (2016)
93. W.Chen, Y.Xu, Q.Luo, Y.Dai, S.Huang, P.-Y.Guo. *J. Porphyrins Phthalocyanines*, **18**, 600 (2014)
94. W.Chen, J.Huang, Q.Luo, Y.Xu, H.-R.Fu. *J. Porphyrins Phthalocyanines*, **19**, 154 (2015)
95. W.-T.Chen, Z.Zhang, L.Lin, Y.Sui, D.Liu, H.-L.Chen. *Cryst. Growth Des.*, **18**, 5456 (2018)
96. J.Demel, P.Kubat, F.Millange, J.Marrot, I.Císarová, K.Lang. *Inorg. Chem.*, **52**, 2779 (2013)
97. T.Rhauderwiek, K.Wolkersdìrfer, S.Øien-Ødegaard, K.-P.Lillerud, M.Wark, N.Stock. *Chem. Commun.*, **54**, 389 (2018)
98. T.Rhauderwiek, H.Zhao, P.Hirschle, M.Dìblinger, B.Bueken, H.Reinsch, D.De Vos, S.Wuttke, U.Kolb, N.Stock. *Chem. Sci.*, **9**, 5467 (2018)
99. B.Wang, T.Rhauderwiek, A.K.Inge, H.Xu, T.Yang, Z.Huang, N.Stock, X.Zou. *Chem. – Eur. J.*, **24**, 17429 (2018)
100. C.F.Pereira, F.Figueira, R.F.Mendes, J.Rocha, J.T.Hupp, O.K.Farha, M.M.Q.Simoées, J.P.C.Tomé, F.A.A.Paz. *Inorg. Chem.*, **57**, 3855 (2018)
101. M.Maares, M.M.Ayhan, K.B.Yu, A.O.Yazaydin, K.Harmandar, H.Haase, J.Beckmann, Y.Zorlu, G.Yücesan. *Chem. – Eur. J.*, **25**, 11214 (2019)
102. Y.Y.Enakieva, A.A.Sinelshchikova, M.S.Grigoriev, V.V.Chernyshev, K.A.Kovalenko, I.A.Stenina, A.B.Yaroslavtsev, Y.G.Gorbunova, A.Y.Tsivadze. *Chem. – Eur. J.*, **25**, 10552 (2019)
103. Y.Y.Enakieva, A.A.Sinelshchikova, M.S.Grigoriev, V.V.Chernyshev, K.A.Kovalenko, I.A.Stenina, A.B.Yaroslavtsev, Y.G.Gorbunova, A.Y.Tsivadze. *Chem. – Eur. J.*, **27**, 1598 (2021)
104. Y.Y.Enakieva, E.A.Zhigileva, A.N.Fitch, V.V.Chernyshev, I.A.Stenina, A.B.Yaroslavtsev, A.A.Sinelshchikova, K.A.Kovalenko, Y.G.Gorbunova, A.Y.Tsivadze. *Dalton Trans.*, **50**, 6549 (2021)
105. M.M.Ayhan, C.Bayraktar, K.B.Yu, G.Hanna, A.O.Yazaydin, Y.Zorlu, G.Yücesan. *Chem. – Eur. J.*, **26**, 14813 (2020)
106. X.S.Wang, L.Meng, Q.Cheng, C.Kim, L.Wojtas, M.Chrzanowski, Y.S.Chen, X.P.Zhang, S.Ma. *J. Am. Chem. Soc.*, **133**, 16322 (2011)
107. L.Meng, Q.Cheng, C.Kim, W.Y.Gao, L.Wojtas, Y.S.Chen, M.J.Zaworotko, X.P.Zhang, S.Ma. *Angew. Chem., Int. Ed.*, **51**, 10082 (2012)
108. B.K.Tripuramallu, S.Goswami, I.Goldberg. *Cryst. Growth Des.*, **18**, 230 (2018)
109. E.Choi, P.M.Barron, R.W.Novotny, H.Son, C.Hu, W.Choe. *Inorg. Chem.*, **48**, 426 (2009)
110. H.Chung, P.M.Barron, R.W.Novotny, H.-T.Son, C.Hu, W.Choe. *Cryst. Growth Des.*, **9**, 3327 (2009)
111. B.J.Burnett, W.Choe. *CrystEngComm*, **14**, 6129 (2012)
112. B.J.Burnett, P.M.Barron, W.Choe. *CrystEngComm*, **14**, 3839 (2012)
113. H.Zhang, J.Wei, J.Dong, G.Liu, L.Shi, P.An, G.Zhao, J.Kong, X.Wang, X.Meng, J.Zhang, J.Ye. *Angew. Chemie, Int. Ed.*, **55**, 14310 (2016)

114. T.-H.Chang, C.Young, M.-H.Lee, R.R.Salunkhe, S.M.Alshehri, T.Ahamad, M.T.Islam, K.C.W.Wu, M.S.A.Hossain, Y.Yamauchi, K.-C.Ho. *Chem.–Asian J.*, **12**, 2857 (2017)
115. T.Li, P.Hu, J.Li, P.Huang, W.Tong, C.Gao. *Colloids Surf. A*, **577**, 456 (2019)
116. S.Biswas, Y.Chen, Y.Xie, X.Sun, Y.Wang. *Anal. Chem.*, **92**, 4566 (2020)
117. A.M.Szczepkowska, M.Janeta, M.Siczek, W.Tylus, A.M.Trzeciak, W.Bury. *Dalton Trans.*, **50**, 9051 (2021)
118. X.S.Wang, M.Chrzanowski, L.Wojtas, Y.S.Chen, S.Ma. *Chem.–Eur. J.*, **19**, 3297 (2013)
119. W.Gao, H.T.Ngo, Z.Niu, W.Zhang, Y.Pan, Z.Yang, V.R.Bhethanabotla, B. Joseph, B.Aguila, S.Ma. *ChemSusChem*, **13**, 6273 (2020)
120. J.Ji, F.Liu, W.Yang, M.Tan, W.Luo, S.Yin. *ChemCatChem*, **12**, 4331 (2020)
121. L.Feng, Y.Wang, S.Yuan, K.Y.Wang, J.L.Li, G.S.Day, D.Qiu, L.Cheng, W.M.Chen, S.T.Madrahimov, H.C.Zhou. *ACS Catal.*, **9**, 5111 (2019)
122. K.Mao, Y.Zhu, J.Rong, F.Qiu, H.Chen, J.Xu, D.Yang, T.Zhang, L.Zhong. *Colloids Surf. A*, **611**, 125888 (2021)
123. Y.-C.Wang, Y.-C.Chen, W.-S.Chuang, J.-H.Li, Y.-S.Wang, C.-H.Chuang, C.-Y.Chen, C.-W.Kung. *ACS Appl. Nano Mater.*, **3**, 9440 (2020)
124. Y.C.Chen, W.H.Chiang, D.Kurniawan, P.C.Yeh, K.I.Otake, C.W.Kung. *ACS Appl. Mater. Interfaces*, **11**, 35319 (2019)
125. T.H.Yang, S.H.Yang, Y.C.Chen, D.Kurniawan, W.H.Chiang, Y.P.Chiu, C.W.Kung. *J. Phys. Chem. C*, **124**, 21635 (2020)
126. S.Takaishi, E.J.De Marco, M.J.Pellin, O.K.Farha, J.T.Hupp. *Chem. Sci.*, **4**, 1509 (2013)
127. J.S.Oh, Y.You, K.C.Park, G.Gupta, D.K.Kang, C.Y.Lee. *Dyes Pigm.*, **170**, 107576 (2019)
128. Z.-W.Huang, K.-Q.Hu, L.Mei, C.-Z.Wang, Y.-M.Chen, W.-S.Wu, Z.-F.Chai, W.-Q.Shi. *Inorg. Chem.*, **60**, 651 (2021)
129. Y.Yang, M.Ishida, Y.Yasutake, S.Fukatsu, C.Fukakusa, M.A.Morikawa, T.Yamada, N.Kimizuka, H.Furuta. *Inorg. Chem.*, **58**, 4647 (2019)
130. S.De, G.C.Quan, B.Gikonyo, C.Martineau-Corcos, C.Bousige, L.Veyre, T.Devic, C.Marichy, A.Fateeva. *Inorg. Chem.*, **59**, 10129 (2020)
131. F.Figueira, F.A.A.Paz. *J. Carbon Res.*, **7**, 47 (2021)
132. B.Karadeniz, D.Zilić, I.Huskić, L.S.Germann, A.M.Fidelli, S.Muratović, I.Loncarić, M.Etter, R.E.Dinnebier, D.Barisić, N.Cindro, T.Islamoglu, O.K.Farha, T.Friscić, K.Uzarević. *J. Am. Chem. Soc.*, **141**, 19214 (2019)
133. B.J.Burnett, P.M.Barron, C.Hu, W.Choe. *J. Am. Chem. Soc.*, **133**, 9984 (2011)
134. J.Goldsmith, A.G.Wong-Foy, M.J.Cafarella, D.J.Siegel. *Chem. Mater.*, **25**, 3373 (2013)
135. G.Anderson, B.Schweitzer, R.Anderson, D.A.Gømez-Gualdrøn. *J. Phys. Chem. C*, **123**, 120 (2019)
136. M.Fernandez, T.K.Woo, C.E.Wilmer, R.Q.Snurr. *J. Phys. Chem. C*, **117**, 7681 (2013)
137. T.Watanabe, D.S.Sholl. *Langmuir*, **28**, 14114 (2012)
138. R.Costa e Silva, L.Oliveira da Silva, A.de Andrade Bartolomeu, T.J.Brocksom, K.T.de Oliveira. *Beilstein J. Org. Chem.*, **16**, 917 (2020)
139. A.G.Mojarrad, S.Zakavi. *Catal. Sci. Technol.*, **8**, 768 (2018)
140. Y.Chen, Z.Huang, L.Wang. In *Phthalocyanines and Some Current Applications*. (Ed. Y.Yilmaz). (Rijeka, Croatia: InTech, 2017). P. 35
141. J.Barona-Castaåo, C.Carmona-Vargas, T.Brocksom, K.de Oliveira. *Molecules*, **21**, 310 (2016)
142. K.A.D.de F.Castro, M.M.Q.Simoes, M.da Graça P.M.S.Neves, J.A.S.Cavaleiro, R.R.Ribeiro, F.Wypych, S.Nakagaki. *Appl. Catal., A: Gen.*, **503**, 9 (2015)
143. C.F.Pereira, M.Q.Simoes, J.P.C.Tomé, F.A.A.Paz. *Molecules*, **21**, 1348 (2016)
144. J.Jin. *New J. Chem.*, **44**, 15362 (2020)
145. C.Liu, K.Liu, C.Wang, H.Liu, H.Wang, H.Su, X.Li, B.Chen, J.Jiang. *Nat. Commun.*, **11**, 1047 (2020)
146. L. Zou, R.Sa, H.Lv, H.Zhong, R.Wang. *ChemSusChem*, **130**, cssc. 202001796 (2020)
147. J.G.Mahy, C.A.Paez, C.Carcel, C.Bied, A.S.Tatton, C.Damblon, B.Heinrichs, M.Wong, C.Man, S.D.Lambert. *J. Photochem. Photobiol. A*, **373**, 66 (2019)
148. K.Epp, B.Bueken, B.J.Hofmann, M.Cokoja, K.Hemmer, D.De Vos, R.A.Fischer. *Catal. Sci. Technol.*, **9**, 6452 (2019)
149. C.Zou, T.Zhang, M.-H.Xie, L.Yan, G.-Q.Kong, X.-L.Yang, A.Ma, C.-D.Wu. *Inorg. Chem.*, **52**, 3620 (2013)
150. J.W.Brown, Q.T.Nguyen, T.Otto, N.N.Jarenwattananon, S.Glöggler, L.-S.Bouchard. *Catal. Commun.*, **59**, 50 (2015)
151. A.D.Cardenal, H.J.Park, C.J.Chalker, K.G.Ortiz, D.C.Powers. *Chem. Commun.*, **53**, 7377 (2017)
152. N.Huang, H.Drake, J.Li, J.Pang, Y.Wang, S.Yuan, Q.Wang, P.Cai, J.Qin, H.-C.Zhou. *Angew. Chem., Int. Ed.*, **57**, 8916 (2018)
153. J.Park, D.Feng, S.Yuan, H.-C.Zhou. *Angew. Chem., Int. Ed.*, **54**, 430 (2015)
154. E.Amayuelas, A.Fidalgo-Marijuán, B.Bazán, M.K.Urtiaga, G.Barandika, M.I.Arriortua. *CrystEngComm*, **19**, 7244 (2017)
155. S.Ou, C.-D.Wu. *Inorg. Chem. Front.*, **1**, 721 (2014)
156. Y.Liu, A.J.Howarth, J.T.Hupp, O.K.Farha. *Angew. Chem., Int. Ed.*, **54**, 9001 (2015)
157. M.E.Kosal, J.H.Chou, S.R.Wilson, K.S.Suslick. *Nat. Mater.*, **1**, 118 (2002)
158. K.S.Suslick, P.Bhyrappa, J.H.Chou, M.E.Kosal, S.Nakagaki, D.W.Smithenry, S.R.Wilson. *Acc. Chem. Res.*, **38**, 283 (2005)
159. J.Liu, L.Chen, H.Cui, J.Zhang, L.Zhang, C.-Y.Su. *Chem. Soc. Rev.*, **43**, 6011 (2014)
160. M.-H.H.Xie, X.-L.L.Yang, Y.He, J.Zhang, B.Chen, C.-D.De Wu. *Chem.–Eur. J.*, **19**, 14316 (2013)
161. M.H.Beyzavi, N.A.Vermeulen, K.Zhang, M.So, C.-W.Kung, J.T.Hupp, O.K.Farha. *ChemPlusChem*, **81**, 708 (2016)
162. M.Chino, L.Leone, G.Zambrano, F.Pirro, D.D'Alonzo, V.Firpo, D.Aref, L.Lista, O.Maglio, F.Nastri, A.Lombardi. *Biopolymers*, **109**, e23107 (2018)
163. S.Oudi, A.R.Oveisi, S.Daliran, M.Khajeh, R.Luque, U.Sen, H.García. *Appl. Catal., A: Gen.*, **611**, 117965 (2021)
164. Y.Zhao, Y.Dong, F.Lu, C.Ju, L.Liu, J.Zhang, B.Zhang, Y.Feng. *J. Mater. Chem. A*, **5**, 15380 (2017)
165. C.Li, W.Qiu, W.Long, F.Deng, G.Bai, G.Zhang, X.Zi, H.He. *J. Mol. Catal. A: Chem.*, **393**, 166 (2014)
166. J.A.Johnson, J.Luo, X.Zhang, Y.S.Chen, M.D.Morton, E.Echeverría, F.E.Torres, J.Zhang. *ACS Catal.*, **5**, 5283 (2015)
167. Y.Wang, M.Zhao, J.Ping, B.Chen, X.Cao, Y.Huang, C.Tan, Q.Ma, S.Wu, Y.Yu, Q.Lu, J.Chen, W.Zhao, Y.Ying, H.Zhang. *Adv. Mater.*, **28**, 4149 (2016)
168. Y.Huang, M.Zhao, S.Han, Z.Lai, J.Yang, C.Tan, Q.Ma, Q.Lu, J.Chen, X.Zhang, Z.Zhang, B.Li, B.Chen, Y.Zong, H.Zhang. *Adv. Mater.*, **29**, 1700102 (2017)
169. J.Liu, Y.-Z.Fan, X.Li, Y.-W.Xu, L.Zhang, C.-Y.Su. *ChemSusChem*, **11**, 2340 (2018)
170. J.Liang, Y.-Q.Xie, Q.Wu, X.-Y.Wang, T.-T.Liu, H.-F.Li, Y.-B.Huang, R.Cao. *Inorg. Chem.*, **57**, 2584 (2018)
171. Y.Zhao, N.Kornienko, Z.Liu, C.Zhu, S.Asahina, T.R.Kuo, W.Bao, C.Xie, A.Hexemer, O.Terasaki, P.Yang, O.M.Yaghi. *J. Am. Chem. Soc.*, **137**, 2199 (2015)
172. Y.Wang, H.Cui, Z.-W.Wei, H.-P.Wang, L.Zhang, C.-Y.Su. *Chem. Sci.*, **8**, 775 (2017)
173. Y.Fu, D.Sun, Y.Chen, R.Huang, Z.Ding, X.Fu, Z.Li. *Angew. Chem., Int. Ed.*, **51**, 3364 (2012)
174. D.Sun, Y.Fu, W.Liu, L.Ye, D.Wang, L.Yang, X.Fu, Z.Li. *Chem.–Eur. J.*, **19**, 14279 (2013)
175. S.Chen, F.Yang, H.Gao, J.Wang, X.Chen, X.Zhang, J.Li, A.Li. *J. CO_2 Util.*, **48**, 101528 (2021)
176. N.Sadeghi, S.Sharifnia, T.-O.Do. *J. Mater. Chem. A*, **6**, 18031 (2018)

177. L.Y.Wu, Y.F.Mu, X.X.Guo, W.Zhang, Z.M.Zhang, M.Zhang, T.B.Lu. *Angew. Chem., Int. Ed.*, **58**, 9491 (2019)
178. C.Zheng, X.Qiu, J.Han, Y.Wu, S.Liu. *ACS Appl. Mater. Interfaces*, **11**, 42243 (2019)
179. Z.-B.Fang, T.-T.Liu, J.Liu, S.Jin, X.-P.Wu, X.-Q.Gong, K.Wang, Q.Yin, T.-F.Liu, R.Cao, H.-C.Zhou. *J. Am. Chem. Soc.*, **142**, 12515 (2020)
180. Z.Wang, Q.Sun, B.Liu, Y.Kuang, A.Gulzar, F.He, S.Gai, P.Yang, J.Lin. *Coord. Chem. Rev.*, **439**, 213945 (2021)
181. J.Liu, Y.Yang, W.Zhu, X.Yi, Z.Dong, X.Xu, M.Chen, K.Yang, G.Lu, L.Jiang, Z.Liu. *Biomaterials*, **97**, 1 (2016)
182. J.Chen, Y.Zhu, S.Kaskel. *Angew. Chem., Int. Ed.*, **60**, 5010 (2021)
183. J.Park, Q.Jiang, D.Feng, L.Mao, H.C.Zhou. *J. Am. Chem. Soc.*, **138**, 3518 (2016)
184. Y.Li, Z.Di, J.Gao, P.Cheng, C.Di, G.Zhang, B.Liu, X.Shi, L.-D.Sun, L.Li, C.-H.Yan. *J. Am. Chem. Soc.*, **139**, 13804 (2017)
185. C.Liu, B.Liu, J.Zhao, Z.Di, D.Chen, Z.Gu, L.Li, Y.Zhao. *Angew. Chem., Int. Ed.*, **59**, 2634 (2020)
186. I.E.Kolesnikov, M.A.Kurochkin, I.N.Meshkov, R.A.Akasov, A.A.Kalinichev, E.Y.Kolesnikov, Y.G.Gorbunova, E.Lähderanta. *Mater. Des.*, **203**, 109613 (2021)
187. L.He, Q.Ni, J.Mu, W.Fan, L.Liu, Z.Wang, L.Li, W.Tang, Yi.Liu, Y.Cheng, L.Tang, Z.Yang, Yu.Liu, J.Zou, W.Yang, O.Jacobson, F.Zhang, P.Huang, X.Chen. *J. Am. Chem. Soc.*, **142**, 6822 (2020)
188. G.Canti, A.Nicolin, R.Cubeddu, P.Taroni, G.Bandieramonte, G.Valentini. *Cancer Lett.*, **125**, 39 (1998)
189. W.Liu, Y.-M.Wang, Y.-H.Li, S.-J.Cai, X.-B.Yin, X.-W.He, Y.-K.Zhang. *Small*, **13**, 1603459 (2017)
190. J.-Y.Zeng, M.-K.Zhang, M.-Y.Peng, D.Gong, X.-Z.Zhang. *Adv. Funct. Mater.*, **28**, 1705451 (2018)
191. Y.Zhao, J.Wang, X.Cai, P.Ding, H.Lv, R Pei. *ACS Appl. Mater. Interfaces*, **12**, 23697 (2020)
192. S.S.Wan, Q.Cheng, X.Zeng, X.Z.Zhang. *ACS Nano*, **13**, 6561 (2019)
193. Z.-X.Chen, M.-D.Liu, M.-K.Zhang, S.-B.Wang, L.Xu, C.-X.Li, F.Gao, B.-R.Xie, Z.-L.Zhong, X.-Z.Zhang. *Adv. Funct. Mater.*, **28**, 1803498 (2018)
194. B.Li, X.Wang, L.Chen, Y.Zhou, W.Dang, J.Chang, C.Wu. *Theranostics*, **8**, 4086 (2018)
195. C.Wang, F.Cao, Y.Ruan, X.Jia, W.Zhen, X.Jiang. *Angew. Chem., Int. Ed.*, **58**, 9846 (2019)
196. Y.Ma, X.Li, A.Li, P.Yang, C.Zhang, B.Tang. *Angew. Chem., Int. Ed.*, **56**, 13752 (2017)
197. S.S.Wan, J.Y.Zeng, H.Cheng, X.Z.Zhang. *Biomaterials*, **185**, 51 (2018)
198. S.Yu, Z.Chen, X.Zeng, X.Chen, Z.Gu. *Theranostics*, **9**, 8026 (2019)
199. Z.Wang, B.Liu, Q.Sun, S.Dong, Y.Kuang, Y.Dong, F.He, S.Gai, P.Yang. *ACS Appl. Mater. Interfaces*, **12**, 17254 (2020)
200. S.-Y.Li, H.Cheng, B.-R.Xie, W.-X.Qiu, J.-Y.Zeng, C.-X.Li, S.-S.Wan, L.Zhang, W.-L.Liu, X.-Z.Zhang. *ACS Nano*, **11**, 7006 (2017)
201. C.Liu, J.Xing, O.U.Akakuru, L.Luo, S.Sun, R.Zou, Z.Yu, Q.Fang, A.Wu. *Nano Lett.*, **19**, 5674 (2019)
202. X.Guo, B.Guo, Y.Wang, S.Guan. *Mater. Sci. Eng. C*, **80**, 698 (2017)
203. X.Liu, Z.Yan, Y.Zhang, Z.Liu, Y.Sun, J.Ren, X.Qu. *ACS Nano*, **13**, 5222 (2019)
204. G.Nandi, I.Goldberg. *Chem. Commun.*, **50**, 13612 (2014)
205. S.Tasleem, M.Tahir, W.A.Khalifa. *Int. J. Hydrogen Energy*, **46**, 14148 (2021)
206. F.E.Dayan, S.O.Duke, K.Grossmann. *Weed Sci.*, **58**, 340 (2010)
207. S.Tasleem, M.Tahir. *Renew. Sustain. Energy Rev.*, **132**, 110073 (2020)
208. A.Ortega-Guerrero, M.Fumanal, G.Capano, I.Tavernelli, B.Smit. *Chem. Mater.*, **32**, 4194 (2020)
209. X.Fang, Q.Shang, Y.Wang, L.Jiao, T.Yao, Y.Li, Q.Zhang, Y.Luo, H.-L.Jiang. *Adv. Mater.*, **30**, 1705112 (2018)
210. H.Hu, L.Zeng, Z.Li, T.Zhu, C.Wang. *Chin. J. Catal.*, **42**, 1345 (2021)
211. C.Lin, C.Han, H.Zhang, L.Gong, Y.Gao, H.Wang, Y.Bian, R.Li, J.Jiang. *Inorg. Chem.*, **60**, 3988 (2021)
212. F.Leng, H.Liu, M.Ding, Q.-P.Lin, H.-L.Jiang. *ACS Catal.*, **8**, 4583 (2018)
213. F.Paquin, J.Rivnay, A.Salleo, N.Stingelin, C.Silva. *J. Mater. Chem. C*, **3**, 10715 (2015)
214. Q.Zuo, T.Liu, C.Chen, Y.Ji, X.Gong, Y.Mai, Y.Zhou. *Angew. Chem., Int. Ed.*, **58**, 10198 (2019)
215. T.He, S.Chen, B.Ni, Y.Gong, Z.Wu, L.Song, L.Gu, W.Hu, X.Wang. *Angew. Chem., Int. Ed.*, **57**, 3493 (2018)
216. G.Xu, K.Otsubo, T.Yamada, S.Sakaida, H.Kitagawa. *J. Am. Chem. Soc.*, **135**, 7438 (2013)
217. H.Wu, F.Yang, X.-L.L.Lv, B.Wang, Y.-Z.Z.Zhang, M.J.Zhao, J.-R.R.Li. *J. Mater. Chem. A*, **5**, 14525 (2017)
218. E.-X.Chen, G.Xu, Q.Lin. *Inorg. Chem.*, **58**, 3569 (2019)
219. S.S.Rajasree, X.Li, P.Deria. *Commun. Chem.*, **4**, 47 (2021)
220. Y.Tian, N.Vankova, P.Weidler, A.Kuc, T.Heine, C.Wöll, Z.Gu, J.Zhang. *Adv. Sci.*, **8**, 2100548 (2021)
221. S.M.Pratik, L.Gagliardi, C.J.Cramer. *Chem. Mater.*, **32**, 6137 (2020)
222. D.-Y.Zheng, E.-X.Chen, C.-R.Ye, X.-C.Huang. *J. Mater. Chem. A*, **7**, 22084 (2019)
223. X.Liu, M.Kozlowska, T.Okkali, D.Wagner, T.Higashino, G.Brenner-Weiß, S.M.Marschner, Z.Fu, Q.Zhang, H.Imahori, S.Bräse, W.Wenzel, C.Wöll, L.Heinke. *Angew. Chem., Int. Ed.*, **58**, 9590 (2019)
224. J.Liu, C.Wöll. *Chem. Soc. Rev.*, **46**, 5730 (2017)
225. A.L.Semrau, Z.Zhou, S.Mukherjee, M.Tu, W.Li, R.A.Fischer. *Langmuir*, **37**, 6847 (2021)
226. I.N.Meshkov, A.I.Zvyagina, A.A.Shiryaev, M.S.Nickolsky, A.E.Baranchikov, A.A.Ezhov, A.G.Nugmanova, Y.Y.Enakieva, Y.G.Gorbunova, V.V.Arslanov, M.A.Kalinina. *Langmuir*, **34**, 5184 (2018)
227. R.Makiura, H.Kitagawa. *Eur. J. Inorg. Chem.*, 3715 (2010)
228. M.Soichiro, R.Makiura, O.Sakata, H.Kitagawa. *J. Am. Chem. Soc.*, **133**, 5640 (2011)
229. G.Xu, T.Yamada, K.Otsubo, S.Sakaida, H.Kitagawa. *J. Am. Chem. Soc.*, **134**, 16524 (2012)
230. M.Zhao, Y.Wang, Q.Ma, Y.Huang, X.Zhang, J.Ping, Z.Zhang, Q.Lu, Y.Yu, H.Xu, Y.Zhao, H.Zhang. *Adv. Mater.*, **27**, 7372 (2015)
231. G.Ding, B.Yang, K.Zhou, C.Zhang, Y.Wang, J.Q.Yang, S.T.Han, Y.Zhai, V.A.L.Roy, Y.Zhou. *Adv. Electron. Mater.*, **6**, 1900978 (2020)
232. M.Jian, R.Qiu, Y.Xia, J.Lu, Y.Chen, Q.Gu, R.Liu, C.Hu, J.Qu, H.Wang, X.Zhang. *Sci. Adv.*, **6**, eaay3998 (2020)
233. M.C.So, S.Jin, H.Son, G.P.Wiederrecht, O.K.Farha, J.T.Hupp. *J. Am. Chem. Soc.*, **135**, 15698 (2013)
234. J.Liu,W.Zhou, J.Liu, I.Howard, G.Kilibarda, S.Schlabach, D.Coupry, M.Addicoat, S.Yoneda,Y.Tsutsui, T.Sakurai, S.Seki, Z.Wang, P.Lindemann, E.Redel, T.Heine, C.Wöll. *Angew. Chem., Int. Ed.*, **54**, 7441 (2015)
235. N.Yanai, N.Kimizuka. *Chem. Commun.*, **52**, 5354 (2016)
236. P.Duan, N.Yanai, N.Kimizuka. *J. Am. Chem. Soc.*, **135**, 19056 (2013)
237. P.Mahato, A.Monguzzi, N.Yanai, T.Yamada, N.Kimizuka. *Nat. Mater.*, **14**, 924 (2015)
238. S.Hisamitsu, N.Yanai, N.Kimizuka. *Angew. Chem., Int. Ed.*, **54**, 11550 (2015)
239. J.S.Lissau, D.Nauroozi, M.P.Santoni, S.Ott, J.M.Gardner, A.Morandeira. *J. Phys. Chem. C*, **119**, 25792 (2015)
240. T.Ogawa, N.Yanai, A.Monguzzi, N.Kimizuka. *Sci. Rep.*, **5**, 1 (2015)

241. K.Kamada, Y.Sakagami, T.Mizokuro, Y.Fujiwara, K.Kobayashi, K.Narushima, S.Hirata, M.Vacha. *Mater. Horizons*, **4**, 83 (2017)
242. M.Oldenburg, A.Turshatov, D.Busko, S.Wollgarten, M.Adams, N.Baroni, A.Welle, E.Redel, C.Will, B.S.Richards, I.A.Howard. *Adv. Mater.*, **28**, 8477 (2016)
243. M.Adams, M.Kozlowska, N.Baroni, M.Oldenburg, R.Ma, D.Busko, A.Turshatov, G.Emandi, M.O.Senge, R.Haldar, C.Wöll, G.U.Nienhaus, B.S.Richards, I.A.Howard. *ACS Appl. Mater. Interfaces*, **11**, 15688 (2019)
244. C.Gu, H.Zhang, J.Yu, Q.Shen, G.Luo, X.Chen, P.Xue, Z.Wang, J.Hu. *Nano Lett.*, **21**, 1102 (2021)
245. Y.Xiao, W.Guo, H.Chen, H.Li, X.Xu, P.Wu, Y.Shen, B.Zheng, F.Huo, W.D.Wei. *Mater. Chem. Front.*, **3**, 1580 (2019)
246. Y.Pan, R.Abazari, J.Yao, J.Gao. *J. Phys. Energy*, **3**, 032010 (2021)
247. Y.Zhao, Y.Kuang, M.Liu, J.Wang, R.Pei. *Chem. Mater.*, **30**, 7511 (2018)
248. P.Ling, C.Qian, J.Yu, F.Gao. *Chem. Commun.*, **55**, 6385 (2019)
249. X.Qiao, M. rsalan, X.Ma, Y.Wang, S.Yang, Y.Wang, Q.Sheng, T.Yue. *Anal. Bioanal. Chem.*, **413**, 839 (2021)
250. S.Hu, Y.Jiang, Y.Wu, X.Guo, Y.Ying, Y.Wen, H.Yang. *ACS Appl. Mater. Interfaces*, **12**, 55324 (2020)
251. Z.Qiu, T.Yang, R.Gao, G.Jie, W.Hou. *J. Electroanal. Chem.*, **835**, 123 (2019)
252. J.Ma, W.Bai, J.Zheng. *Microchim. Acta*, **186**, 1 (2019)
253. Y.Han, Z.Liu, F.Zheng, Y.Bai, Z.Zhang, X.Li, W.Xiong, J.Zhang, A.Yuan. *J. Alloys Compd.*, **881**, 160531 (2021)
254. J.Meng, Y.Zhou, H.Chi, K.Li, J.Wan, Z.Hu. *ChemistrySelect*, **4**, 8661 (2019)
255. V.V.Arslanov, M.A.Kalinina, E.V.Ermakova, O.A.Raitman, Y.G.Gorbunova, O.E.Aksyutin, A.G.Ishkov, V.A.Grachev, A.Y.Tsivadze. *Russ. Chem. Rev.*, **88**, 775 (2019)
256. M.S.Yao, J.W.Xiu, Q.Q.Huang, W.H.Li, W.W.Wu, A.Q.Wu, L.A.Cao, W.H.Deng, G.E.Wang, G.Xu. *Angew. Chem., Int. Ed.*, **58**, 14915 (2019)
257. A.I.Zvyagina, A.A.Shiryaev, A.E.Baranchikov, V.V.Chernyshev, Y.Y.Enakieva, O.A.Raitman, A.A.Ezhov, I.N.Meshkov, D.A.Grishanov, O.S.Ivanova, Y.G.Gorbunova, V.V.Arslanov, M.A.Kalinina. *New J. Chem.*, **41**, 948 (2017)
258. E.V.Ermakova, A.A.Ezhov, A.E.Baranchikov, Y.G.Gorbunova, M.A.Kalinina, V.V.Arslanov. *J. Colloid Interface Sci.*, **530**, 521 (2018)
259. D.T.Lee, J.D.Jamir, G.W.Peterson, G.N.Parsons. *Small*, **15**, 1805133 (2019)
260. M.R.Sokolov, Y.Y.Enakieva, A.D.Yapryntsev, A.A.Shiryaev, A.I.Zvyagina, M.A. Kalinina. *Adv. Funct. Mater.*, **30**, 2000681 (2020)
261. S.R.Ahrenholtz, C.C.Epley, A.J.Morris. *J. Am. Chem. Soc.*, **136**, 2464 (2014)
262. P.M.Usov, S.R.Ahrenholtz, W.A.Maza, B.Stratakes, C.C.Epley, M.C.Kessinger, J.Zhu, A.J.Morris. *J. Mater. Chem. A*, **4**, 16818 (2016)